

**This pdf file contains all figure pages in the dissertation:**

LATE STRUCTURES AND STRAIN HISTORY ACCOMPANYING FLUID FLOWS IN  
THE WESTERN TACONIC OROGEN OF THE NEW YORK-VERMONT  
APPALACHIANS

and

STRUCTURAL GEOLOGY AND TECTONIC EVOLUTION OF THE NAMCHE  
BARWA REGION, TIBET

by

Chul Lim

A Dissertation

Submitted to the University at Albany, State University of New York

in Partial Fulfillment of

the Requirements for the Degree of

Doctor of Philosophy

College of Arts and Sciences

Department of Earth and Atmospheric Sciences

2007

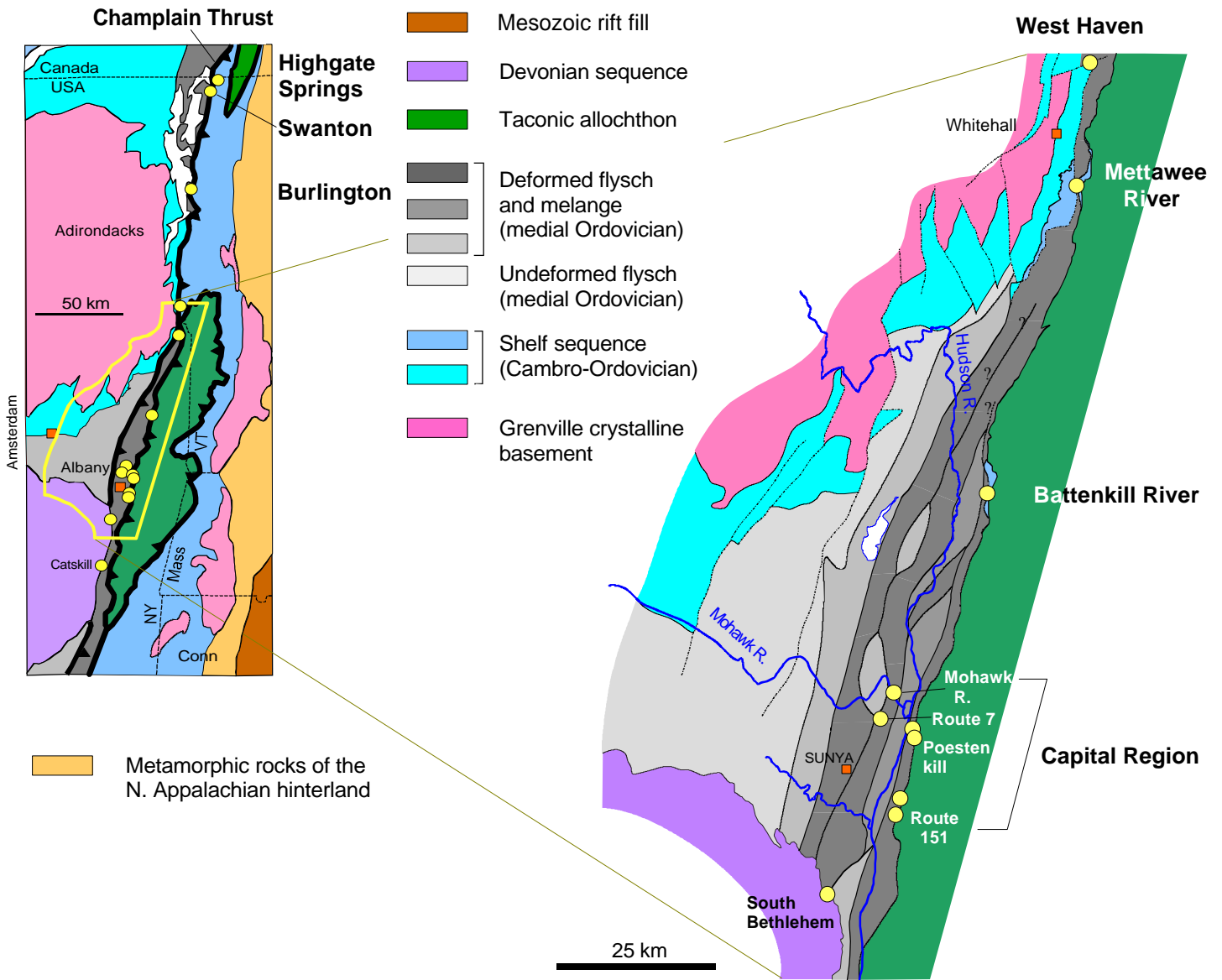


**Figure 1.** Geologic maps showing the general geology of western margin of the Taconic orogen and the foreland, and locations of the outcrops for measurement and sampling (circles). SUNYA: University at Albany



**Figure 2.** Reverse-motion vein with a multilayer mat of mineral slickenfibers. The orientations of fibers are slightly different in each layer, but all of them indicate essentially the same movement direction and shear sense, westward displacement of a hanging wall that was in contact with the vein when it precipitated. Route 7 roadcut, Latham, New York.

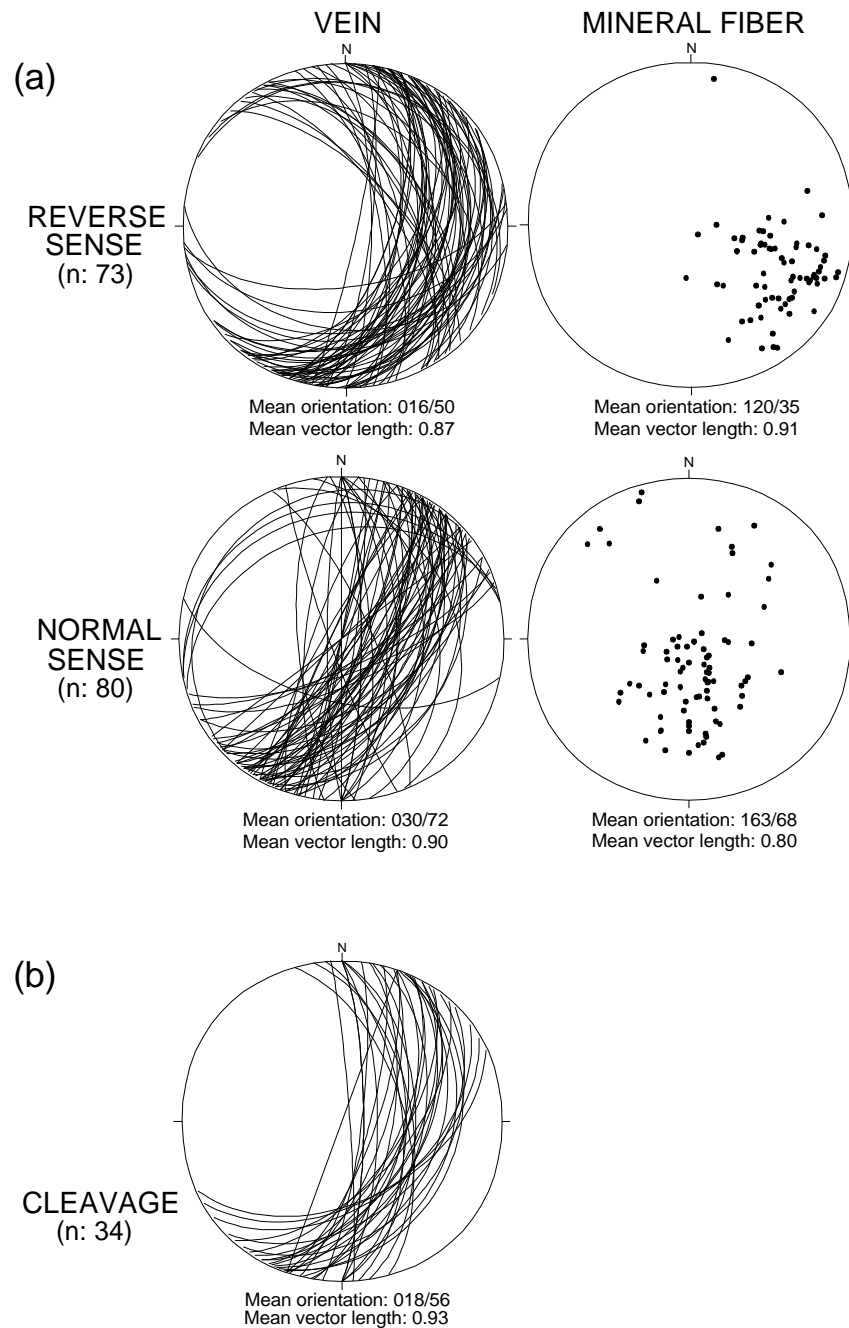


**Figure 3.** Results of field measurements. (a) Equal area stereonet of the vein and mineral fiber orientations. The mineral fibers with reverse motion plunge toward the southeast, and the displacement of the hanging wall was toward  $300^\circ$  in average orientation. The mineral fibers with normal motion plunge more toward the south and show large variation in orientation. Mean vector length refers to the length of the mean vector divided through the number of measurements (value 1 means all vectors are parallel, and value 0 vectors are randomly oriented). Lower hemisphere projection. (b) Equal area stereonet for orientation of phacoidal cleavage. Reverse- and normal-motion veins are close to the cleavage in strike, despite different slip directions (See text for discussion). Lower hemisphere projection.

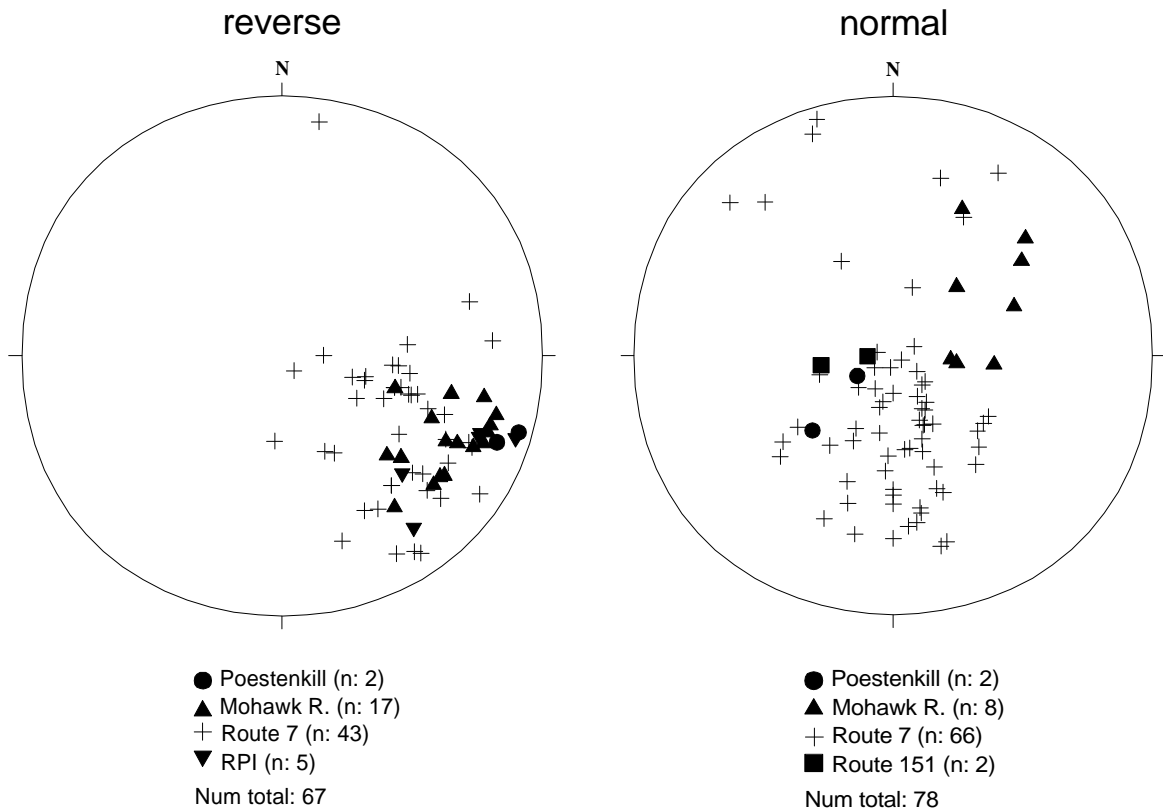


**Figure 4.** Equal area stereonet showing orientation of mineral fibers in each locality. The reverse-motion fibers indicate a consistent, ESE direction regardless of localities. By contrast, the orientation of normal-motion fibers shows large variations within each locality as well as among the localities. Localities with only one measurement for each type of vein are not included. Lower hemisphere projection. RPI: outcrops in the Rensselaer Polytechnic Institute, located 1.5 km north of the Poestenkill gorge outcrops.

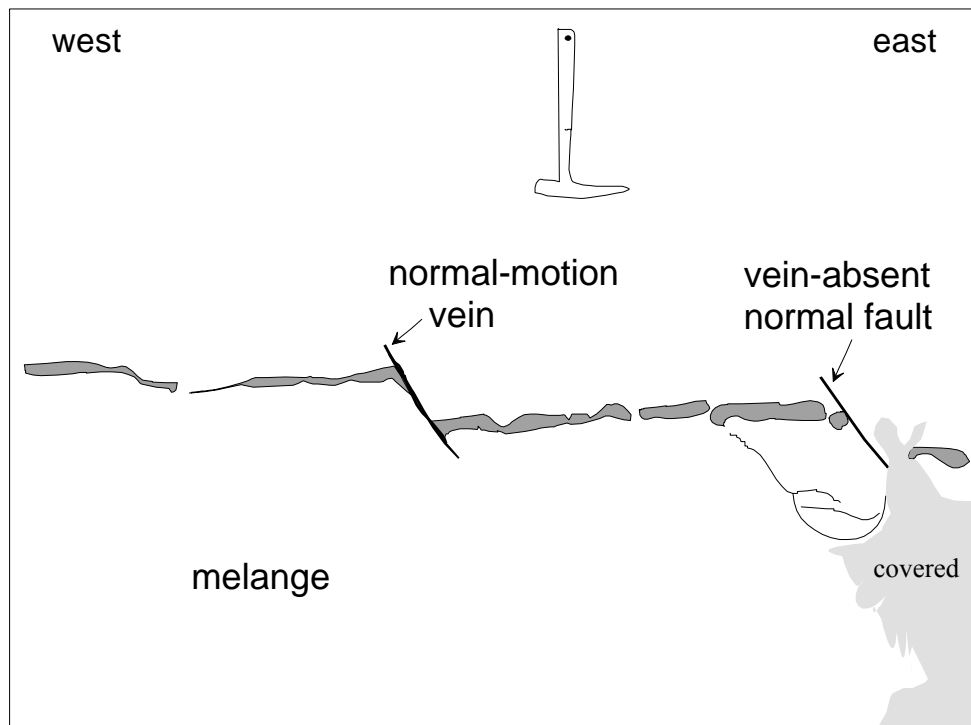


**Figure 5.** Normal-motion vein and a normal fault cut across a thick vein dipping gently to the northwest. The block above the thick vein moved toward northwest. Roadcut on northern side of Route 7, Latham, New York.

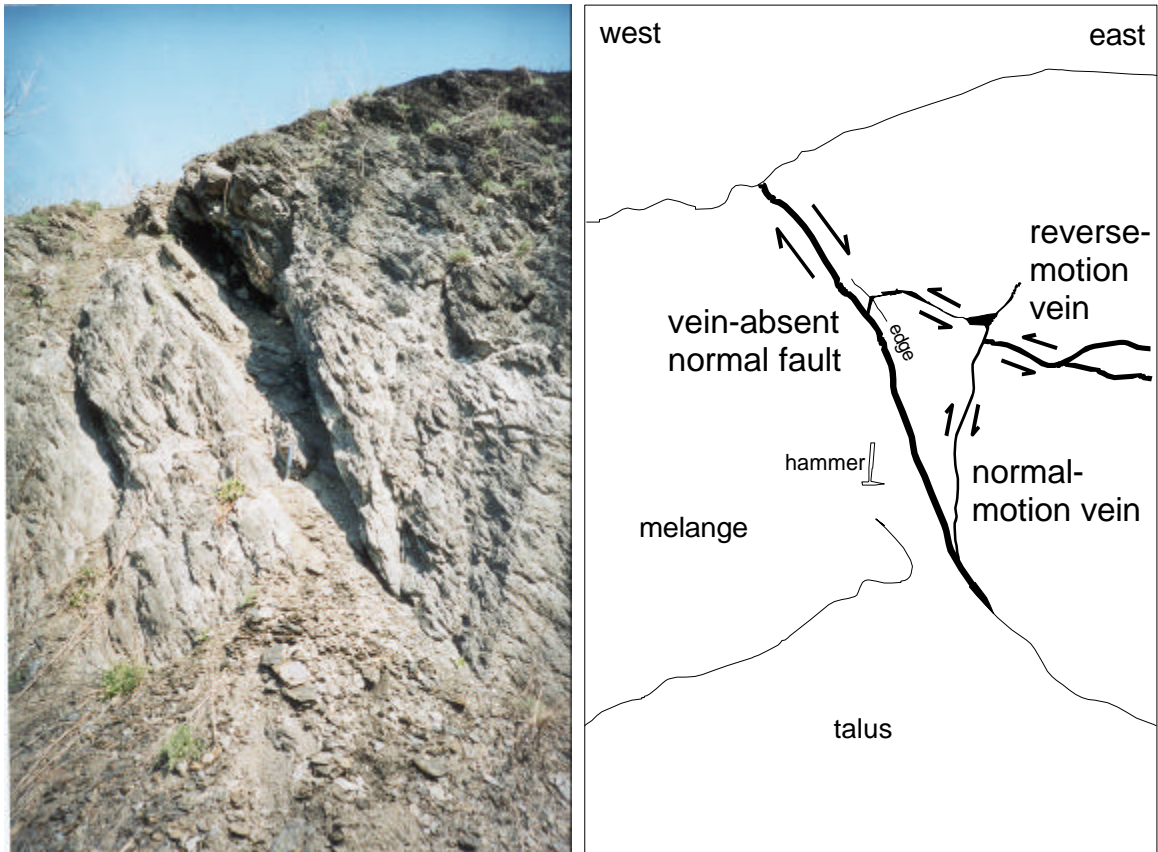


**Figure 6.** Reverse-motion vein (east-side-up) is cross-cut by a nearly vertical normal-motion vein (east-side-down), and both veins are truncated by a vein-absent normal fault. Roadcut on northern side of Route 7, Latham, New York.

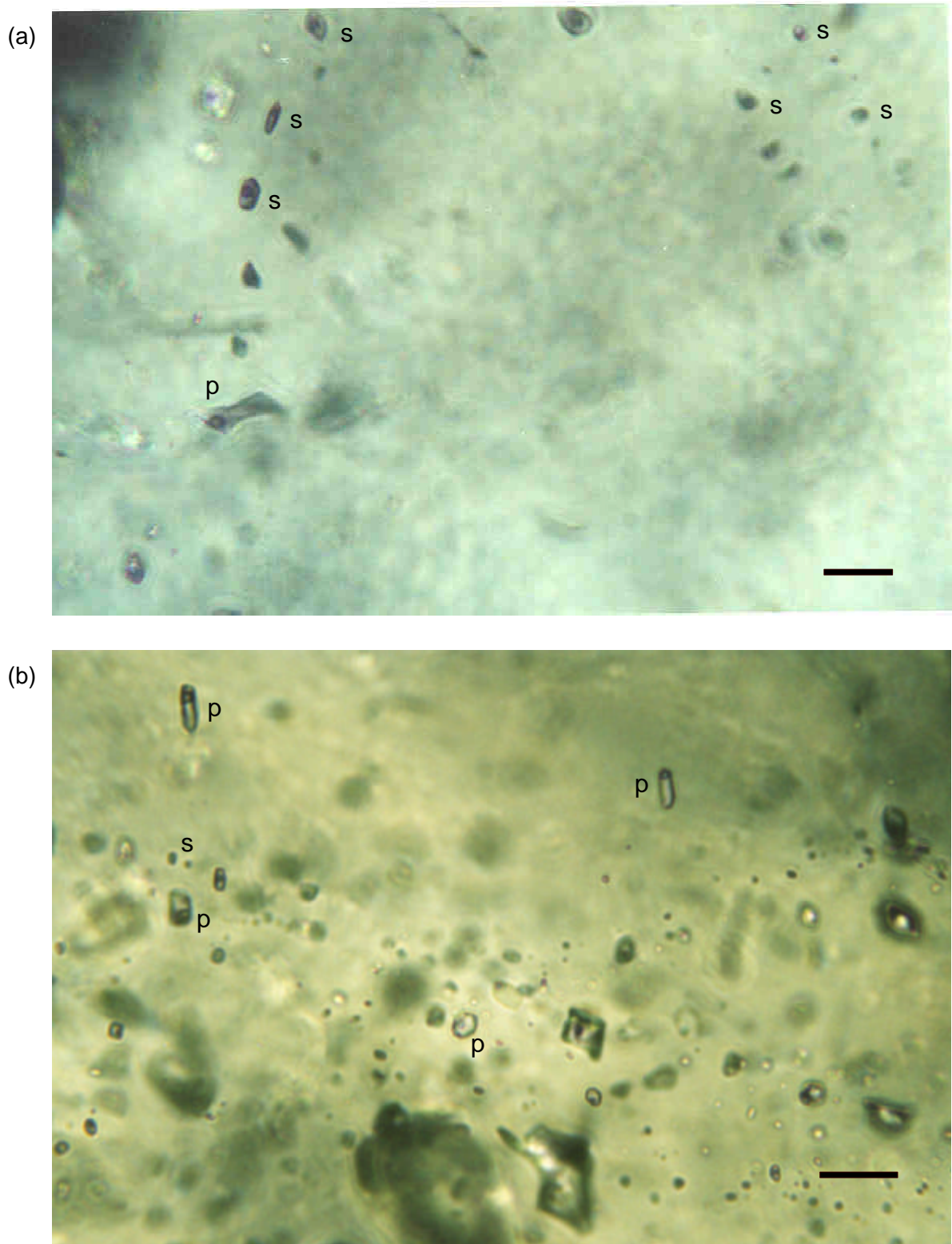


**Figure 7.** Photomicrographs of aqueous fluid inclusions in the vein quartz. (a) shows a number of secondary fluid inclusion trails in MH-1 (Cohoes gorge), and (b) shows many primary fluid inclusions in TR418-2 (Poestenkill gorge). p: primary inclusion, s: secondary inclusion. The black bars are 20 micrometers long in both photos.

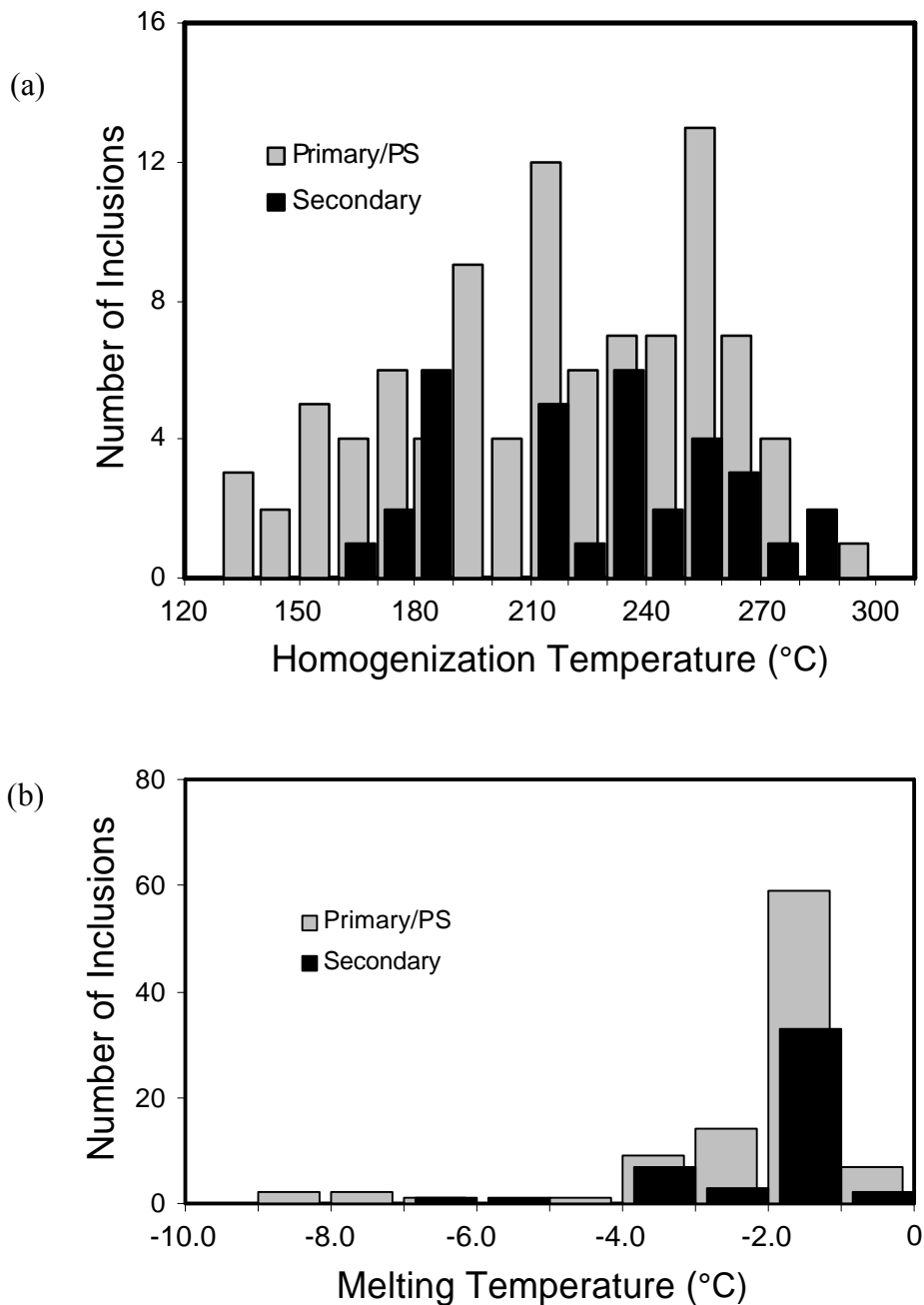


**Figure 8.** Histograms showing all measurement data from the Taconic vein samples. (a) Homogenization temperature of aqueous fluid inclusions in the veins shows a wide variation among the veins. This variation is generally a function of locations (reverse-motion veins) and strain type of the vein. (b) Ice melting temperatures of fluid inclusions show little variation for most samples, with a strong peak in the -1.0 to -2.0°C interval. Some low melting temperatures are probably due to mixing of this fluid with other high-salinity fluid. PS: pseudosecondary.

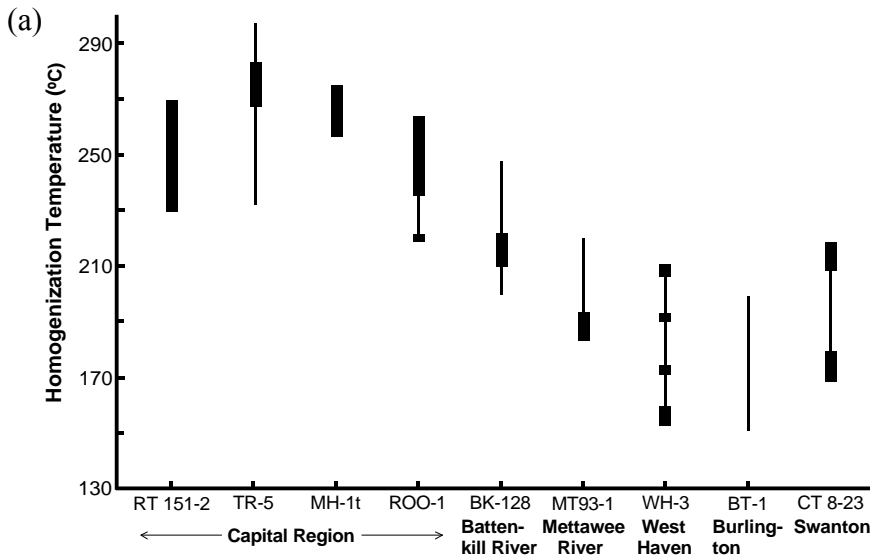
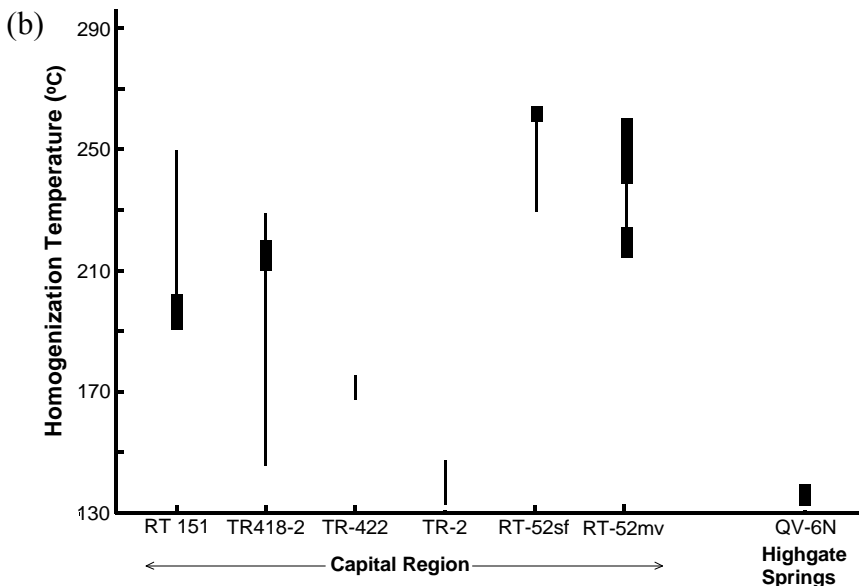
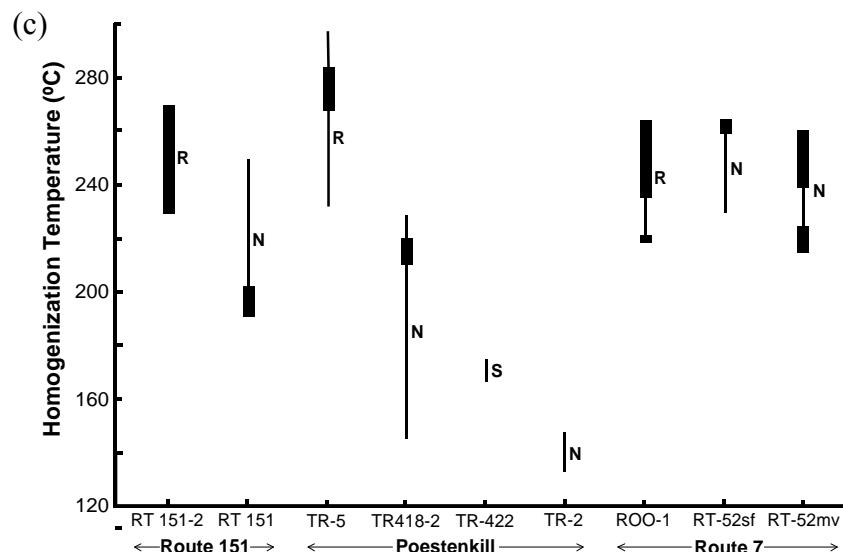


**Figure 9.** Ranges of homogenization temperatures. The thin lines are whole temperature ranges including outliers. The heavy lines mark a temperature range where two or more inclusions plot within 10°C of each other.

(a). Homogenization temperatures in the reverse-motion veins. Along-strike variation of temperatures refers to the variation from the Capital Region northward to Swanton. Across-strike variation is the variation to the west from TR-5 (Poestenkill), through MH-1t (Mohawk River), to ROO-1 (Route 7). Note that variation of homogenization temperatures is gradual.



(b). Homogenization temperatures in the normal-motion veins. Plot includes a strike-slip vein at Poestenkill Falls (TR-422). The variation of temperatures is irregular and abrupt.



(c). Comparison of homogenization temperatures of the reverse- and normal-motion veins occurring in the same outcrops. In Route 7, there is little difference in homogenization temperature between the reverse- and normal-motion veins. In Route 151 and Poestenkill Falls, however, the normal-motion veins yield homogenization temperatures lower than the reverse-motion veins. In contrast to homogenization temperatures, there are virtually no differences in salinity among different vein types. See the salinity ranges of the Capital Region in Figure 10. R: reverse-motion vein, N: normal-motion vein, S: strike-slip vein.

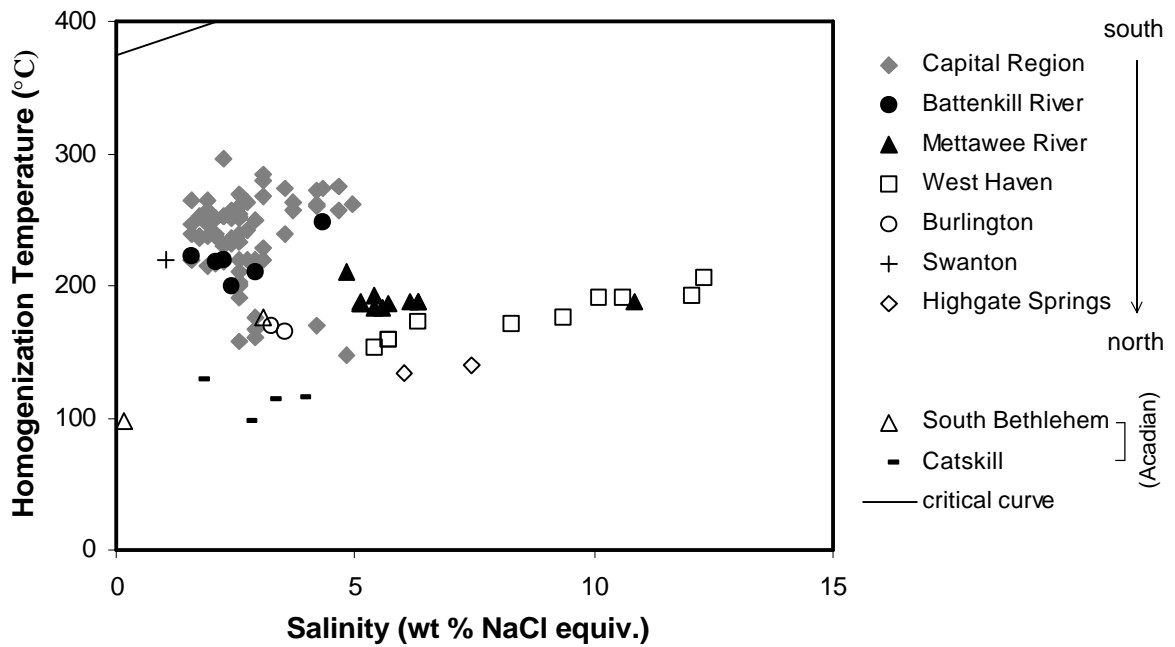


**Figure 10.** Homogenization temperature and salinity of fluid inclusions in the observed veins. Most inclusions have salinity below 7 %. Some samples with higher salinity are from outcrops that are close to carbonate rocks. Only inclusions in which both homogenization temperature and melting temperature were determined are shown. The Devonian (Acadian) samples from South Bethlehem and Catskill are shown for comparison. Critical curve after Shepherd et al. (1985).

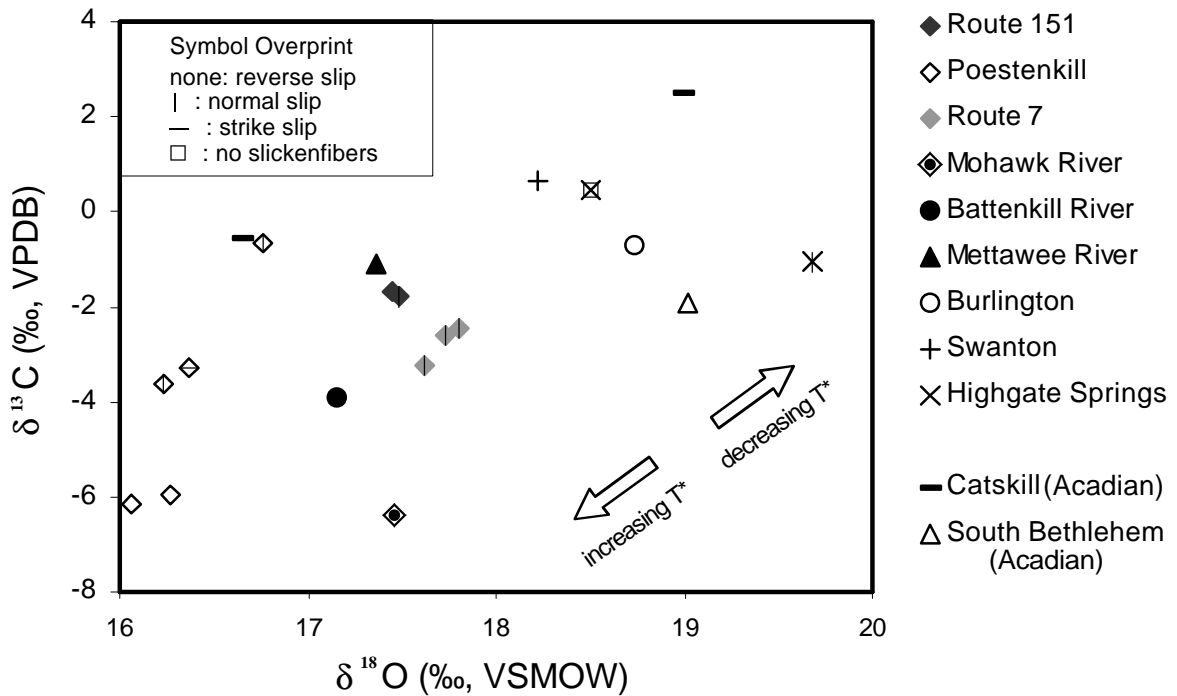


**Figure 11.** Isotopic compositions of vein calcite. In general, samples with higher homogenization temperatures are more depleted, and those with lower homogenization temperatures are more enriched. One problem could be that majority of fluid inclusion data are from quartz, while all isotope data are from calcite. However, when fluid inclusions in both minerals are analyzed in the same sample, they give essentially the same temperature range. Taconic vein calcite is suggested to have precipitated from metamorphic fluids. Fluid-source type or types is not determined for the Acadian samples. Samples without overprinted symbol are reverse-motion veins. For samples with overprinted symbols, the shear senses are normal, strike-slip, or not determined. T\*: homogenization temperatures of fluid inclusions.



**Figure 12.** Contact between the Taconic Allochthon and melange (white arrows) exposed on the southern bank of the falls in the Poestenkill gorge in South Troy. The contact does not bear any vein around the base of the hill, but it contains a thin slickensided vein above and to right of the area shown. The contact has been known as the Taconic Frontal Thrust, but the vein indicates normal slip and has a homogenization temperature lower than a nearby reverse-motion vein in the melange. View is to the southeast. A scale bar on the left is 1 m long.

## Sequence of Events

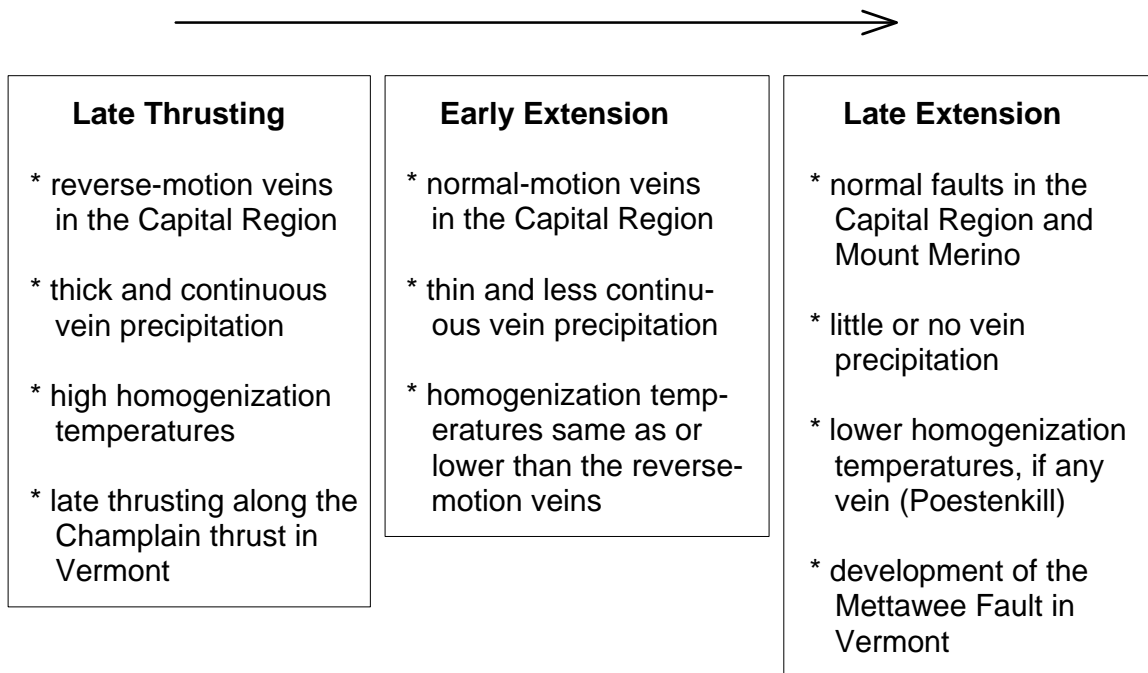


**Figure 13.** Reconstruction of the strain history based on cross-cutting relationships, fluid cooling trends, and scale and abundance of veining.

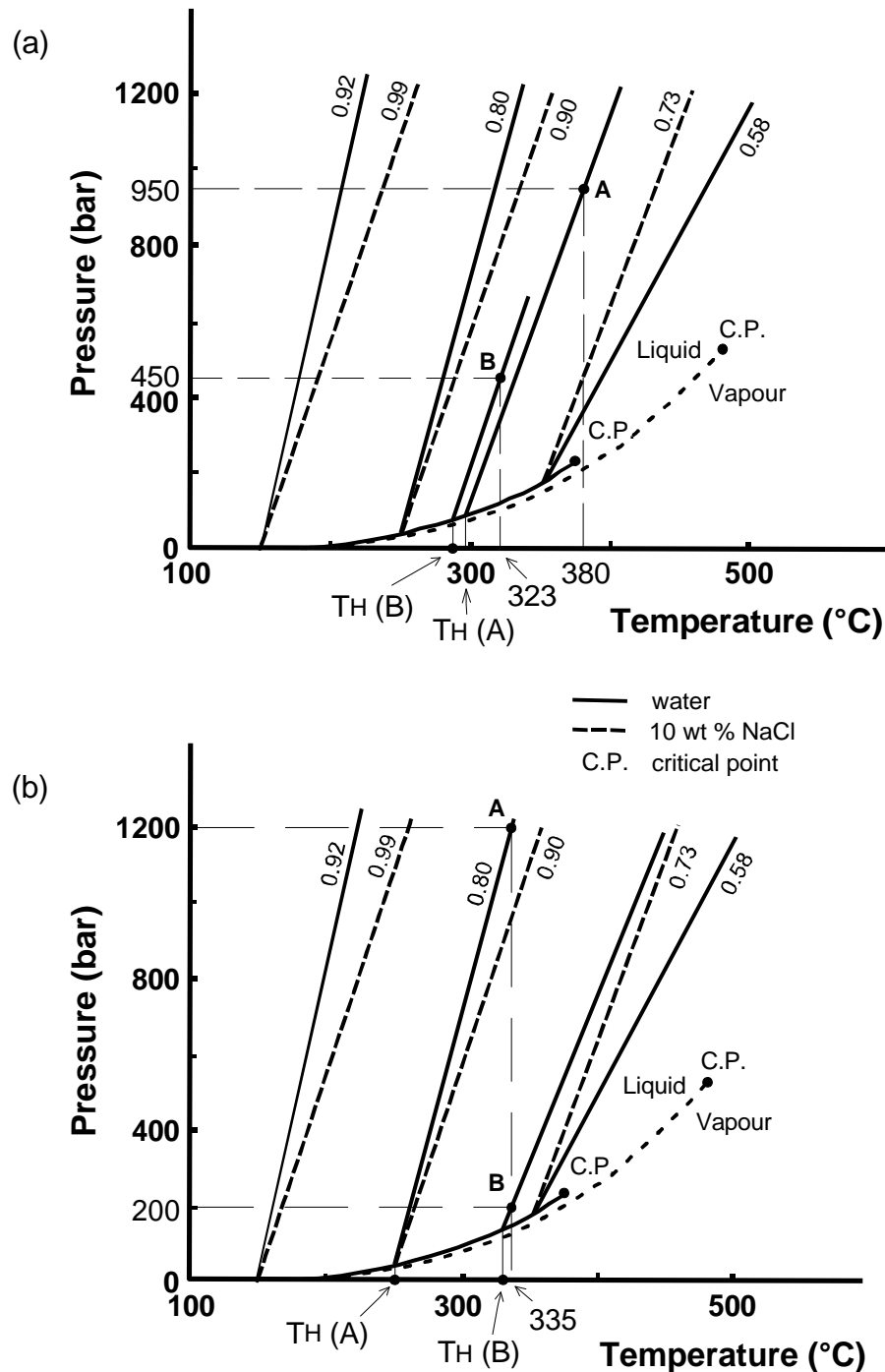


**Figure 14.** Parts of simulations of the homogenization temperatures of fluid inclusions that initially trapped a single-phase water in a hypothetical crust that has only a vertical geothermal gradient and no horizontal gradient. Numbers on the upper part of curves are fluid density. Diagrams modified after Shepherd et al. (1985). (a) Fluid inclusions A and B form at different temperatures and pressures, but there is only a small difference in homogenization temperature. Results of full simulations are presented in Table 1. (b) Fluid inclusion A is trapped at a pressure 1 kbar higher than inclusion B and at the same temperature. However, the homogenization temperature of inclusion A is only 78°C lower than that of inclusion B.

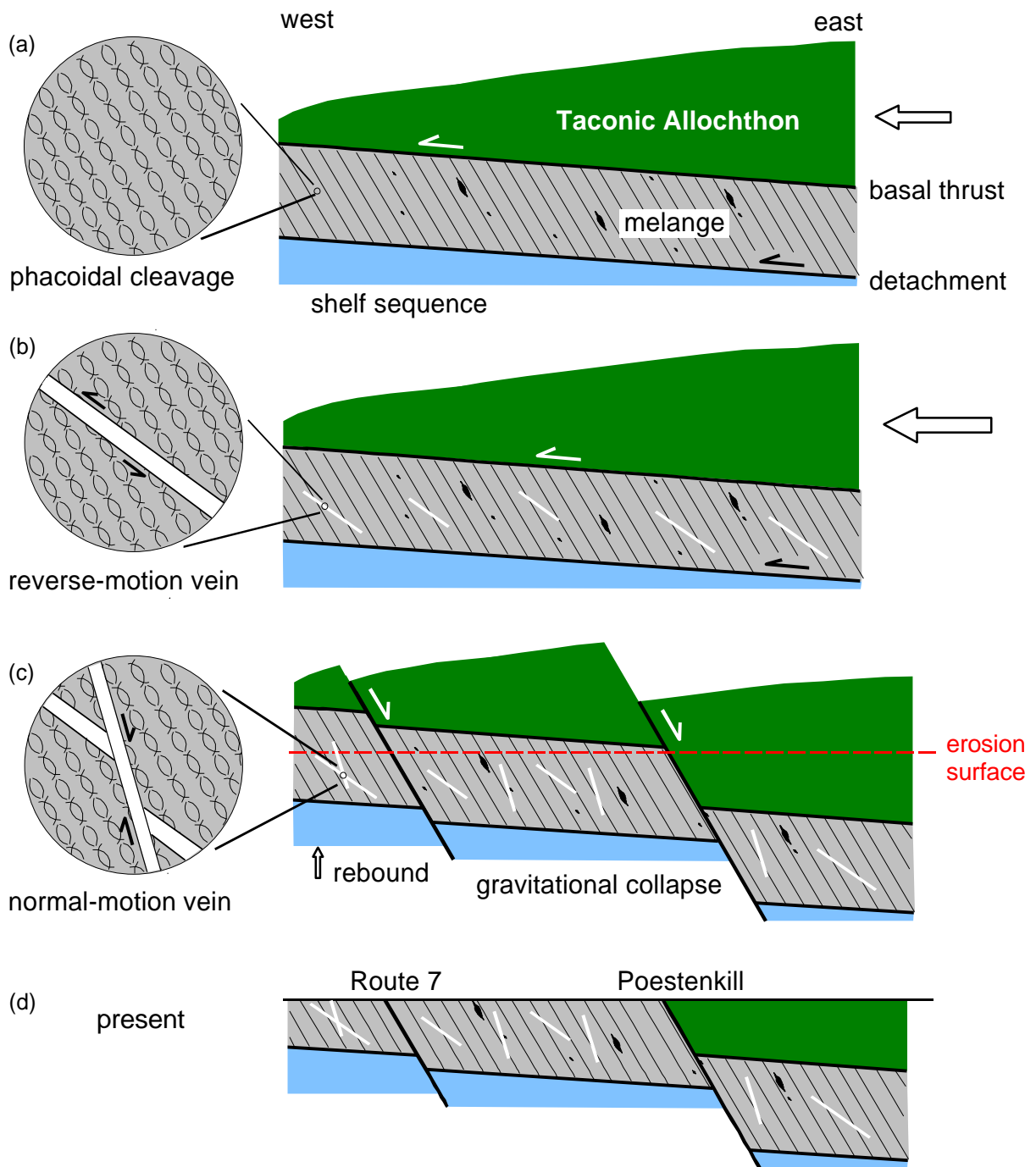


**Figure 15.** Schematic temporal cross sections through the western margin of the Taconic orogen in the Capital Region. (a) Transport of the Allochthon over melange is shown. During this stage, the melange was deformed in a dominantly ductile manner. (b) The last shortening event of the reverse-motion veins from the Capital Region through West Haven is correlated with the late shortening along the Champlain thrust in Vermont. During this stage, deformation in the melange was brittle due to a rapid shortening (See PART III). (c) The early extension is manifested as the normal-motion veins in the melange. The later extension occurred with little or no veining, and good examples are the vein-free normal faults in the Route 7 roadcuts and the western bounding fault of the Allochthon in the Poestenkill Falls outcrop. To the north, this later extension is correlated with the normal faulting along the Mettawee Fault.

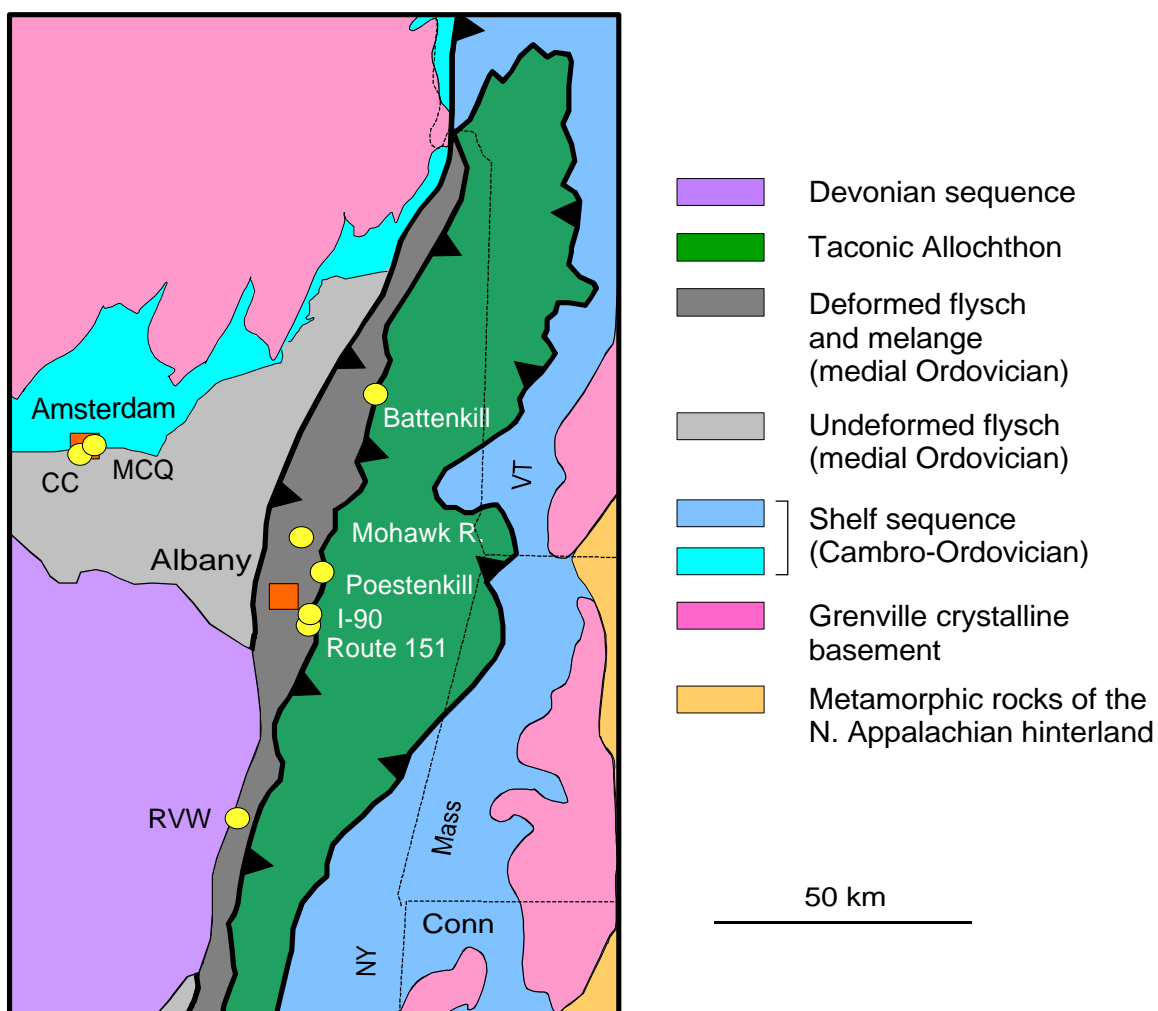


**Figure 1.** A geologic map of the study area and locations of the sampled outcrops.  
 RVW: Rip Van Winkle Bridge, CC: Chuctanunda Creek, MCQ: Manny Corners Quarry

(a)



(b)



**Figure 2.** Quartz-calcite veins exposed in the Route 7 roadcuts, Latham, New York. (a) An overhanging vein surface with stepping-down of slickenfibers indicating normal motion. View is toward south. (b) A layered vein with indistinct slip sense. The wall rocks for both veins are melange predominantly consisting of intensely-sheared shale and siltstone, with well-developed phacoidal cleavage.

(c)



**Figure 2** (continued), (c) a large normal-motion vein 1-7 cm thick. It dips southeastward at a steep angle ( $62^\circ$ ), within the melange.

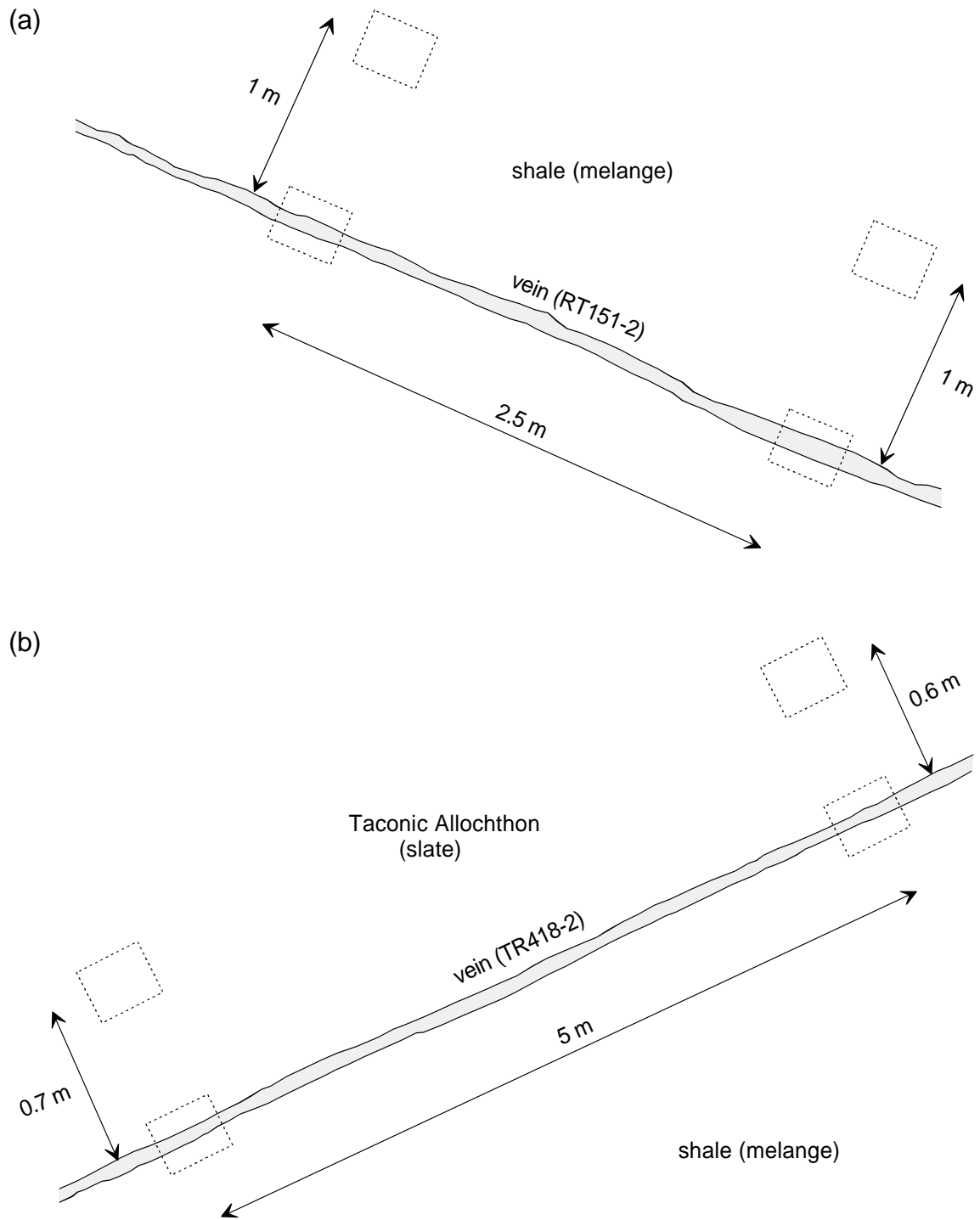


**Figure 3.** Sketches of sites where the vein and host rock samples were collected in individual outcrops. (a) Route 151 roadcut, east end, north side. (b) Poestenkill Falls, Troy, south bank. The dashed boxes are sampling locations.

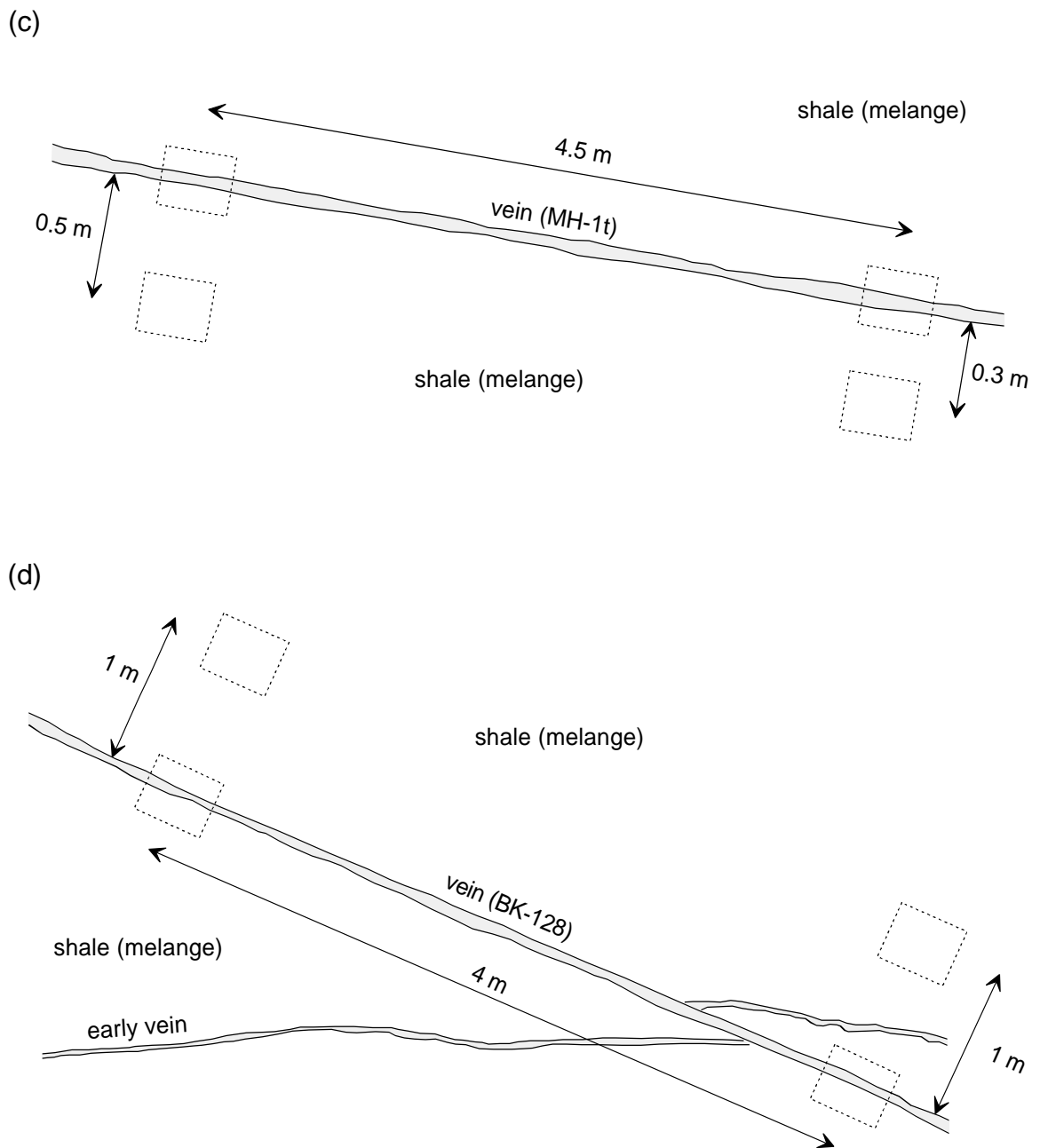


**Figure 3** (continued), (c) North bank of Mohawk River, near and below the Cohoes Falls. (d) Battenkill River, north bank. The vein (BK-128) crosscuts an earlier vein at low angle in thrust sense.

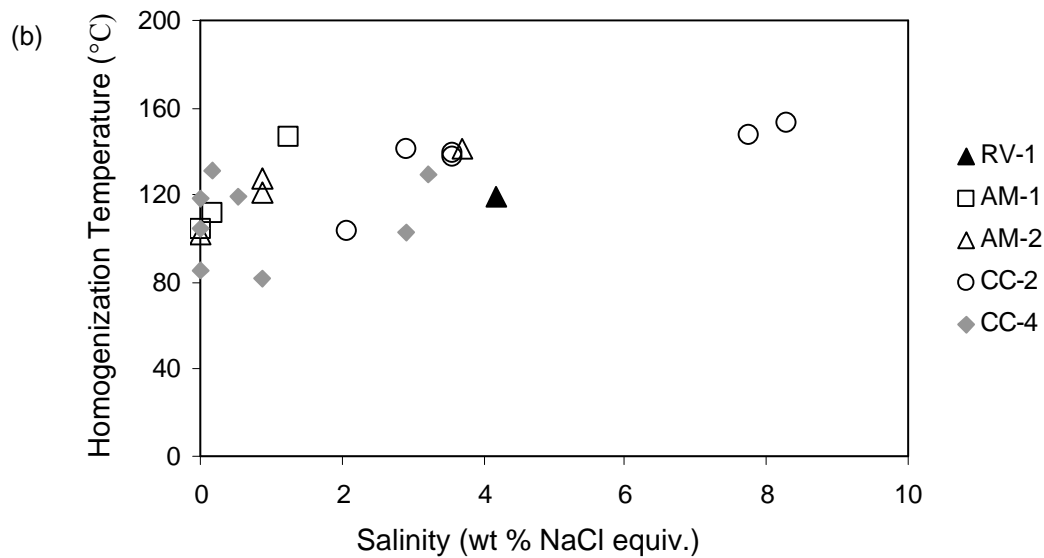
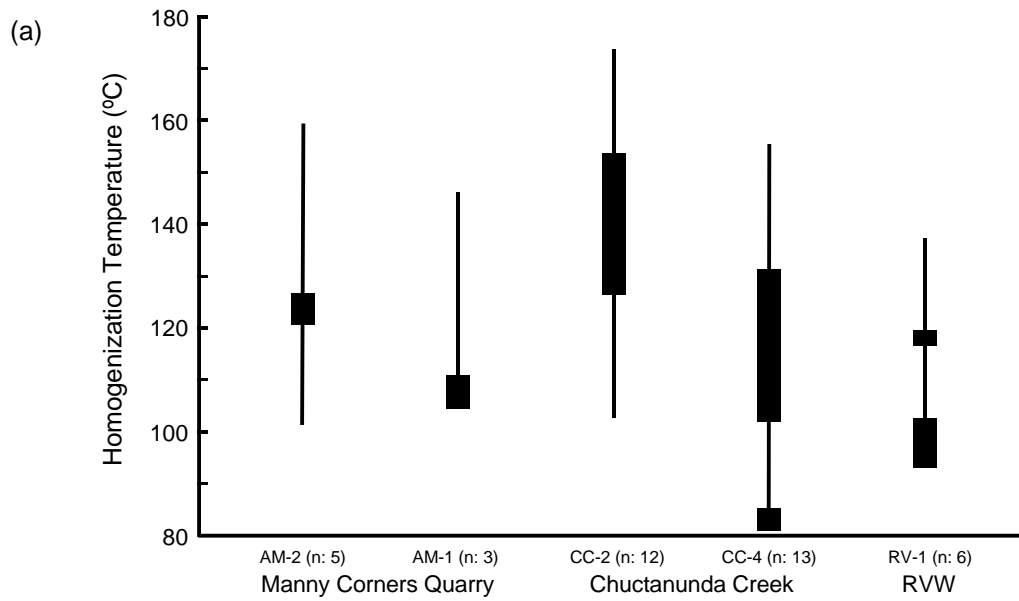


**Figure 4.** Results of fluid inclusion analysis for the strike-slip veins. (a) homogenization temperature, and (b) salinity. Homogenization temperatures in this chapter are presented following the convention in the previous chapter. The thin line indicates a temperature range including outliers, and the thick line a range where two or more data points are less than 10°C apart. Sample RV-1 is from a vein filling tension gash of a left-lateral strike-slip fault set with no veins along the fault surface. RVW: Rip Van Winkle Bridge, west entrance. n: number of analyzed fluid inclusions.

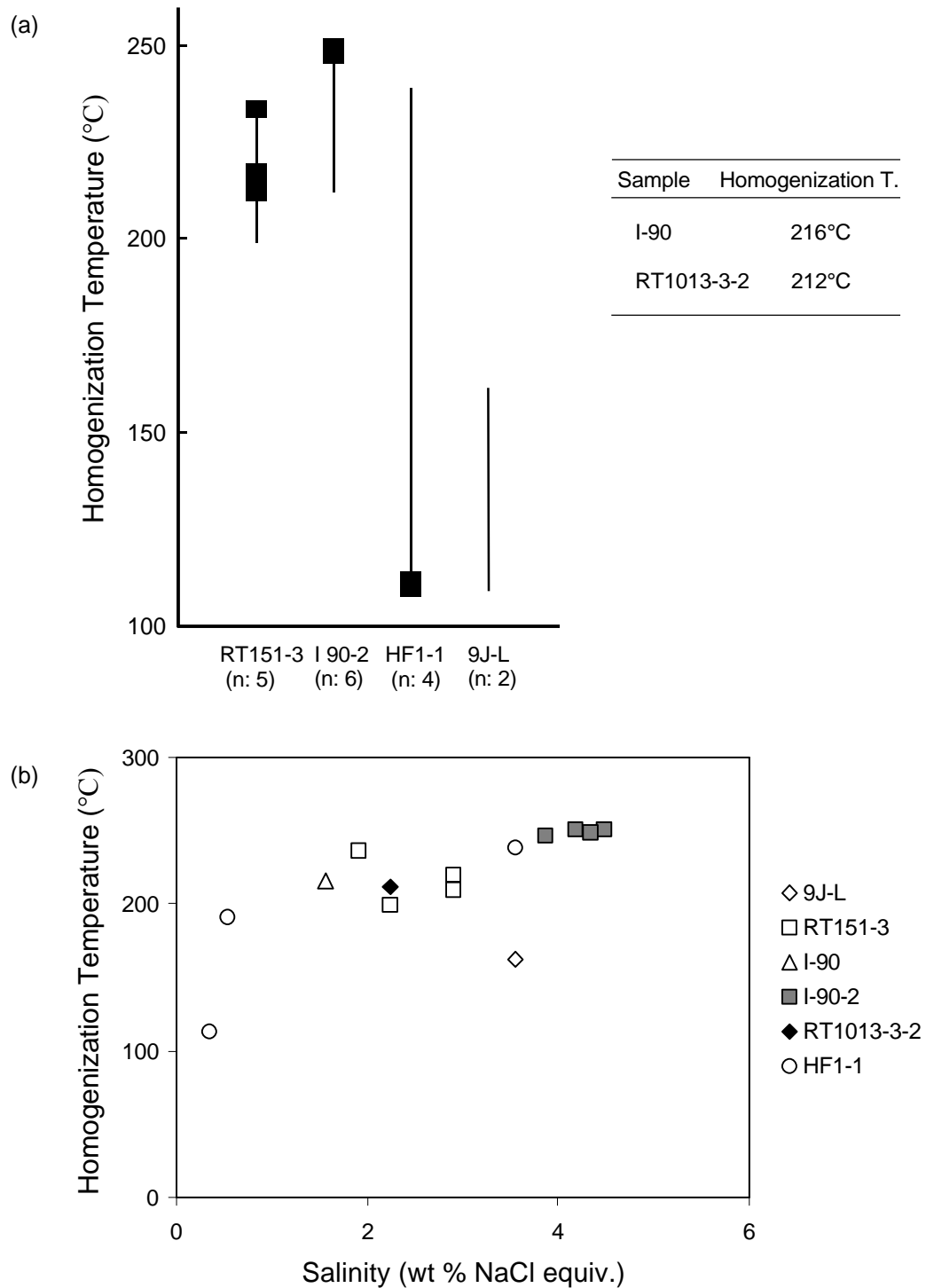


**Figure 5.** Results of fluid inclusion analysis for the dip-slip-veins and vug-quartz. (a) homogenization temperature. Only one fluid inclusion was successfully measured in two other samples as presented in the Table. (b) salinity. RT1013-3-2 is from a vein in the Route 7 roadcut that merges with a thrust-motion vein (ROO-1) reported in PART I. For location, see Figure 1 and Figure 1 in PART I. HF-1 is from the Halfmoon Graywacke Zone, immediately north of the Route 7 locality.

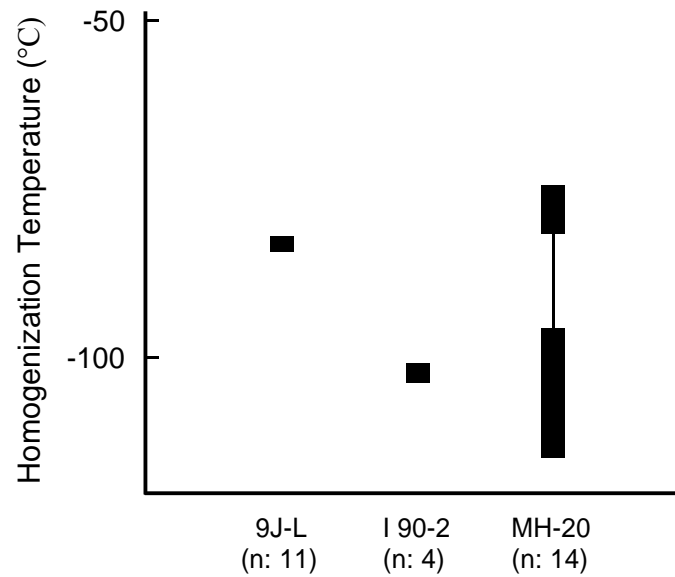


**Figure 6.** Homogenization temperature of hydrocarbon fluid inclusions. Most inclusion fluids in the 9J-L are pure methane. Some aqueous inclusions were also measured in the same samples 9J-L (immediately south of Rensselaer Town line along Route 9J) and I-90-2, while solely hydrocarbon fluid inclusions were measured in the MH-20 (Mohawk River section, above Cohoes Falls).

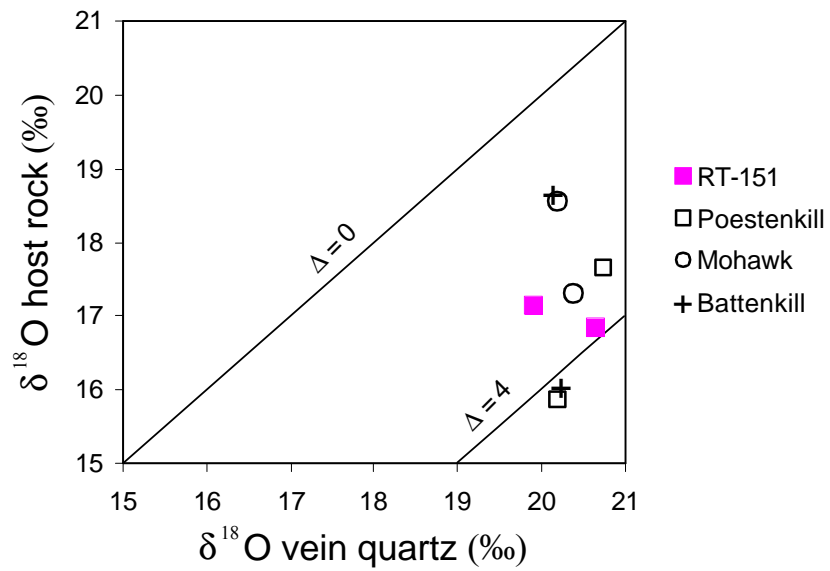


**Figure 7.** Comparison of  $\delta^{18}\text{O}$  values of vein quartz with those of host rocks. The amount of fractionation ( $\Delta$ ) ranges over more than 4 ‰. The vein quartz shows limited variations of  $\delta^{18}\text{O}$  relative to host rocks within and among outcrops, which results in near vertical alignments of the vein quartz-host rock pairs. This pattern is indicative of a rock-buffered system.

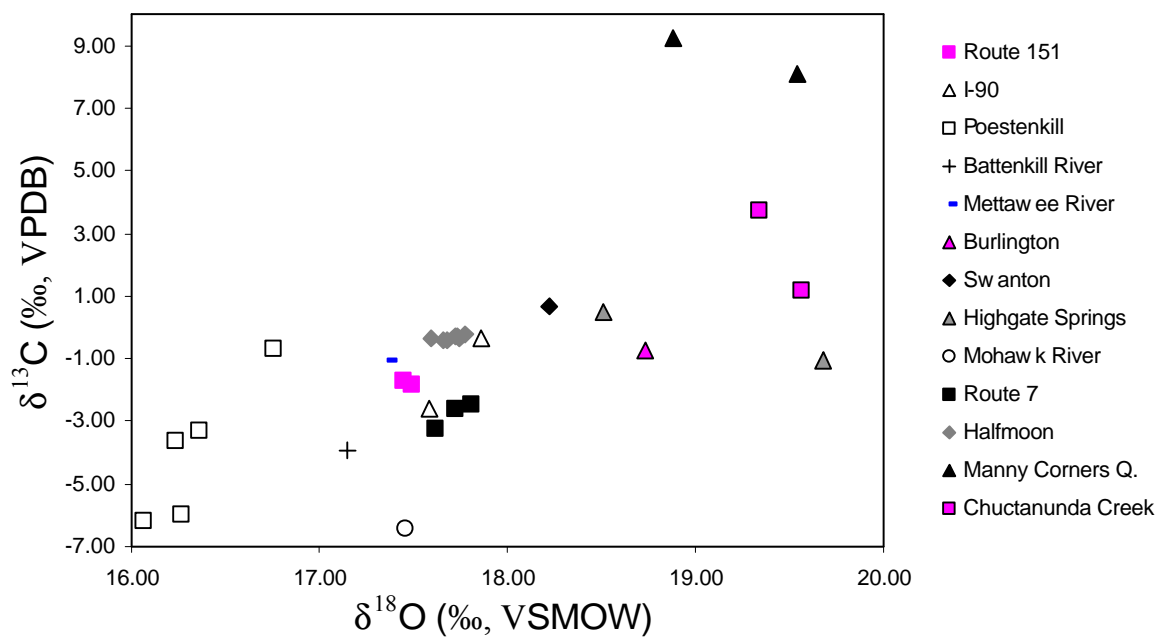


**Figure 8.** Results of stable isotope analysis of vein calcite in 22 veins. The Isotope compositions of 7 new veins analyzed in this chapter show a variation consistent with the isotope composition-temperature relationship exhibited by the 15 veins incorporated from the previous chapter.

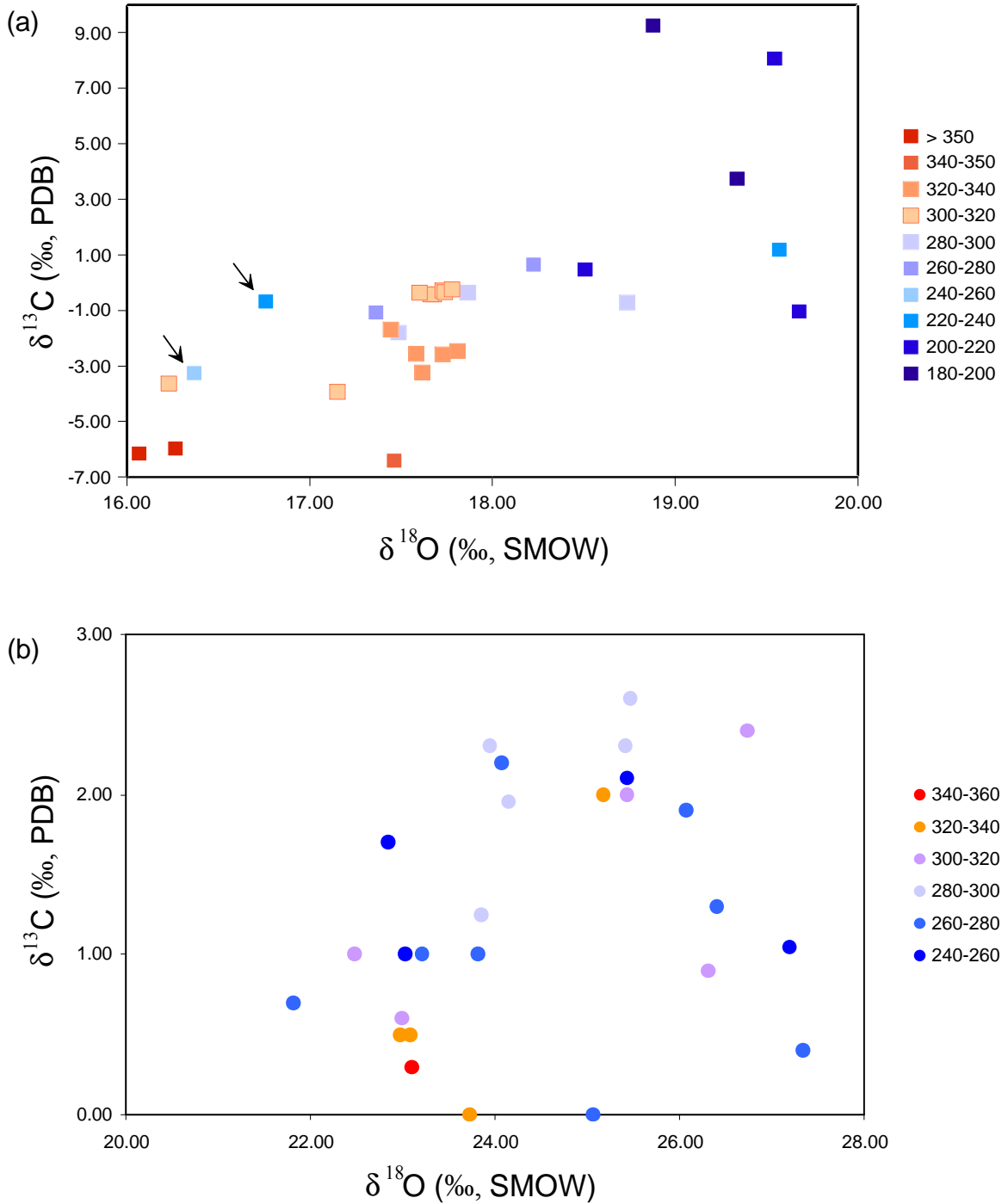


**Figure 9.** Isotope compositions of vein calcite deposited in the (a) fluid-buffered system (this study) and (b) rock-buffered system (Kirschner et al., 1995). In (a), temperatures are based on pressure correction of 80°C. The two low-temperature data (arrowed), all from the Poestenkill gorge, are plotted in lower left indicating interaction with depleted carbonate rocks (probably thrust-motion calcite vein(s)). See text. Except for these two, it is clearly shown that the isotope compositions vary according to temperatures. In (b), the isotope compositions do not show any relationship with temperatures.

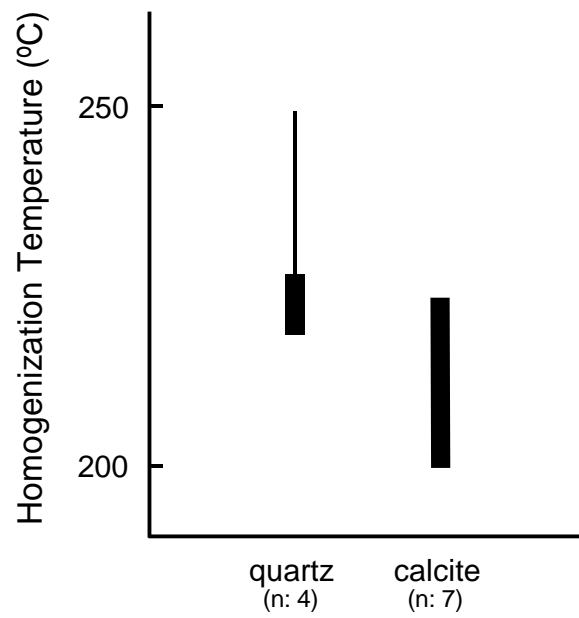


**Figure 10.** Homogenization temperatures of fluid inclusions in quartz and calcite of a thrust-motion vein in the bank of Battenkill River (BK-128). n: number of analyzed fluid inclusion

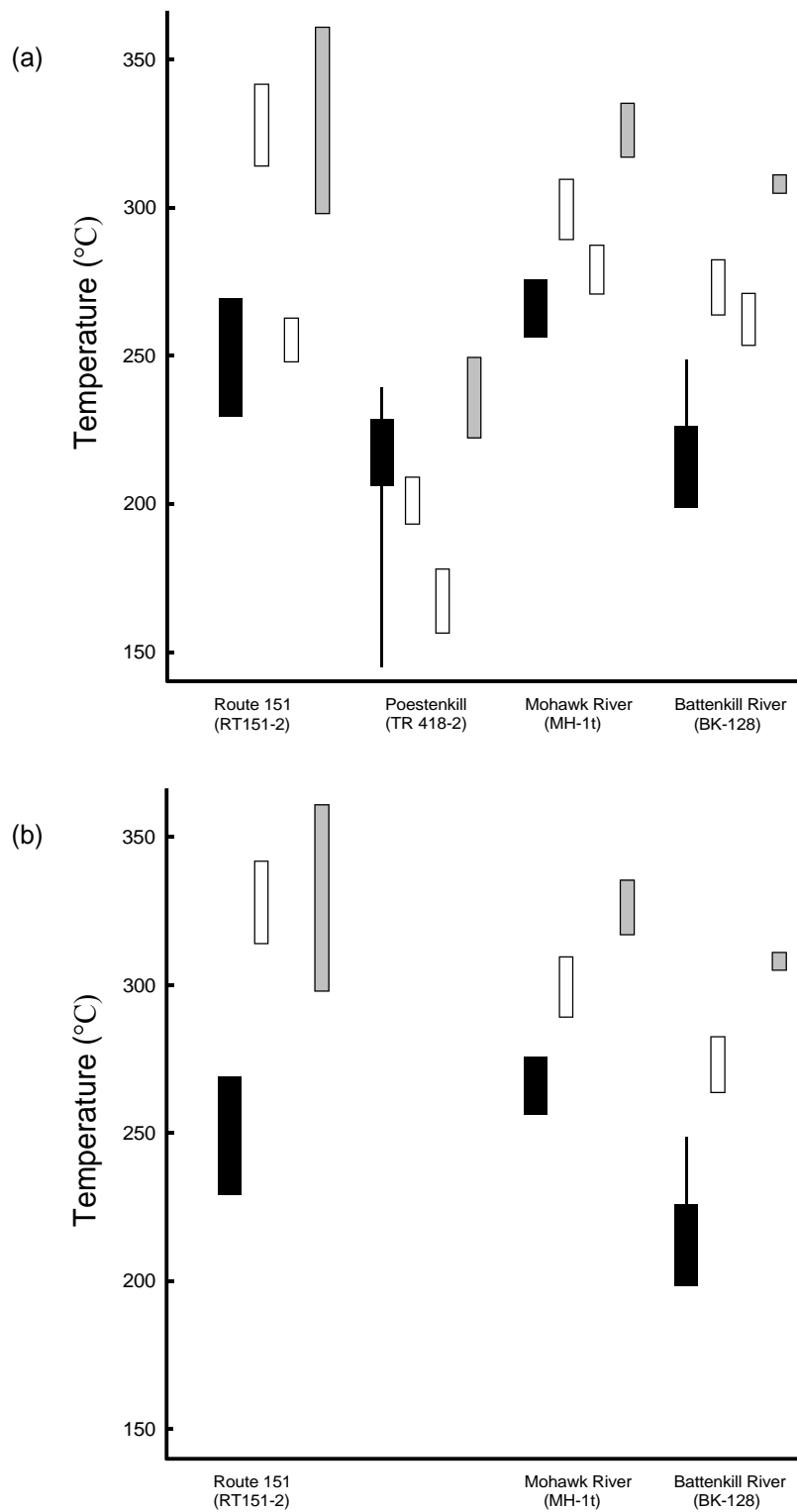


**Figure 11.** Estimations of precipitation temperatures (white and gray bars) for the four veins analyzed. (a) Presentation of all values from Table 2. (b) Preferred values (See text). White bars indicate temperature ranges based on the calibration of Sharp and Kirschner (1994), and gray bars based on that of Friedman and O'Neil (1977). Black bars and lines indicate homogenization temperatures.

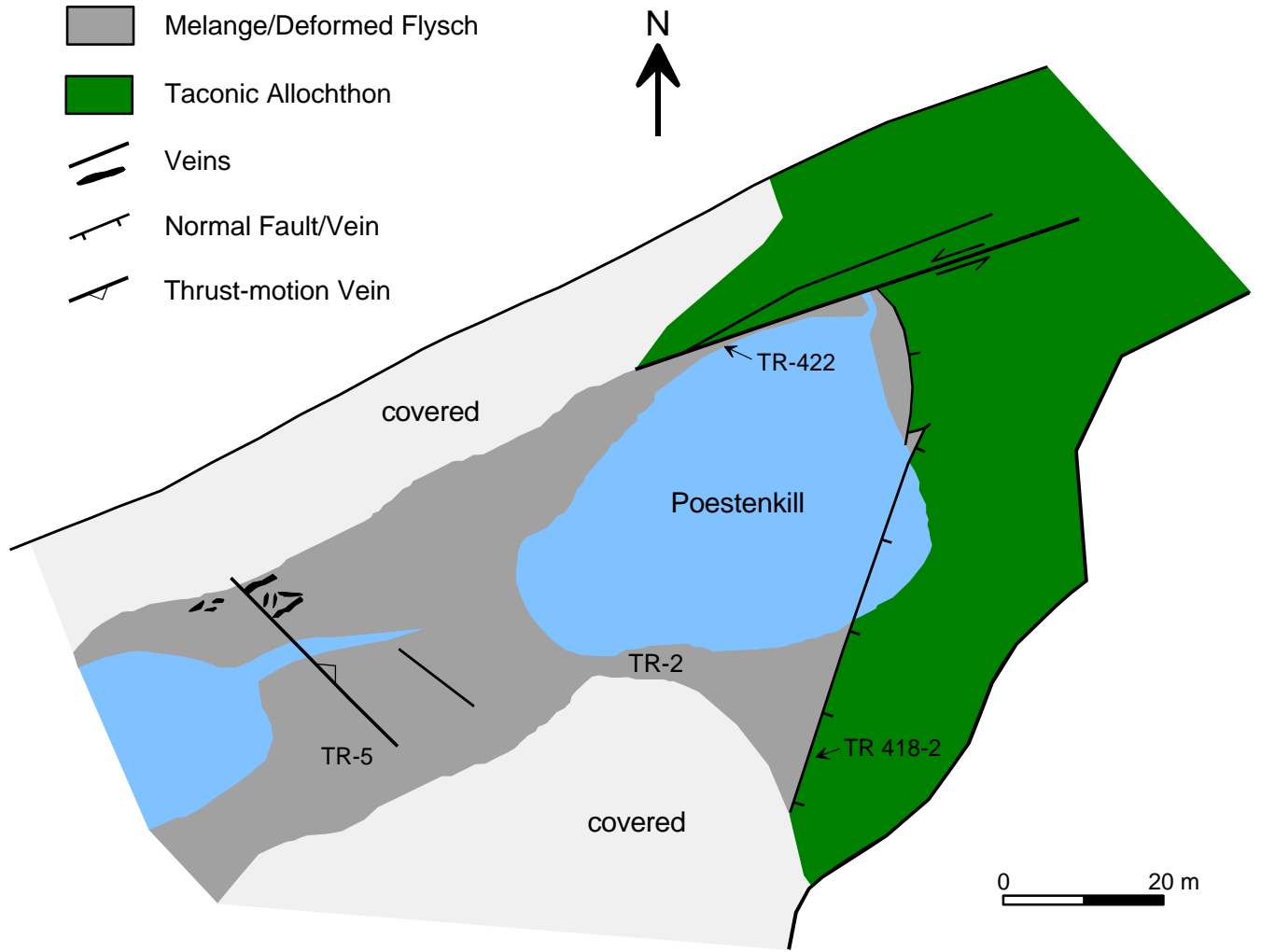


**Figure 12.** The Poestenkill Falls locality and sampling sites. Note that the normal fault along the Allochthon-melange contact is truncated by a left-lateral strike-slip fault. Map modified after Plesch (1994).

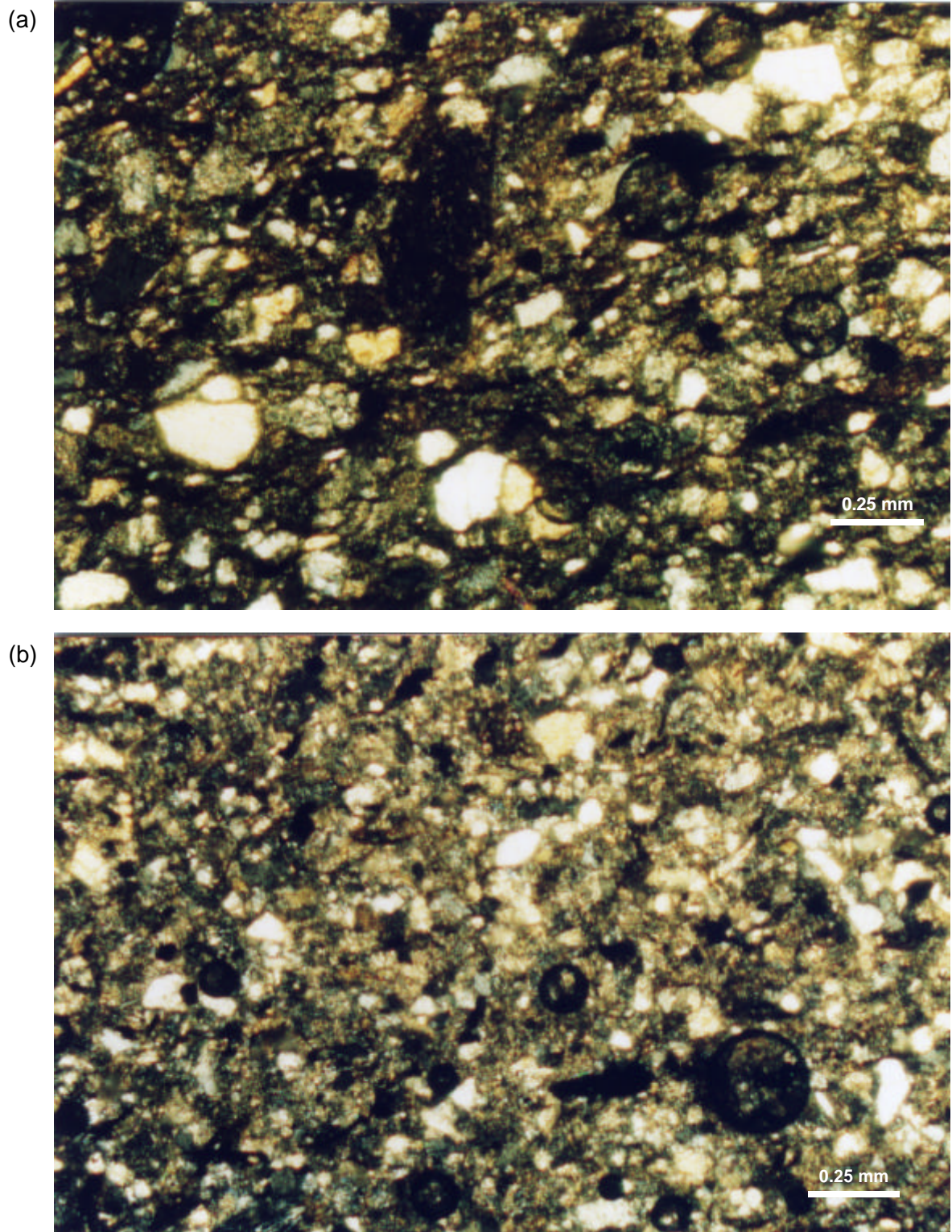


**Figure 13.** Photomicrographs of the melange. (a) shows detrital quartz, rock fragments, and altered feldspar grains, sample TR115. (b) shows the same in sample TR115-5. In both samples, a little serrulated boundary of quartz grains indicate incipient pressure solution process, but no chlorite has been found and original sedimentary texture is well preserved, indicating that both samples are from a sedimentary rock that has not experienced significant metamorphism. It is remarkable that both samples, collected only 20-30 cm away from high-temperature thrust-motion veins in the Poestenkill gorge, contain some calcite cement but no metamorphic minerals visible at this magnification.

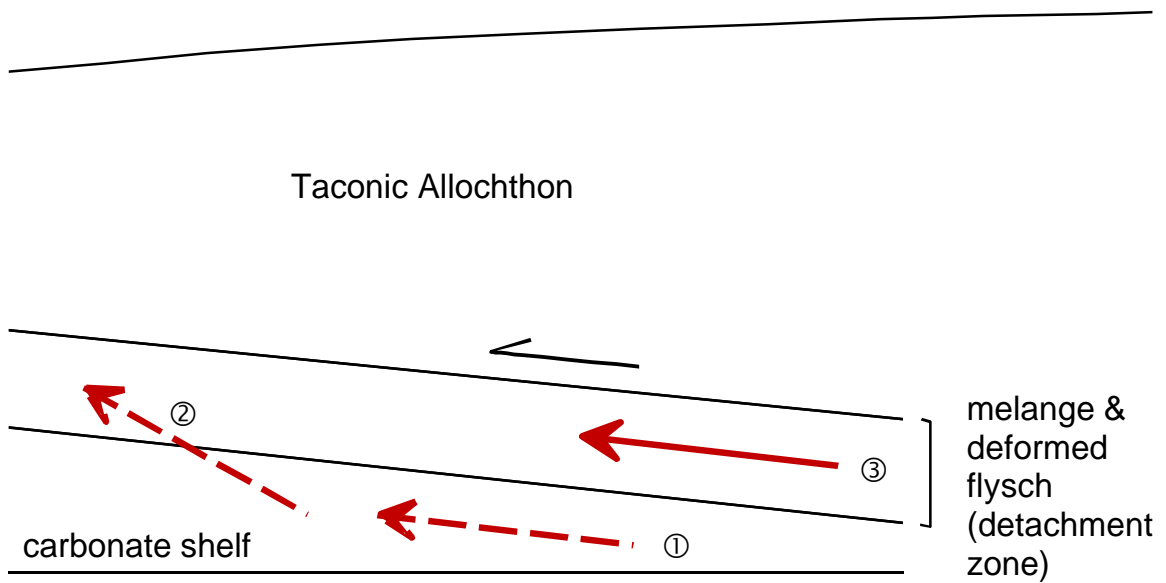


**Figure 14.** Possible pathways for the fluid flows. If the vein-forming fluids migrated through the courses ① and/or ②, they should have been buffered by the carbonate shelf sequence. If the fluids followed the path ③, they should have been buffered by the clastic sediments of melange and flysch, and would have little contact with the carbonate shelf sequence. Preferred pathway (③) shown as solid line.

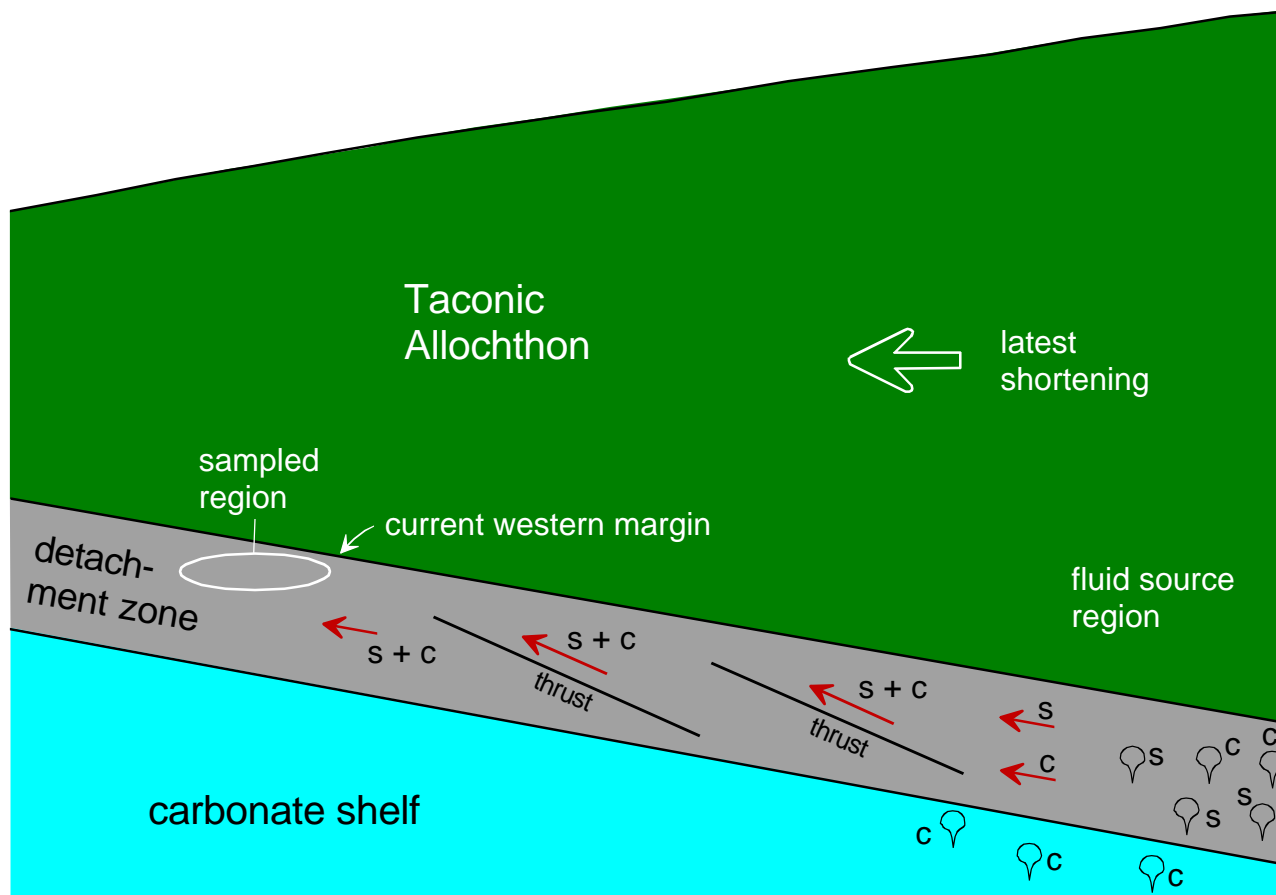


**Figure 15.** A diagram illustrating the fluid event model. In the fluid source region, metamorphic waters are expelled, with some enriched in silica (s) and some in carbonate (c). These waters are mixed and migrate rapidly toward west (red arrows) within and following the detachment zone. Thrusts and fractures created by the latest shortening provided easy pathways for the fluids. During the migration, the fluids undergo extensive interaction with the flysch and melange, a consistent lithology of wall rocks.

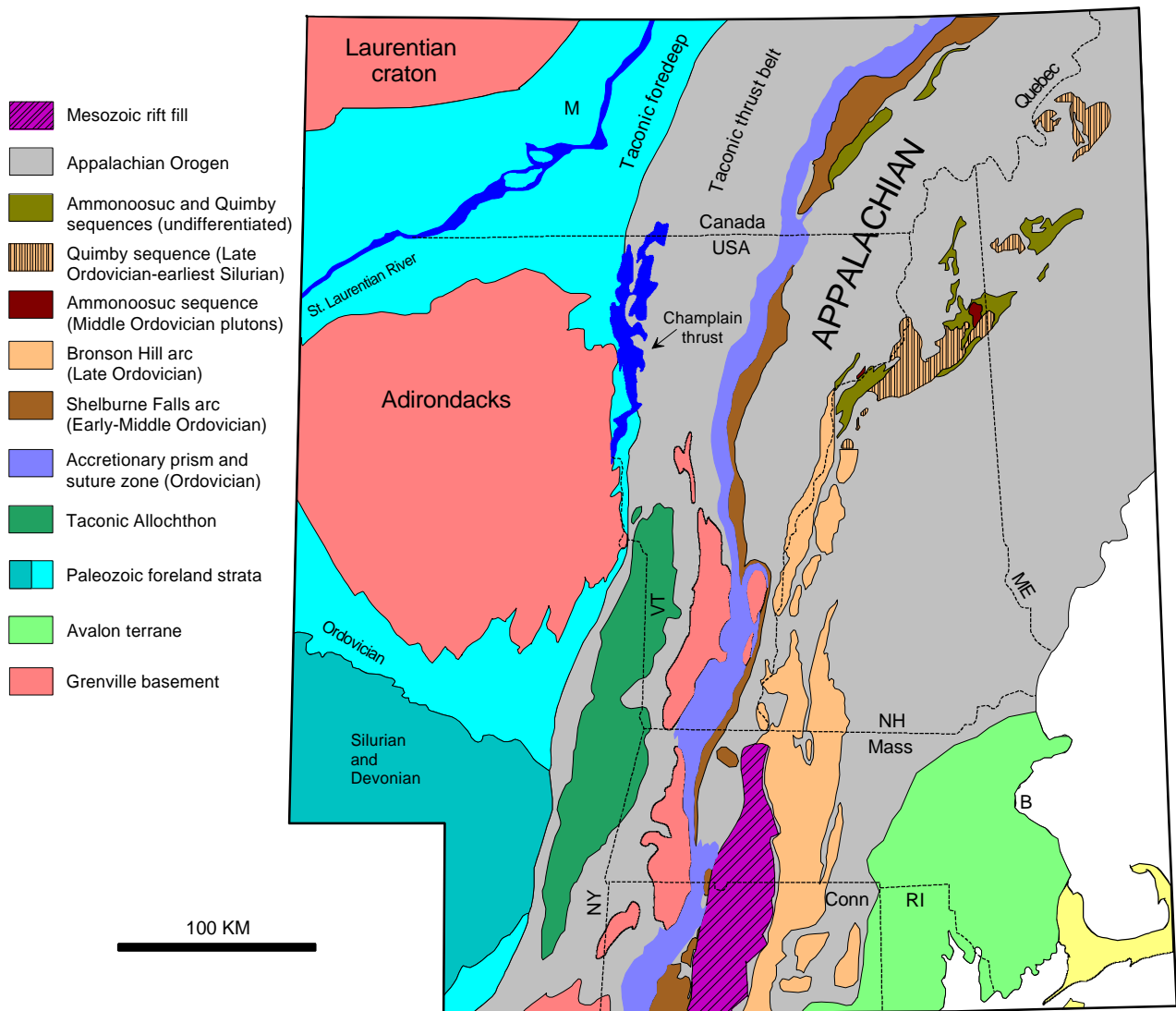
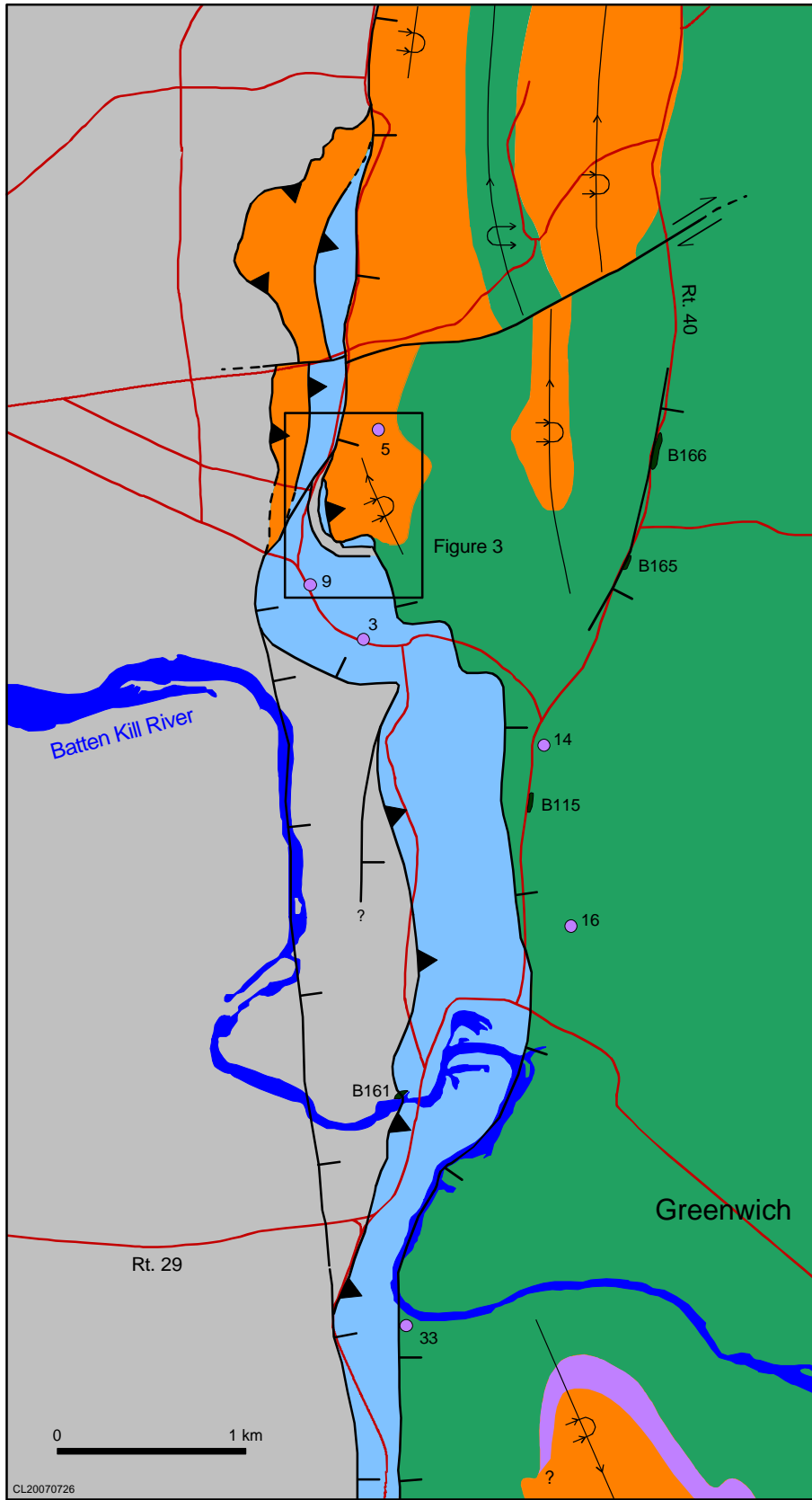


**Figure 1.** Regional geology of the Taconic orogen and foreland. The Shelburne Falls arc comprises the Barnard volcanic member, Whetstone Hill member, and Moretown member (forearc sequence) of Missisquoi Formation in US and the St. Victor Formation (forearc sequence) in Canada. The accretionary prism and suture zone comprise the Stowe Formation in US and the St. Daniel Formation in Canada. Compiled after Doll et al. (1961), Rowley and Kidd (1981), Avramtchev (1989), Karabinos et al. (1998), and Moench and Aleinikoff (2002). B: Boston, M: Montreal.



- Flysch, Melange
- Bald Mountain carbonate
- Hatch Hill
- Browns Pond
- Bomoseen
- Thrust
- Thrust (Inferred)
- Normal Fault
- well with lithic log
- B56 outcrops discussed in the text

**Figure 2.** Geologic map of the Bald Mountain region. To supplement the field data, I compiled a total of 22 well log data from archives of the New York State Department of Environmental Conservation (well completion reports from water well drillers). The anticlines/synclines are from Platt (1960) and Bosworth (1980).

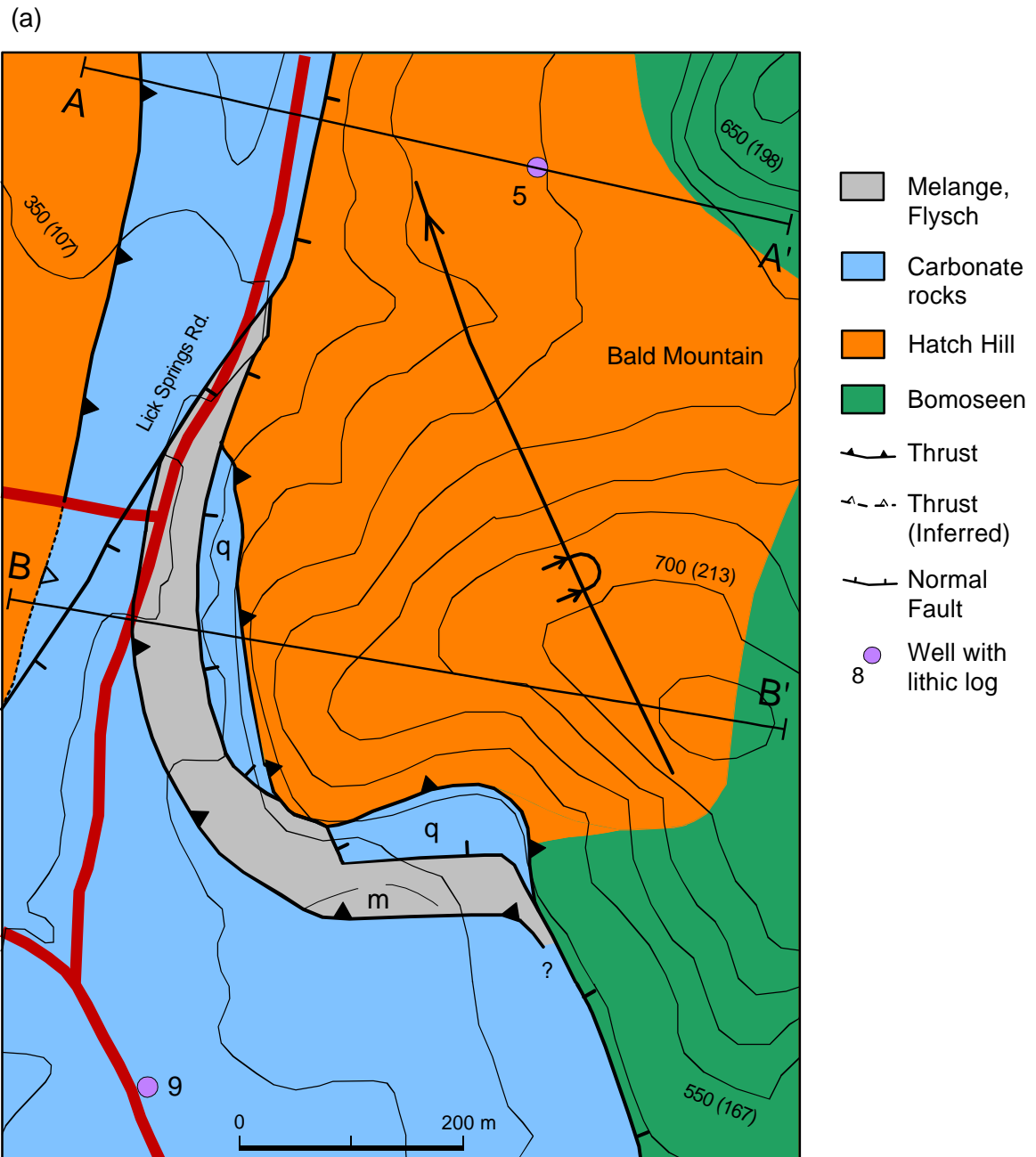


**Figure 3.** (a) Detailed geologic map around Bald Mountain showing the Taconic Allochthon (Bomoseen and Hatch Hill) and the quarry limestones (q) in contact with a "L-shaped" flysch/melange unit that overrides the carbonate slice to the west. All of them are cut by the normal faults. The southern part of the "L-shaped" flysch/melange unit is a typical melange with phacoidal cleavage, while the northern part of this L-shaped unit is the Glens Falls limestone (interbeds of limestone and shale). The elevation is shown in feet (meter). m: melange outcrop where veins were measured (See Figure 7a), q: Bald Mountain quarry.

(b)

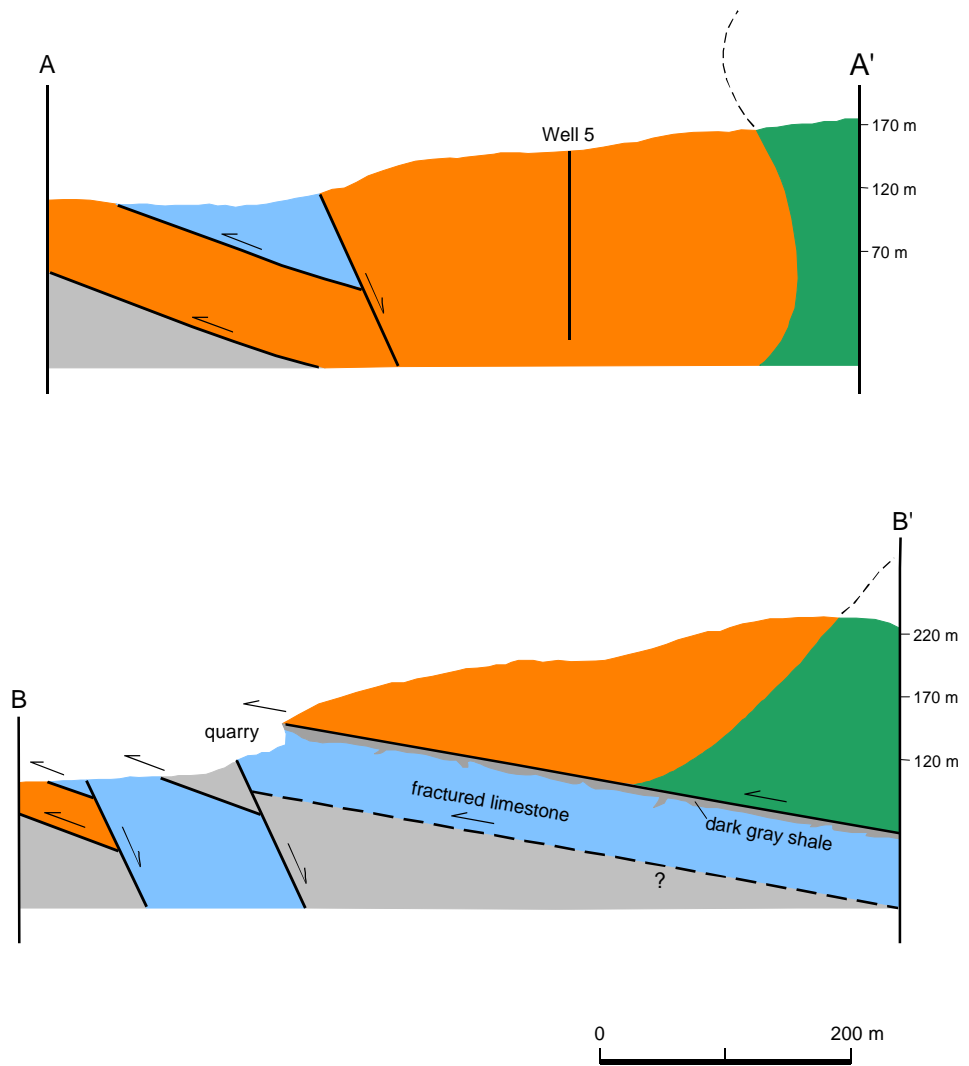


**Figure 3** (continued), (b) Cross sections A-A' and B-B' showing the folded Allochthon that thrust westward and was later cut by the normal fault.

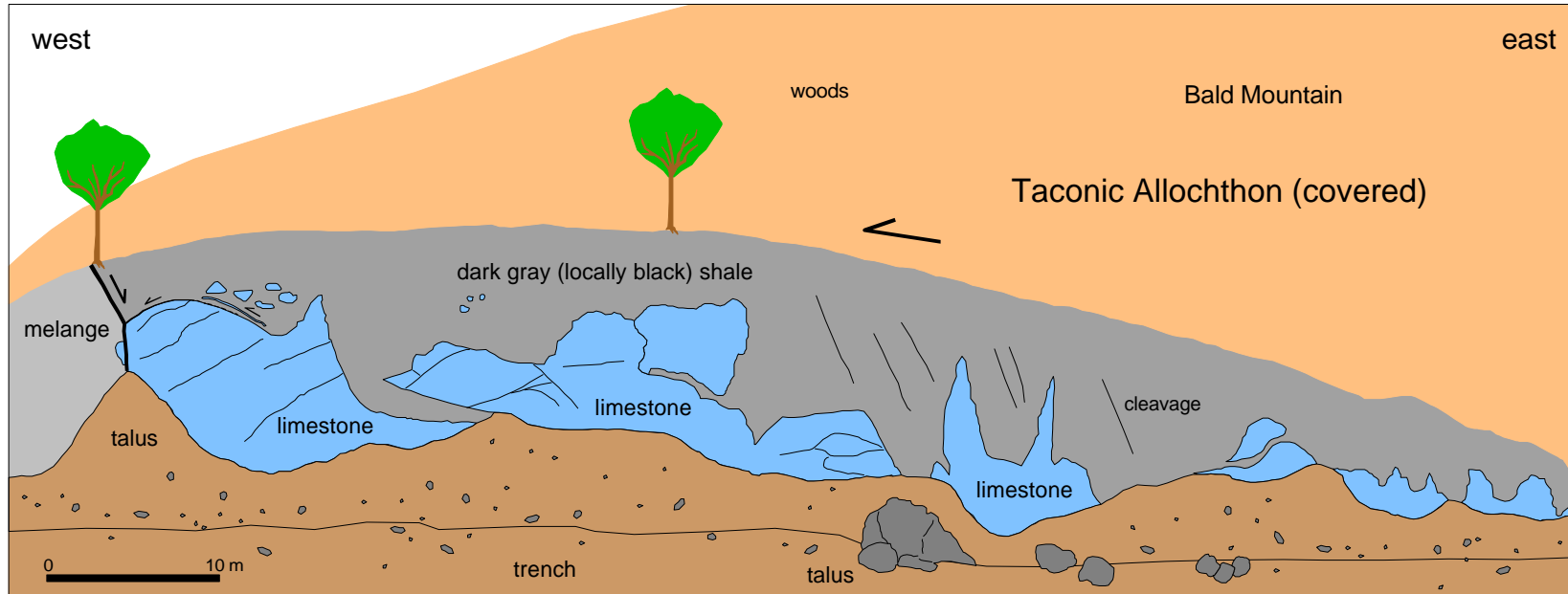


**Figure 4.** Sketch of the southern quarry in Bald Mountain. View is to the north. Fragmented limestones of various sizes and shapes (even a thin layer near the western end of the quarry) are progressively incorporated into the overlying shale. At the western corner of the quarry, the dark gray shale is thrust over the limestone, and the thrust and both rocks are cut by a normal fault (See Figure 9a for photograph). The large limestone pieces are severely fractured, from overthrusting of the Taconic Allochthon. This fracturing caused the rugged top of the limestones, some with saw-teeth-like shapes (See Figures 5 and 6).

(a)



**Figure 5.** (a) Top of the limestone in the southern quarry with saw-teeth-like shape. The narrow and tapering limestones protrude into the overlying shale, and cleavage is well developed between the limestone teeth, generally parallel with the cleavage in the shale. Hammer for scale in white circle.

(b)



**Figure 5** (continued), (b) A close view of small limestone teeth. The shale was squeezed into the space between the teeth during the overthrusting. Hammer for scale near lower edge of photograph.

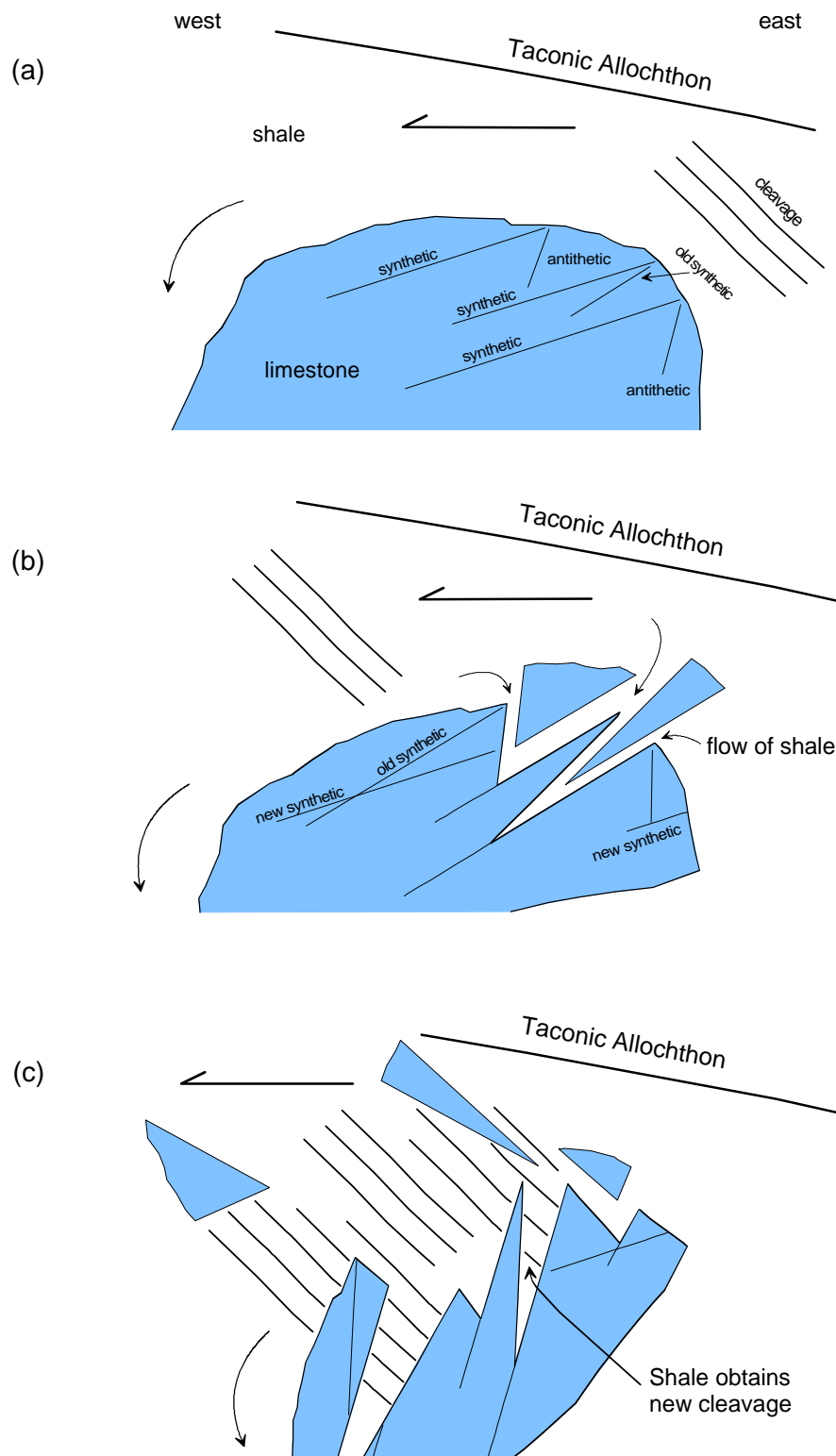


**Figure 6.** Diagram showing a development process of the saw-teeth-like shape of the limestones. (a) Synthetic and antithetic fractures form in response to the shortening. (b) New fractures form as the limestone rotates and fragments begin to separate, driven by flow of the surrounding shale, some of which is squeezed into the fracture openings. (c) The fragments are incorporated within the shale as inclusions and new cleavage is developed in the shale between the "teeth."

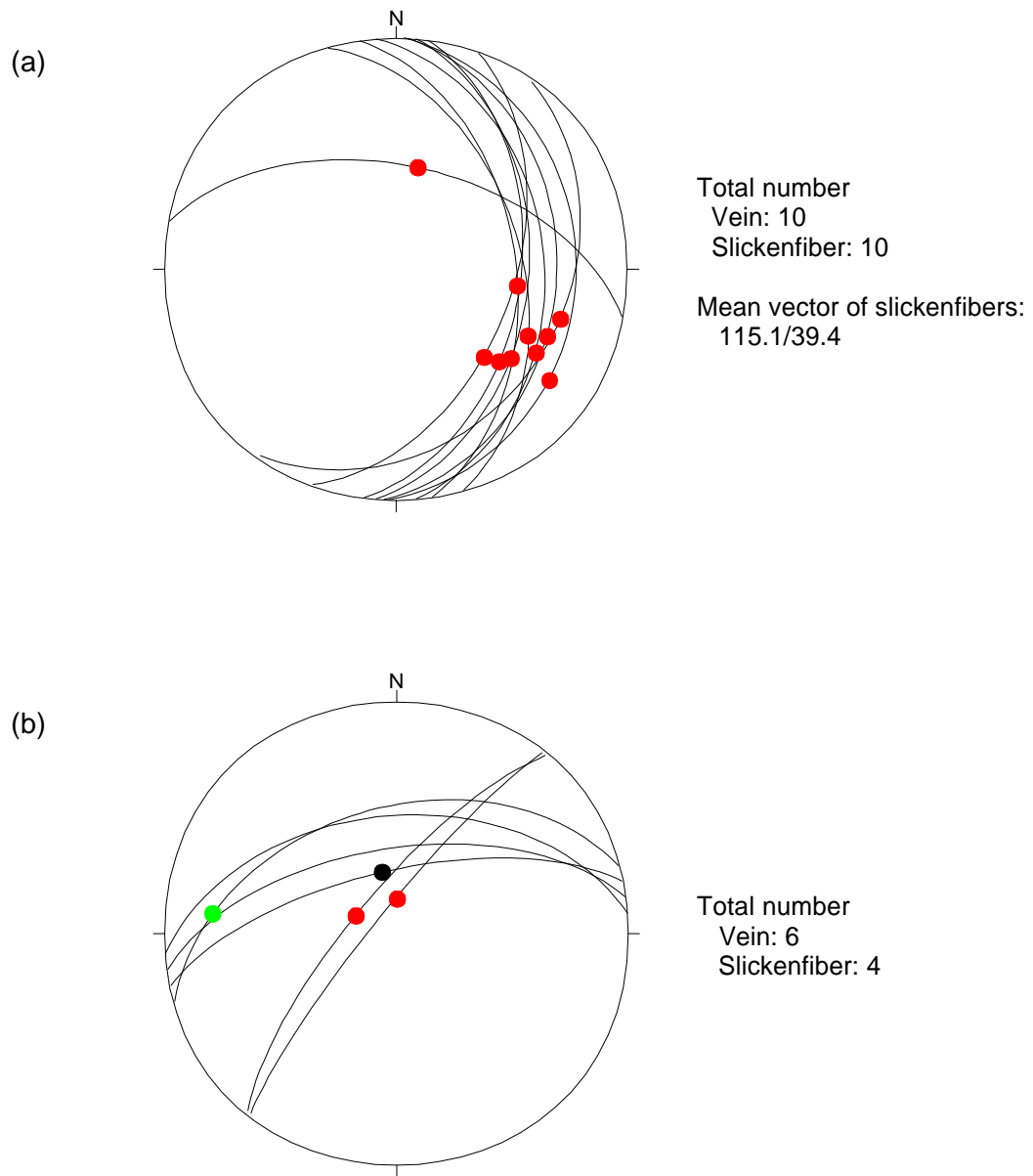


**Figure 7.** Orientations of the veins and slickenfibers (a) in the melange wall ("m" in Fig. 3a) standing across a trench south of the southern quarry in the foot of Bald Mountain, and (b) in the southern quarry. The colors of dots indicate slip sense determined from field and microscope observations (See text). red: reverse, green: normal, black: not clear. Equal area projections.



**Figure 8.** Photograph illustrating the quartz-calcite veins in the southern quarry and their relationship with carbonate blocks. The veins formed along surfaces of carbonate blocks or in the shale between the blocks.

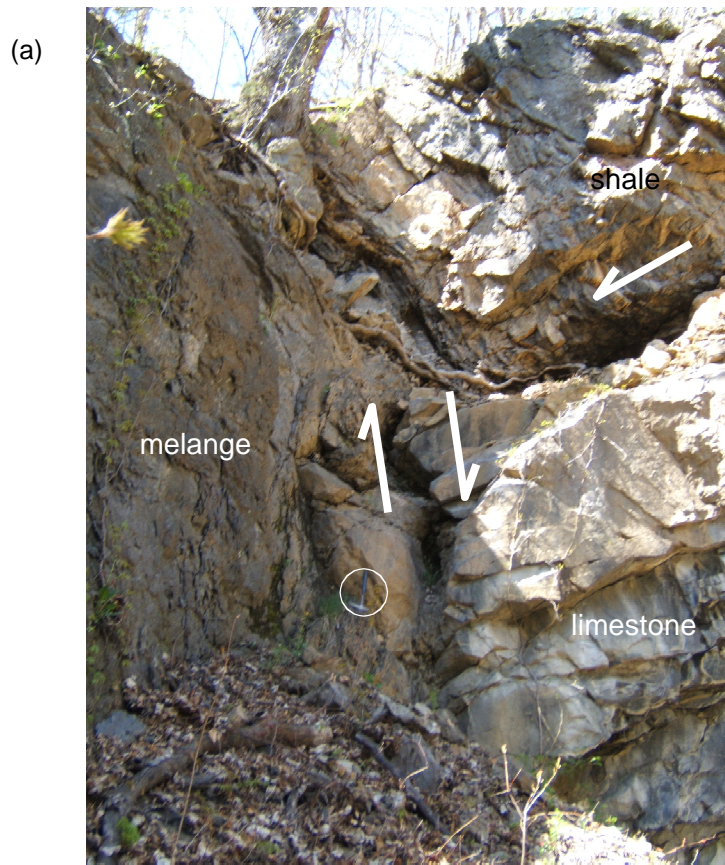


**Figure 9.** (a) A normal fault exposed in the southern quarry of Bald Mountain. View is toward north. Hammer for scale in white circle. (b) Exposure of the western bounding fault of the Allochthon in the Poestenkill gorge in Troy (white arrows). View is to the southeast. Black scale bar on the left is 1 m long.

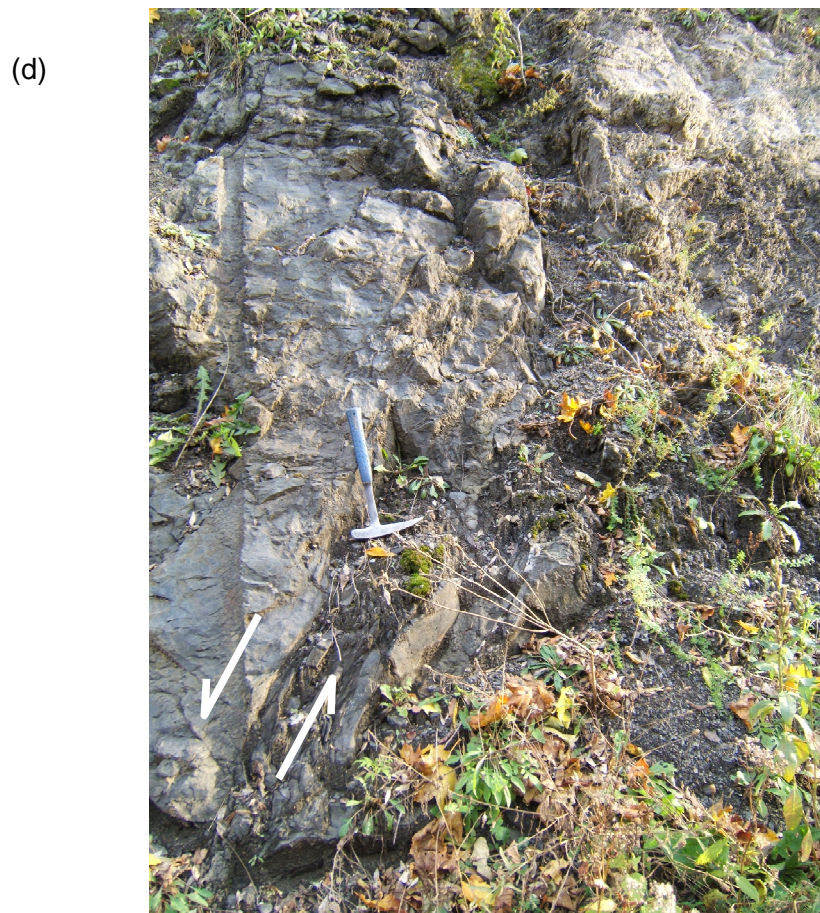
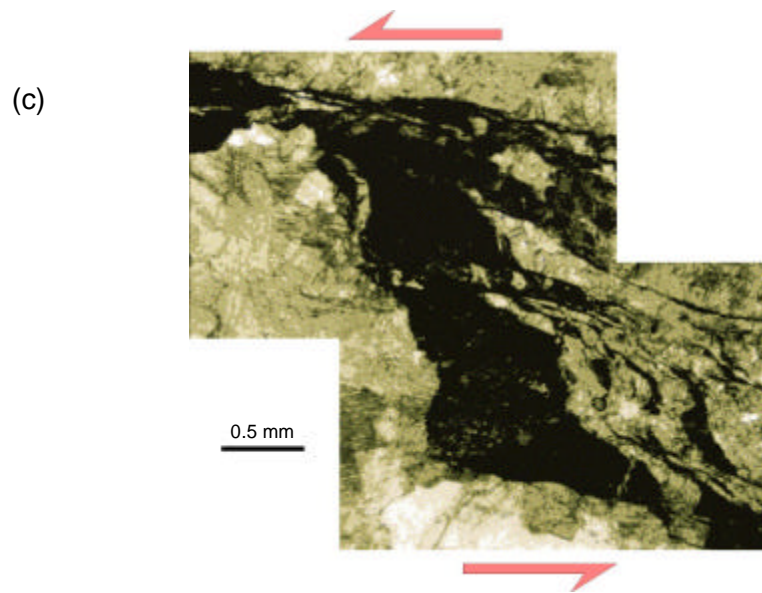


**Figure 9** (continued), (c) Photomicrograph of a vein developed along part of the bounding fault in (b). Host rock inclusions in the vein are deformed in sinistral sense, consistent with the normal slip. View is to the south. (d) The western bounding fault exposed in the Route 9G roadcut near Mount Merino. View is toward south.

(a)



(b)

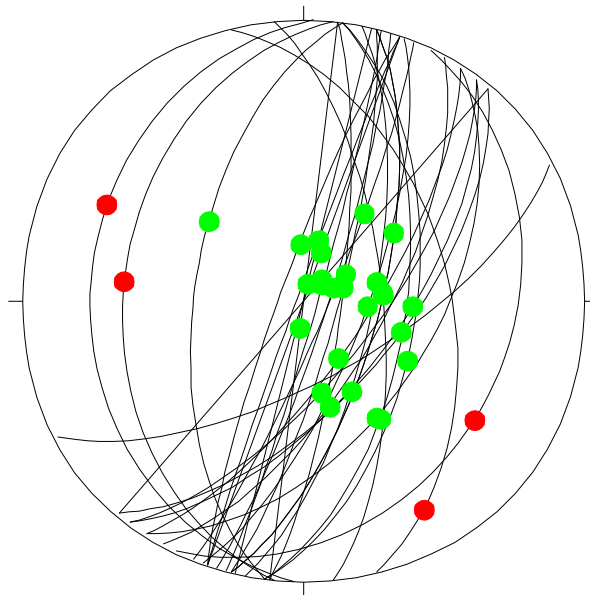


**Figure 10.** Normal faults observed along Route 40. (a) Photograph of an overhanging fault surface exposed in the Bomoseen Formation at the western edge of the Taconic Allochthon north of Middle Falls (B115 in Figure 2). View is to the east. Steps on the quartz vein clearly indicate that this hanging wall moved down. (b) A stereogram showing orientations of faults or veins and striations or slickenfibers on them, measured in the outcrop of (a) and B165 and B166 in Figure 2. They show mostly east-down slip (green dots) and some of them east-up movement (red dots). All veins consist of quartz in those outcrops. 30 measurements for each planar and linear fabrics.

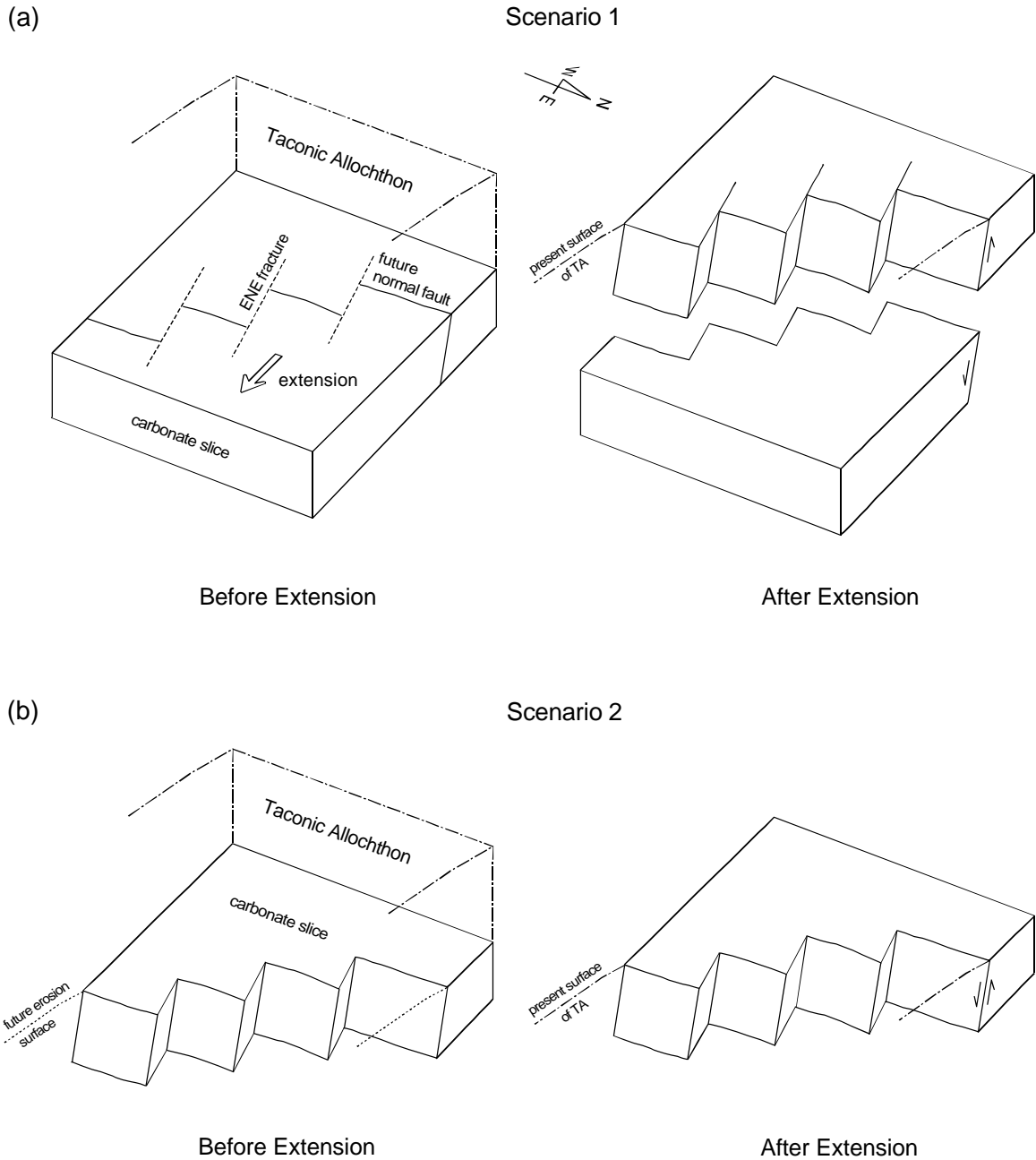


**Figure 11.** Diagrams illustrating possible scenarios of how the zigzag fault between the Taconic Allochthon and the carbonate slice formed. In (a), the carbonate slice broke up along the left-stepping normal faults connected by the ENE fractures, when the Allochthon extended during the later part of the Taconic orogeny. In this scenario, the western half of the carbonate slice is exposed and there must be the eastern half beneath the Allochthon. In (b), the carbonate slice was already in zigzag shape when it reached the current western margin of the Taconic orogen. In this scenario, the Allochthon simply moved down along the zigzag-shaped eastern margin of the carbonate slice during the extension.



**Figure 12.** Western margin of the carbonate slice exposed in the bank of Battenkill River (B161 in Figure 2). Here, the limestone sheet is thrust over the melange. View is to the north.

(a)



(b)

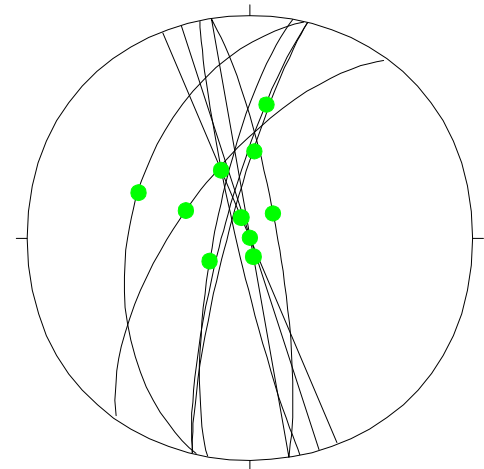


**Figure 13.** The western margin of the carbonate slice exposed along Route 40. (a) A fault surface in a large limestone roadcut about 2.5 km south of the map area in Figure 2. View is toward east. The steps of veins indicate that the east side of this fault moved down. All veins consist of calcite. (b) A stereogram showing orientations of veins or faults and slickenfibers or striations on them, measured in the western margin of the carbonate slice (the roadcut of (a) and an outcrop about 1 km north of it along Route 40). The green dots indicate east-down sense of slip. 10 measurements for each planar and linear fabrics. Equal area projection.

(a)

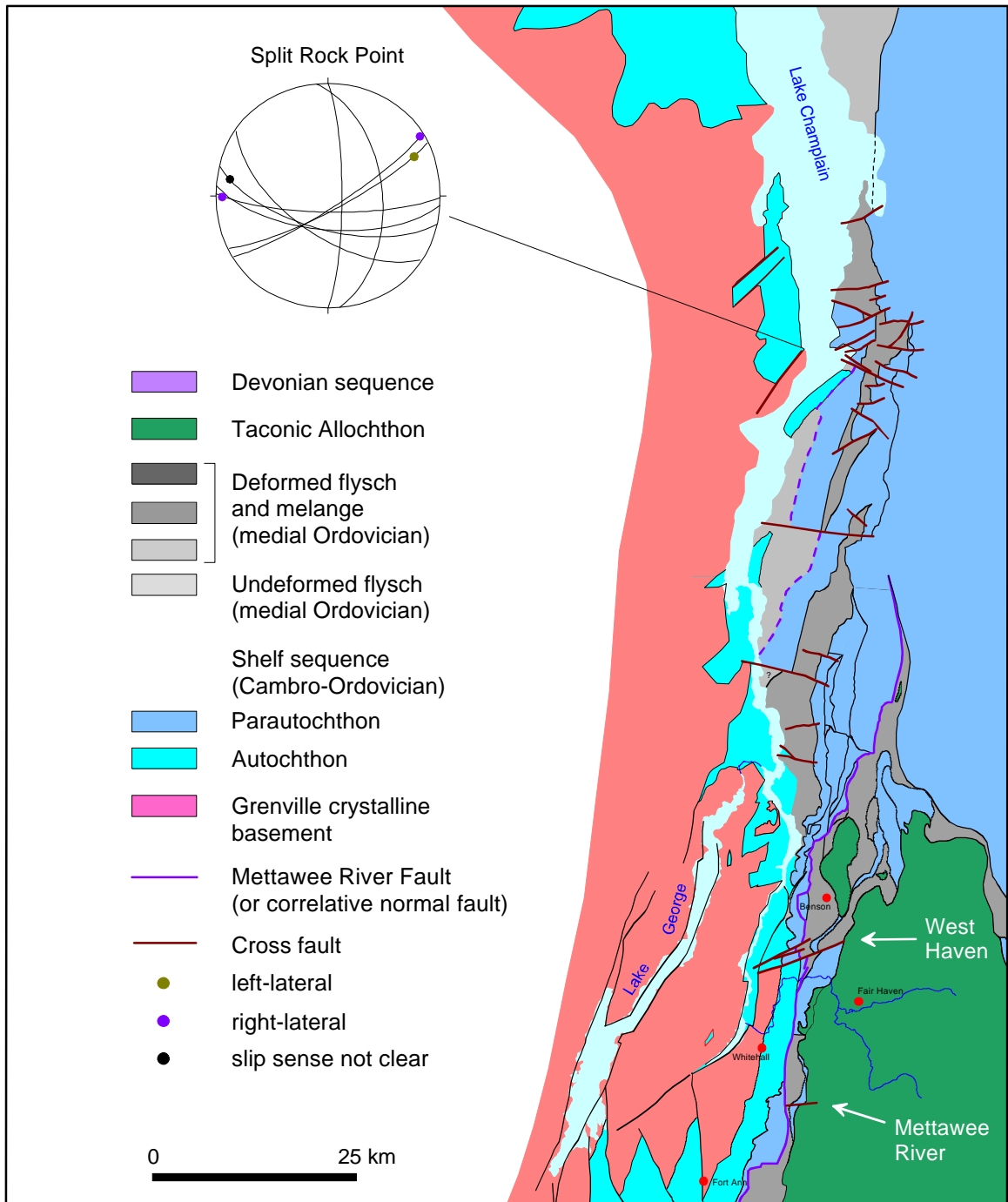


**Figure 14.** A geologic map of the Taconic orogen and foreland showing distribution and orientations of strike-slip cross faults of substantial size (mapped) or of outcrop-scale (stereogram). (a) A northern map. Compiled after Welby (1961), Isachsen and Fisher (1970), and Hayman and Kidd (2002a).

(b)

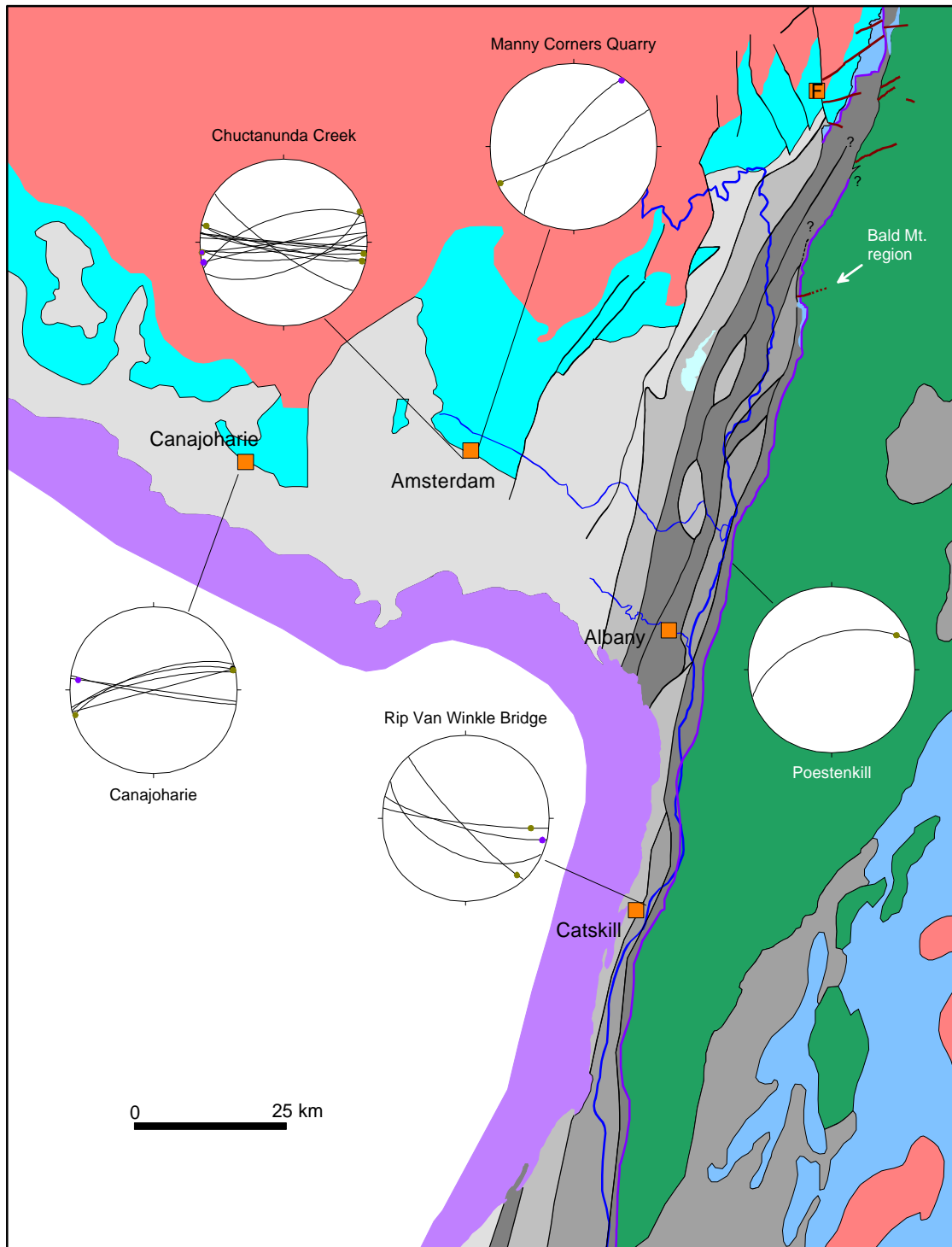


**Figure 14** (continued), (b) A geologic map of the Taconic orogen and foreland showing distribution and orientations of strike-slip cross faults. A southern map. Compiled after Fisher et al. (1970), Isachsen and Fisher (1970), W. Shaw (unpublished map), Plesch (1994), and Hayman and Kidd (2002a). The "F" in small square is Fort Ann. Legend same as Fig. 14a is used.

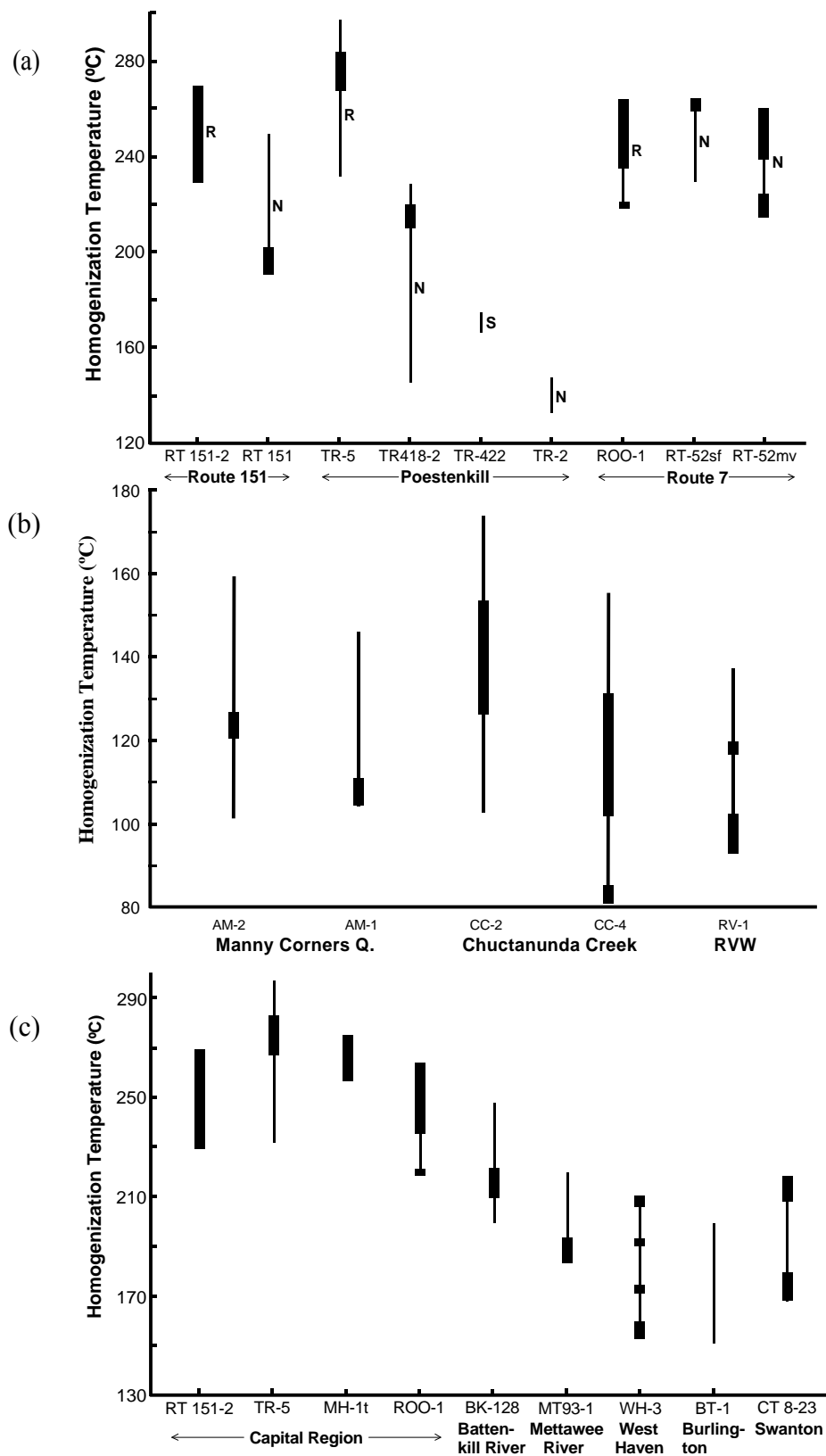


**Figure 15.** Homogenization temperatures of aqueous fluid inclusions in veins. (a) Measurements from veins with slip senses of; reverse (R), normal (N), and left-lateral strike-slip (S). Note that the temperature range of strike-slip vein (TR-422) is lower than the major temperature range (thicker line) of a normal-motion vein (TR418-2) but higher than another normal-motion vein (TR-2) in the same locality (Poestenkill). Data from PART I. (b) Measurements from 5 more strike-slip veins. RVW: Rip Van Winkle Bridge. Data from PART II. (c) Along-strike variation of the temperatures of reverse-motion veins, from south (RT151-2) to north (CT8-23). Data from PART I. See Figure 1 of PART I for locations.

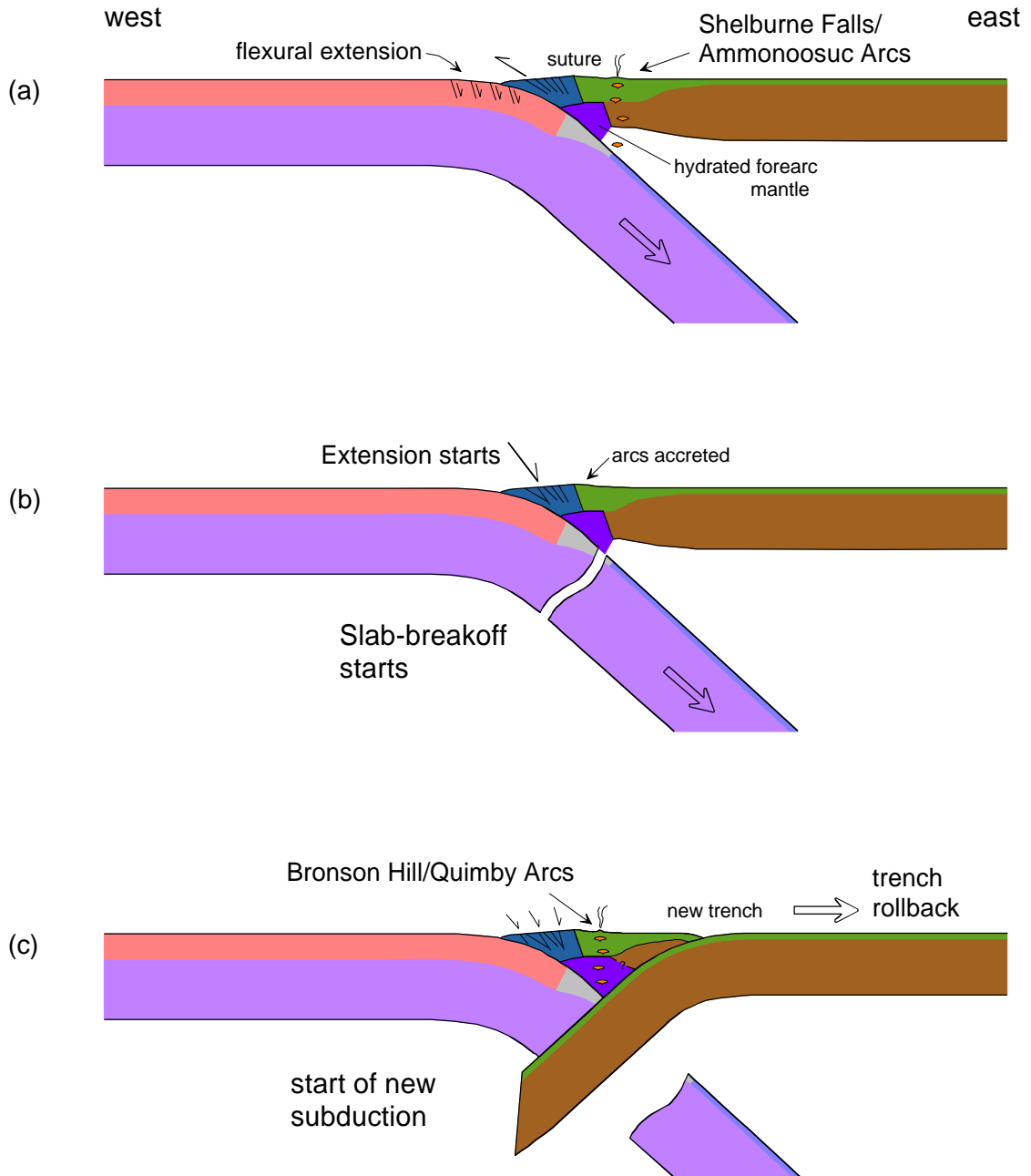


**Figure 16.** Schematic diagrams illustrating evolution of the Taconic orogen in association with plate interactions during the Late Ordovician through the earliest Silurian. (a) An early stage of the arc-continent collision. Regional stress field was compressional. However, normal faulting occurred in the foreland by down bending of the crust (Bradley and Kidd, 1991). (b) Late stage of the collision. The slab started to undergo breakoff. The stress field began to switch from compressional to tensional where the slab was broken off, and regional extension started. The broken off slab sank into the mantle. (c) Initiation of a westward subduction to accommodate the plate convergence. An Andean-type continental margin was developed, and younger arc magmatism was active until the earliest Silurian. This new subduction could have involved a trench rollback. In all diagrams, the structure of forearc follows Hyndman et al. (2005).

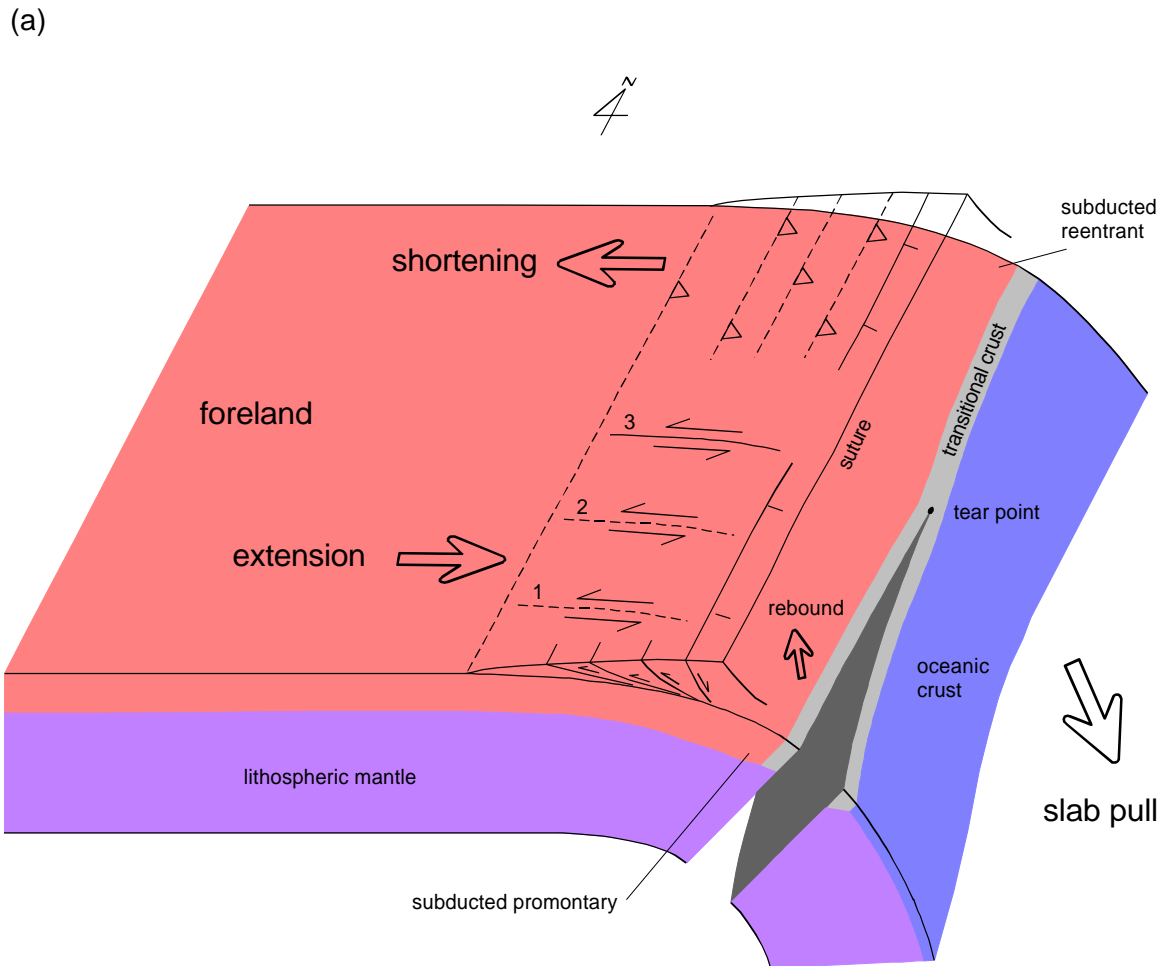


**Figure 17.** Diagrams illustrating the slab breakoff that started in the south (at the New York promontory) and propagated to the north toward the Quebec reentrant. The accretionary complex is shown transparent to illuminate the breakoff process. Active cross faults at this snapshot are shown by solid line, and inactive (older) cross faults by dashed lines. The diagram (a) shows development of left-lateral cross faults which are required to reconcile the coexisting shortening and extension in a region located up-dip of the tear point. The left-lateral cross faults form in the order 1, 2, and 3 as the tear point migrated northward. In this model, both the shortening and extension rates are assumed to be constant, and the right-lateral cross faults cannot form.

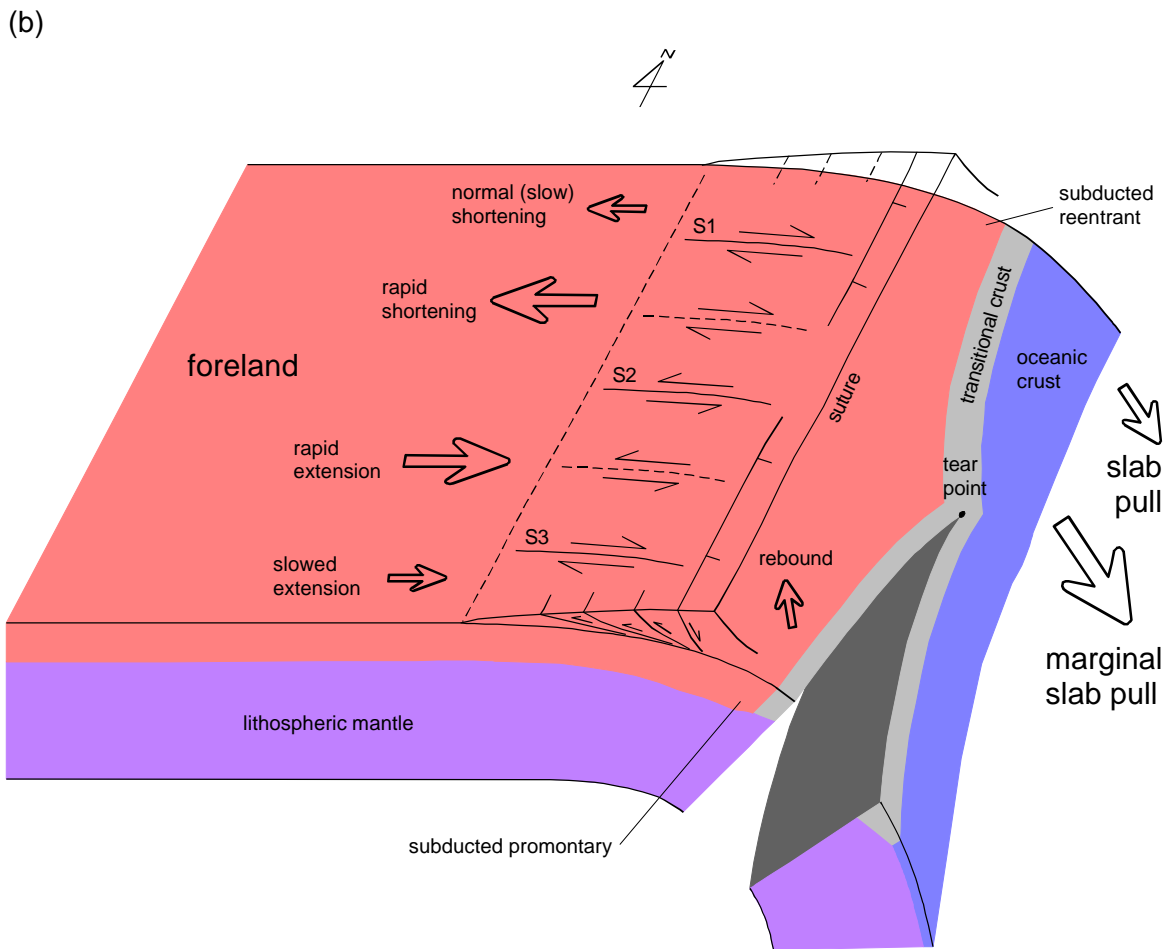


**Figure 17** (continued), (b) A diagram showing an effect of the marginal slab pull. During propagation of the slab breakoff in the untorn part, the slab pull suddenly increases as the tear point approaches, because of the dangling partly-broken-off slab. In the untorn part, the shortening rate suddenly increases as the tear point approaches, which results in a right-lateral cross fault (S1). To the south, left-lateral cross fault (S2) forms above the tear point in the same way shown in Fig. 17a. Farther to the south, another right-lateral cross fault (S3) forms if the extension rate decreases rapidly with time following passage of the tear point. In both (a) and (b), the slab is shown to breakup at right angle (symmetrically) through its whole thickness for illustration purpose, but it could occur asymmetrically along a plane tilted relative to top and bottom of the lithosphere if the breakoff process is similar with rifting.

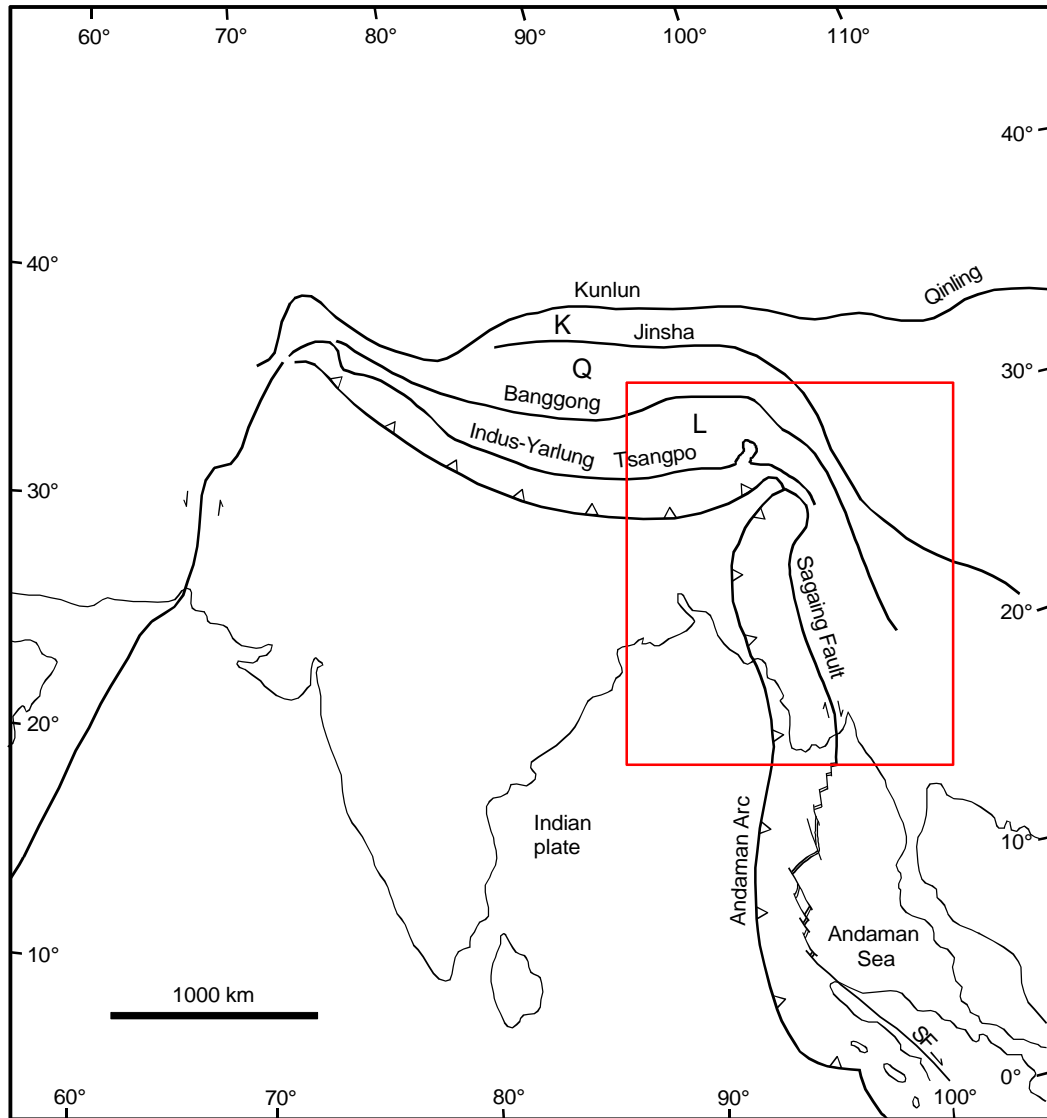


**Figure 1.** Distribution of major suture zones and structures in the India-Asia collision zone. The red box is an area shown in Figure 2. L: Lhasa Terrane, Q: Qiangtang Terrane, K: Kunlun Terrane, SF: Sumatra Fault. Modified after Curray et al. (1979), Dewey et al. (1988), and Guzman-Speziale and Ni (1996).

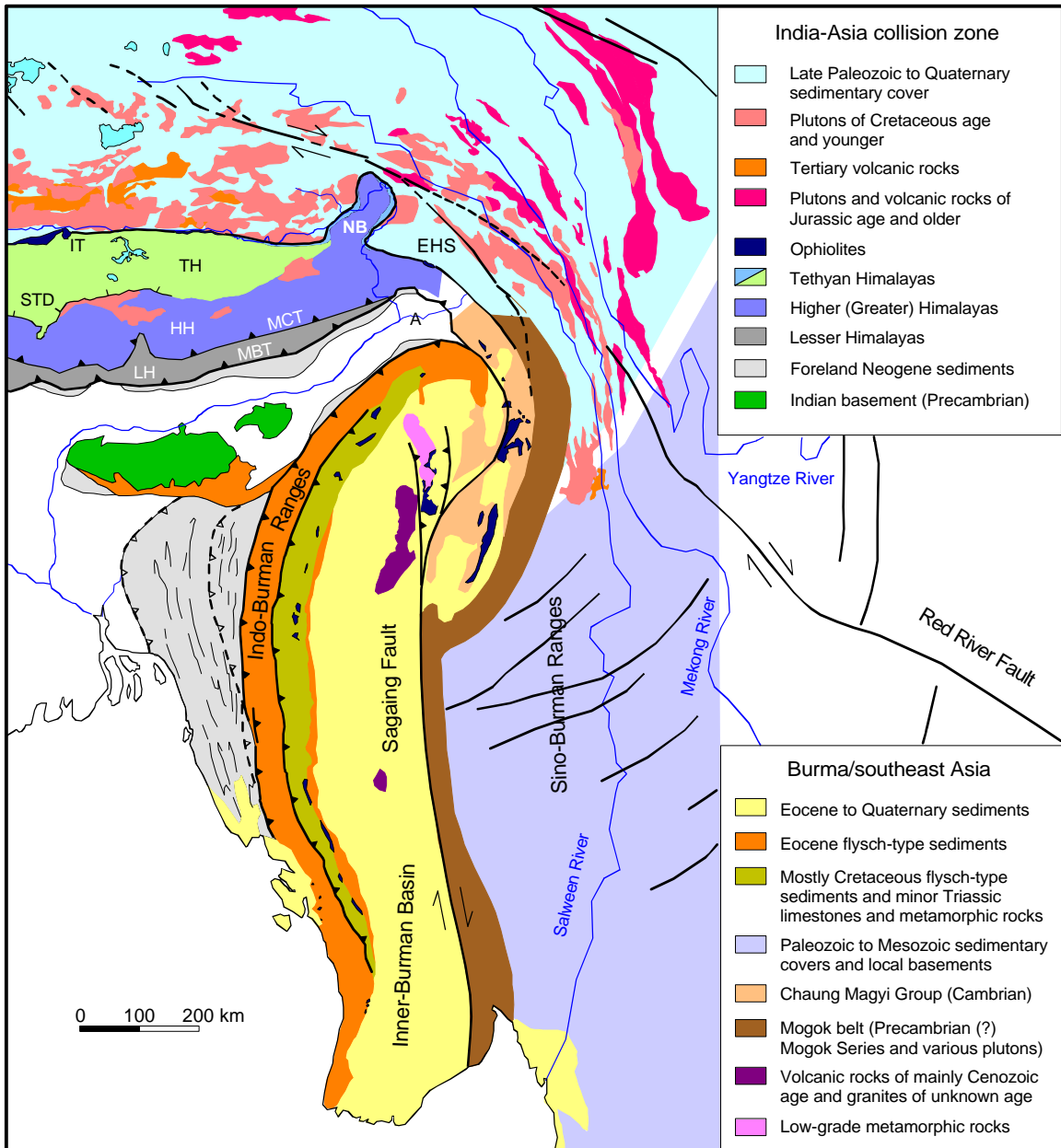


**Figure 2.** Location of the eastern Himalayan syntaxis and its regional relationships to the eastern Himalayas/Tibet, the Assam region, Burma, and western Indochina. EHS: Eastern Himalayan syntaxis, NB: Namche Barwa massif, IT: Indus-Tsangpo suture, TH: Tethyan Himalayas, HH: Higher Himalayas, LH: Lesser Himalayas, MBT: Main Boundary Thrust, MCT: Main Central Thrust, STD: South Tibetan detachment system, A: Assam, Compiled from Bender (1983), Armijo et al. (1989), Burchfiel et al. (1992), Mitchell (1993), Wang and Burchfiel (2000), Luo et al. (2004), and Schoenbohm et al. (2006).

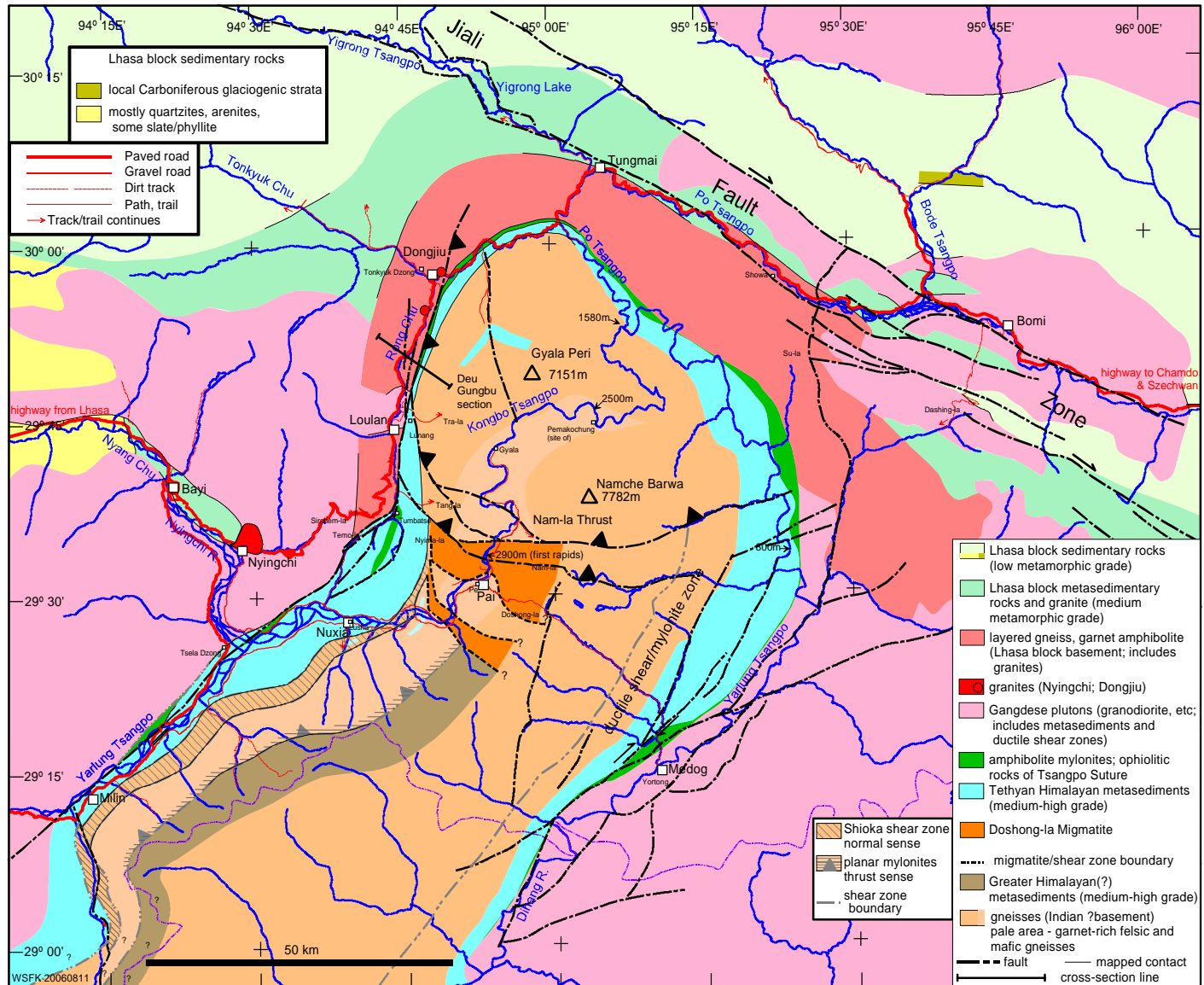


**Figure 3.** Geologic map compiled by W. S. F. Kidd from field observations of this project, and previous works of Burg et al. (1997), and Geng et al. (2006).

(a)



(b)

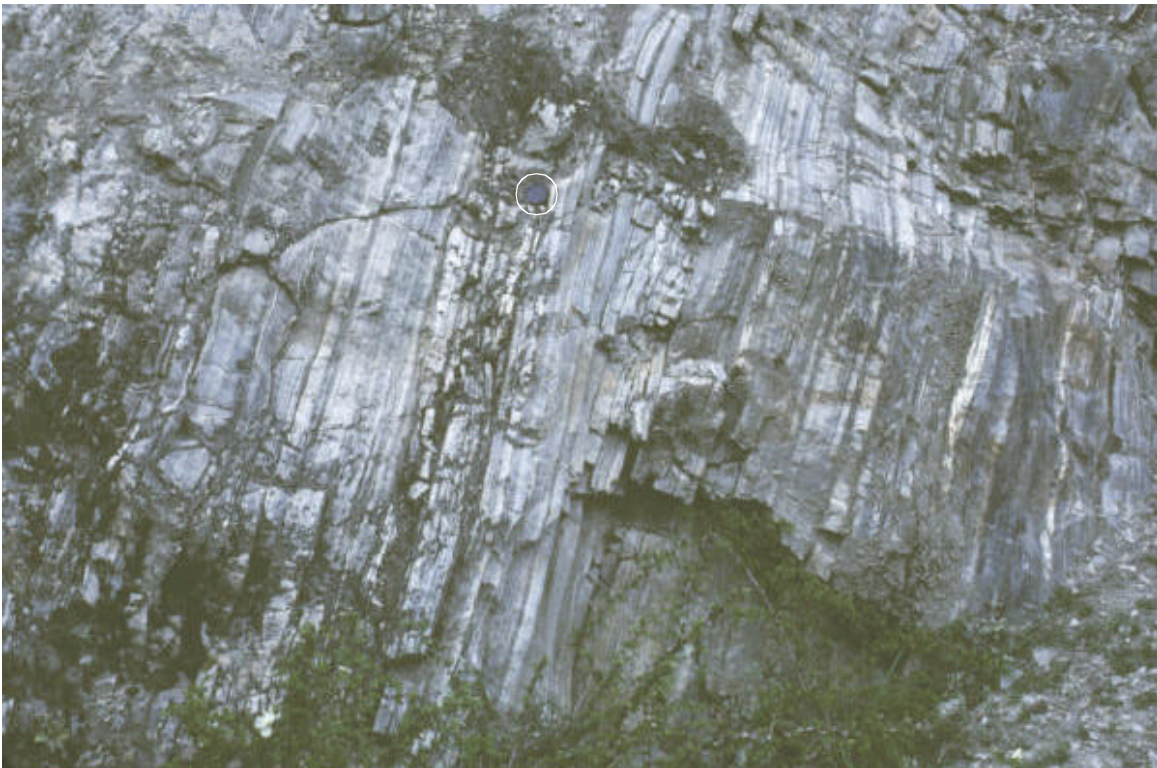


**Figure 4.** The Tethyan Himalaya metasedimentary sequences exposed along a road along the north bank of Yarlung-Tsangpo River across from Nuxia. (a) View of the Yarlung-Tsangpo River and roadcuts of the Tethyan sequences. outcrop no. 03 (2002). (b) A roadcut consisting of mylonitic quartzites and thin pelitic layers. A camera cap for scale in the circle. outcrop no. 03 (2002).

(c)



**Figure 4** (continued), (c) A roadcut in the Yarlung-Tsangpo River section. It shows a part of the Tethyan sequences mostly consisting of quartzite mylonites and thin intercalations of metapelites. A camera cap for scale in the circle. All photographs by W. S. F. Kidd.



**Figure 5.** The garnet-rich pelitic gneiss. Many large garnets are densely distributed. One large feldspar porphyroclast is seen near the center. This rock is also highly strained. Southeast bank of Tsangpo River near outcrop no: 30 (2003). Photograph by W. S. F. Kidd.

(a)



(b)



**Figure 6.** The Shioka shear zone. (a) Overview from the northeast wall of the Shioka valley. View is to the northeast. outcrop no: 55 (2005), (b) Highly strained, porphyroclastic gneisses of outcrop 55 (2005). Note the planar foliation. Lineations are oriented oblique to this page. View is toward north.

(c)



**Figure 6** (continued), (c) Highly-strained porphyroclastic feldspathic gneiss in outcrop 55 (2005). Sigma-type feldspar porphyroclasts indicate apparent sinistral sense of shear. All photographs by W. S. F. Kidd.

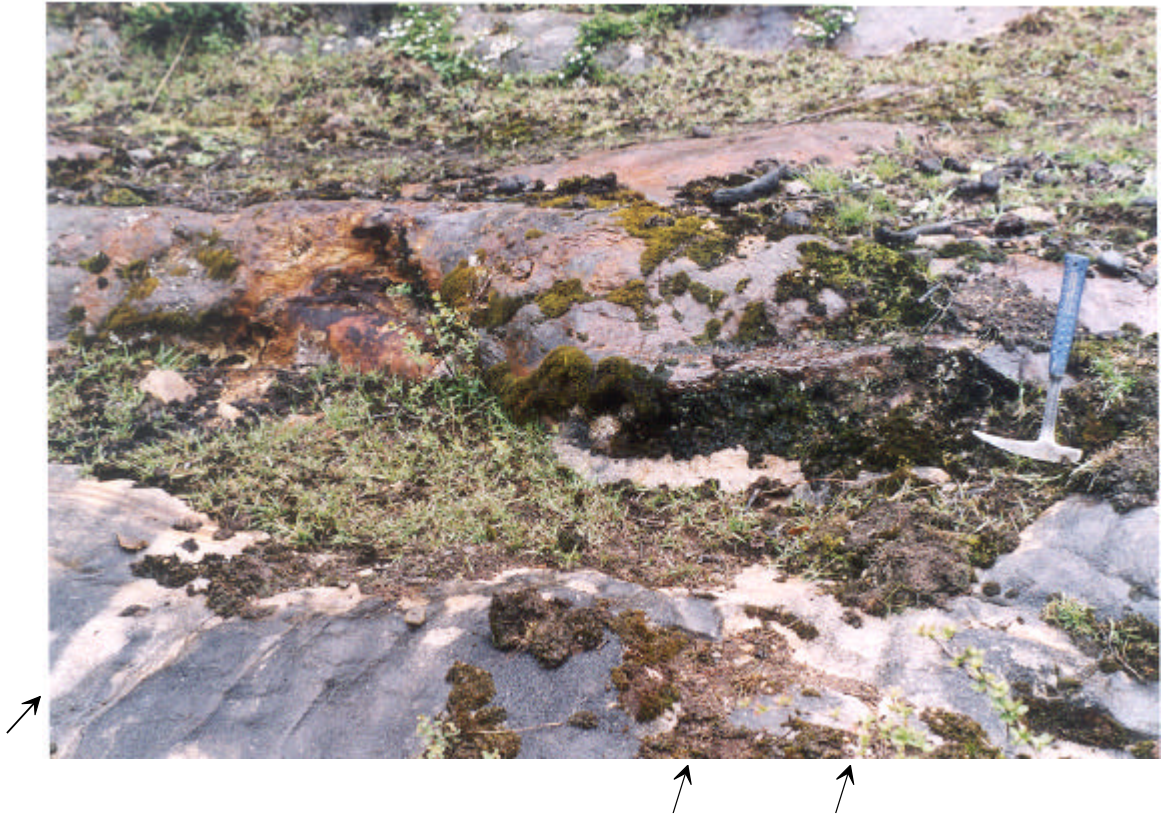


**Figure 7.** An outcrop of the Lhasa Terrane metasedimentary cover sequence. It consists of marble and rusty pyrrhotite schist intruded by thin granite dikes (arrows). outcrop no. 36 (2002).

(a)



(b)



**Figure 8.** The Gangdese batholith. (a) A far view to south from the main high pass (Mt. Milha) on the highway between Lhasa and Bayi, (b) Massive granitoid with prominent jointing. About 100 km west of Bayi.

(c)



(d)

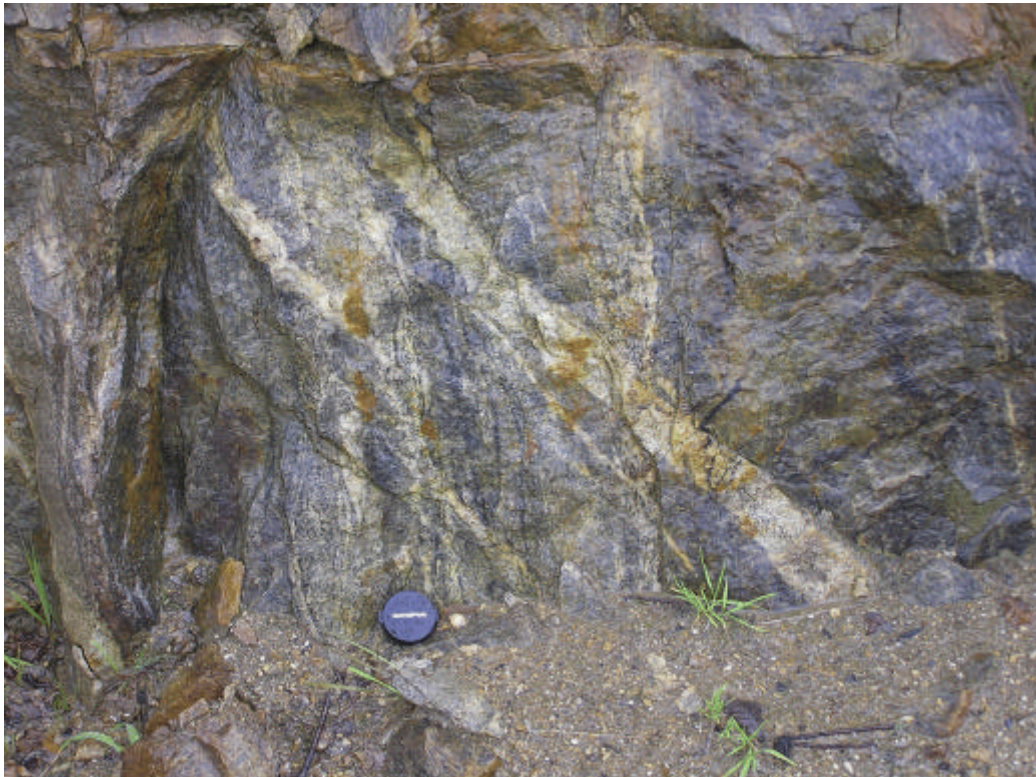
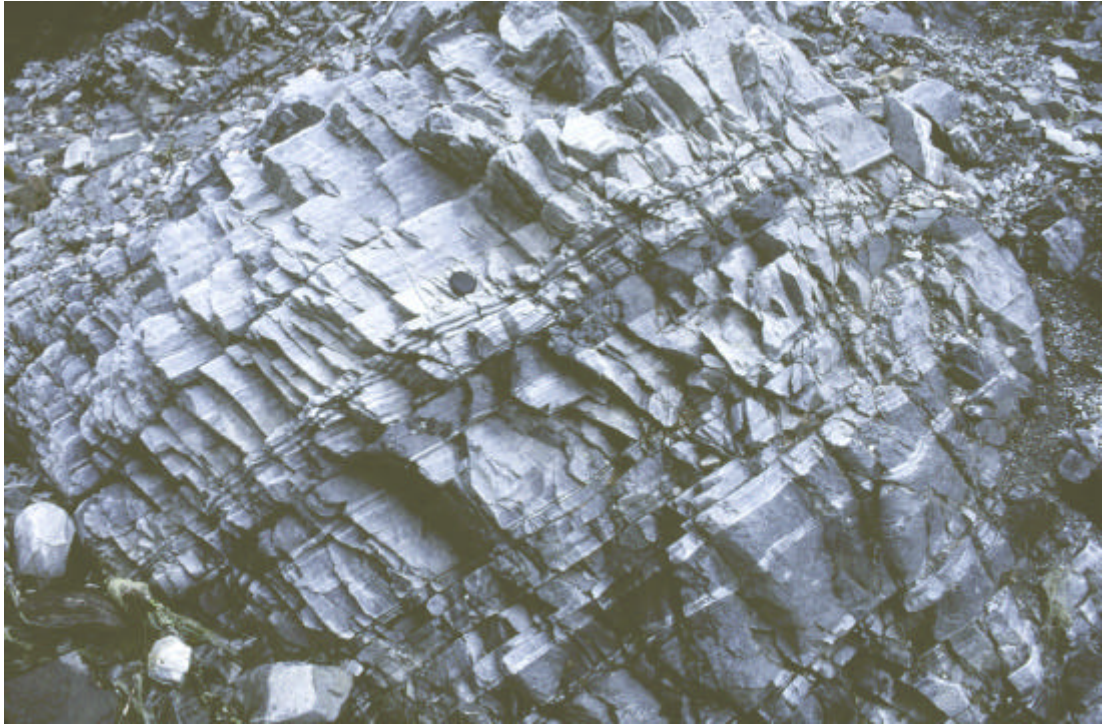


**Figure 8** (continued), (c) A view north to Bayi across Nyingchi River. (d) A foliated granitoid cross-cut by granitic dikes. outcrop no: 36 (2006). All photographs by W. S. F. Kidd.

(a)



(b)



**Figure 9.** Outcrops of rocks interpreted as belonging to the Tsangpo suture in the map area. (a) Mylonitic amphibolite and quartzite in the Deu Gungbu valley. (b) Mylonitic amphibolite beside the road between Dongjiu and Parlung.

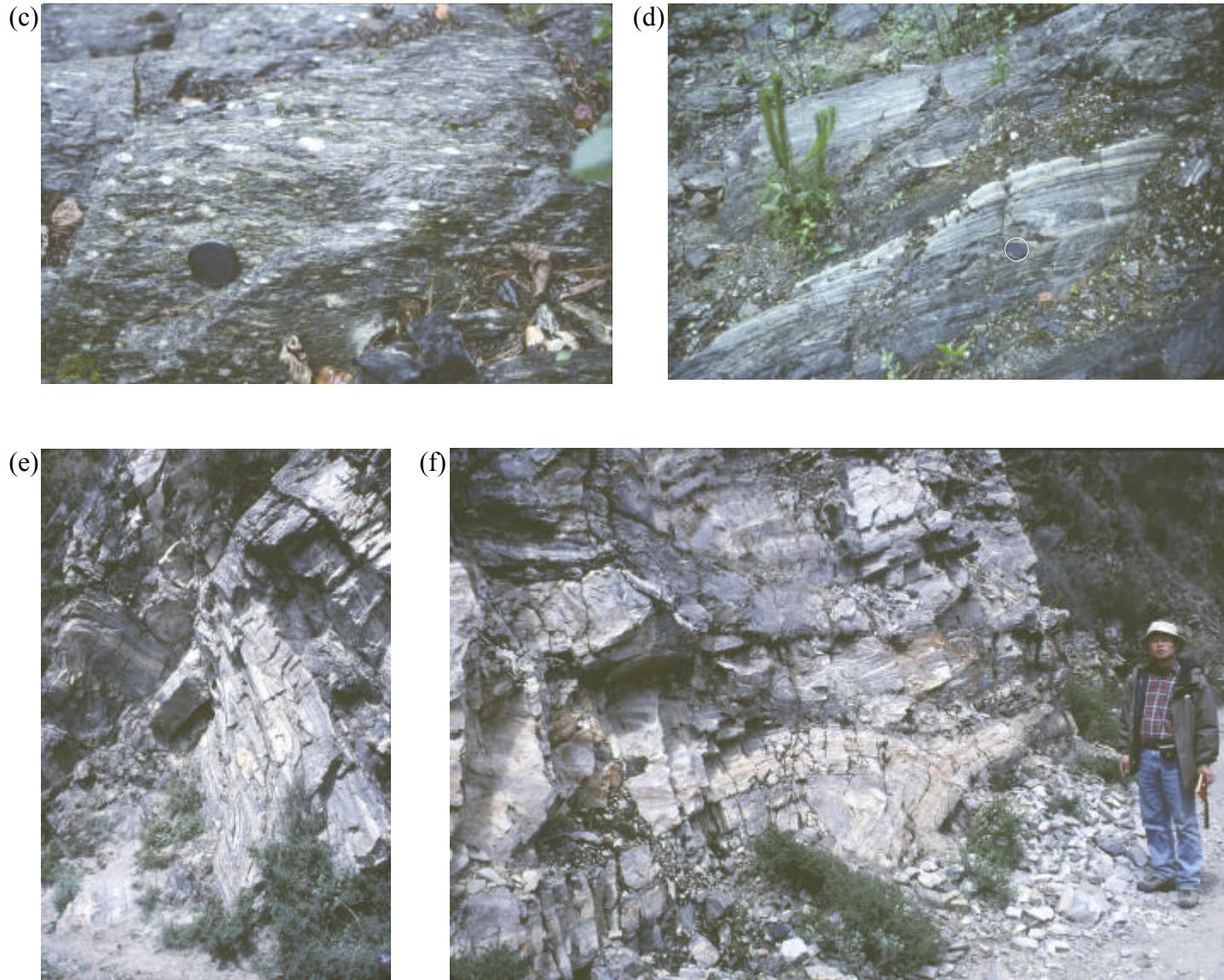


**Figure 9** (continued), The Tsangpo suture rocks. (c) Feldspar porphyroclasts in granitoid-derived mylonite. (d) Asymmetric folds in mafic mylonite near a camera cap for scale. Outcrop no. for (b), (c), and (d) is 39 (2002). (e) and (f) is a roadcut of mostly mylonitic amphibolites and lesser felsic veins and pegmatites. They are folded in various directions. Parts of the folds have a sheath fold geometry with an elliptical "eye", beside the author. Outcrop no. for (e) and (f) is 12 (2002). All photographs by W. S. F. Kidd.

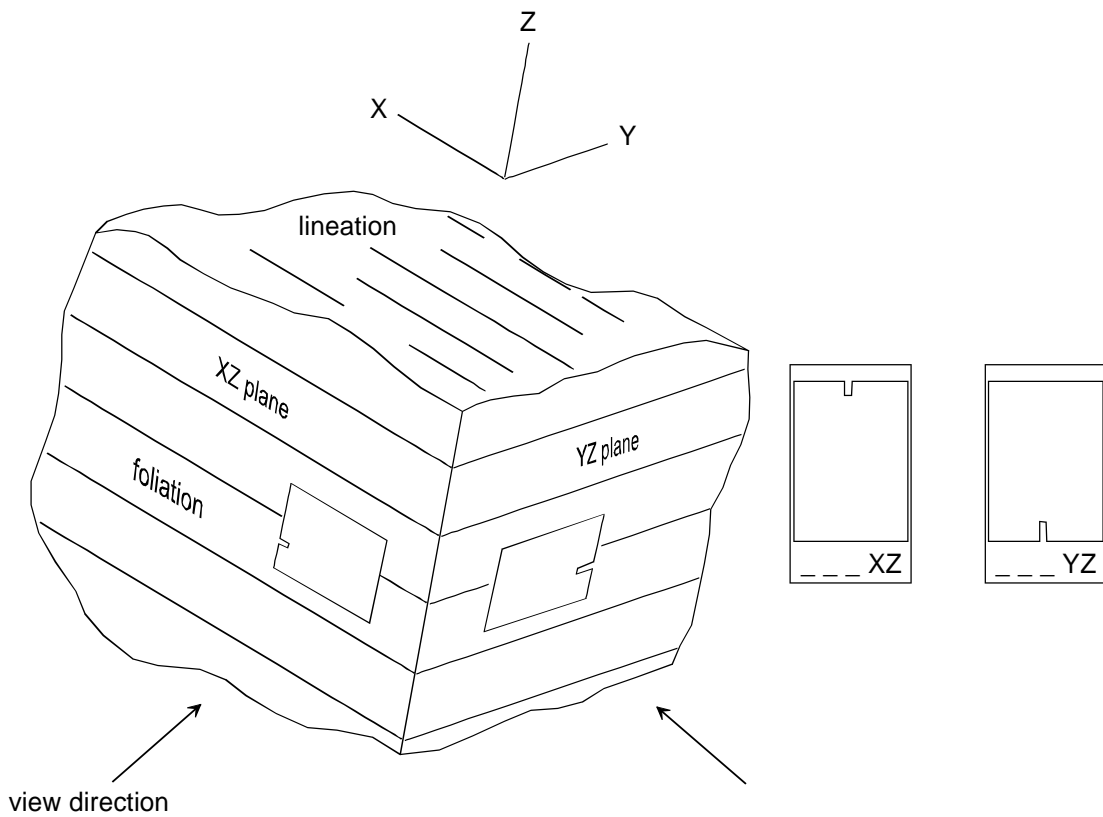
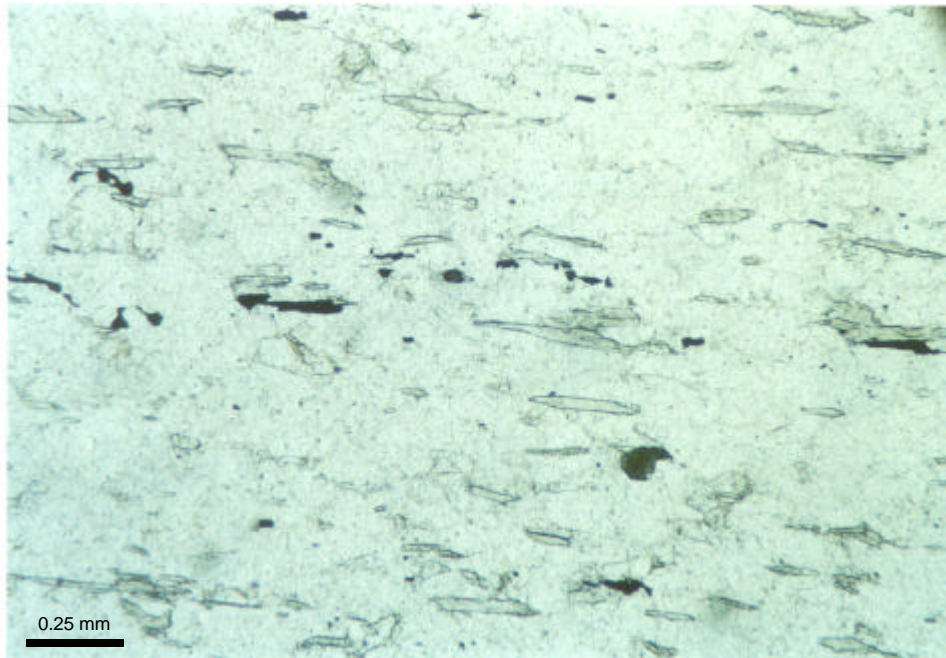


**Figure 10.** Definition of XZ and YZ planes and the way oriented rock chips are cut. The samples are tilted to match with original orientation and a view direction is recorded when the rock chips are glued to slide glass. The cut marks indicate upper ends. The cartoon modified after Turner and Weiss (1963).

(a)



(b)

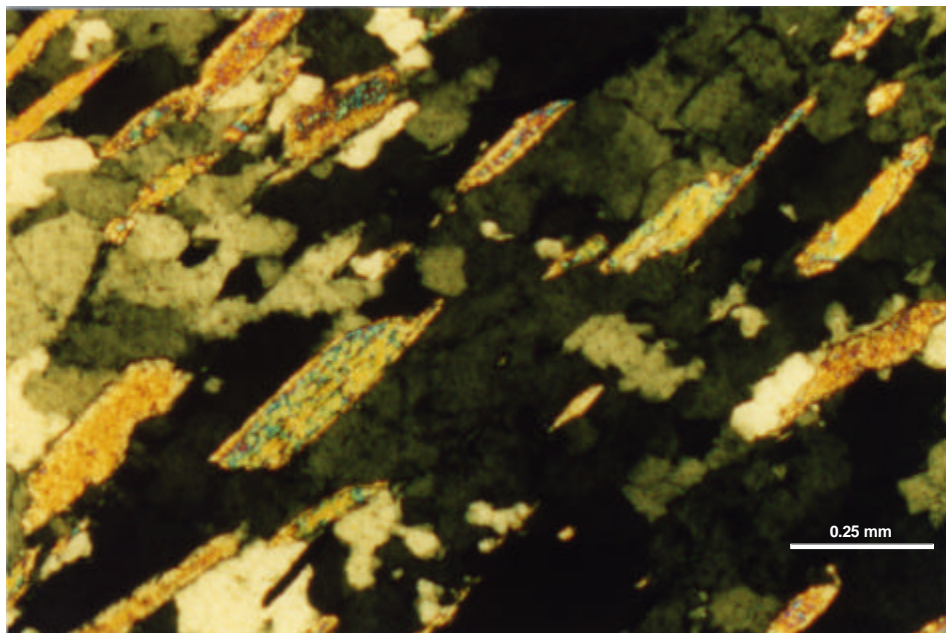


**Figure 11.** Microscopic shear criteria. Monoclinic symmetry of mica fishes (muscovite) in quartzite samples indicate sinistral sense of shear (a) in NB02-08, and (b) in NBK-73X-05.

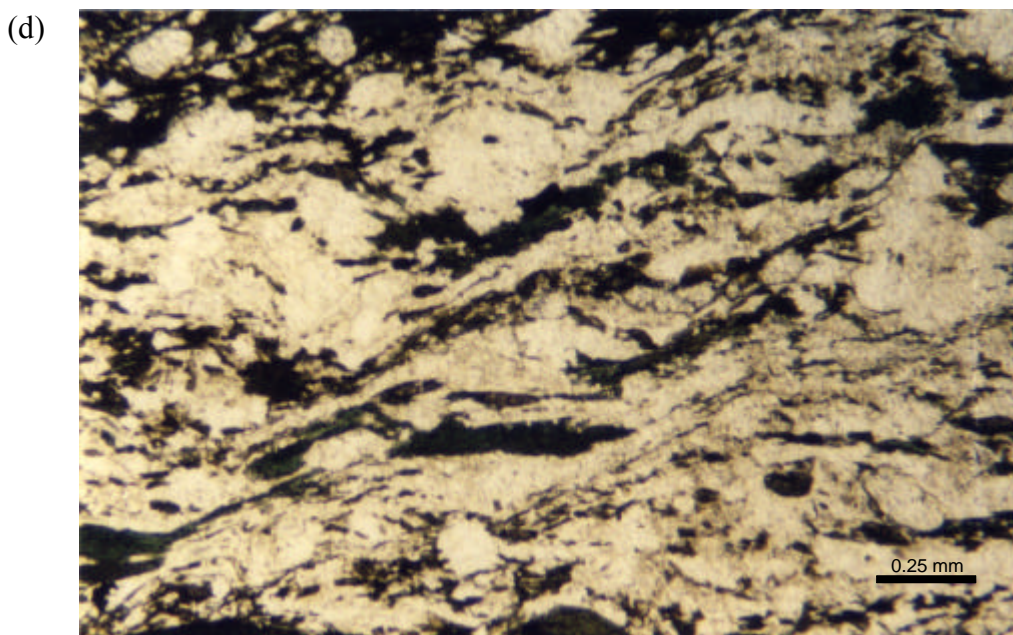
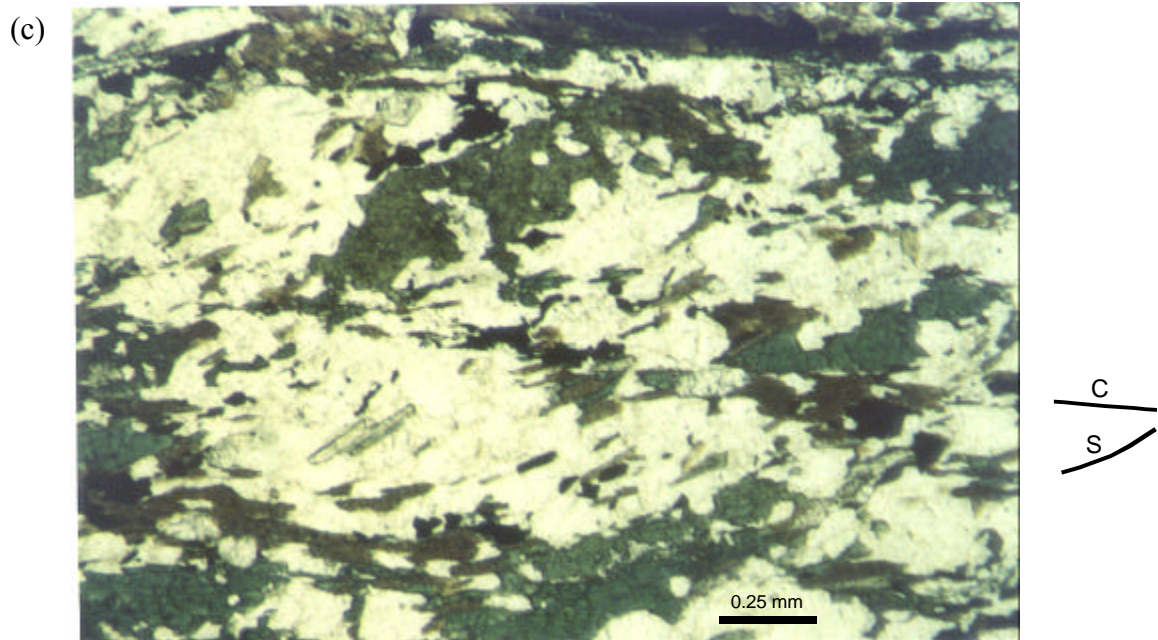


**Figure 11** (continued), (c) S-C fabrics defined by amphibole and biotite indicate apparent dextral sense of shear. NB02-77B. (d) Amphibole, biotite, and titanite form shear bands and S-C fabrics that clearly indicate sinistral sense of shear. NB02-78. Both (c) and (d) are mylonites from the Deu Gungbu section.

(e)

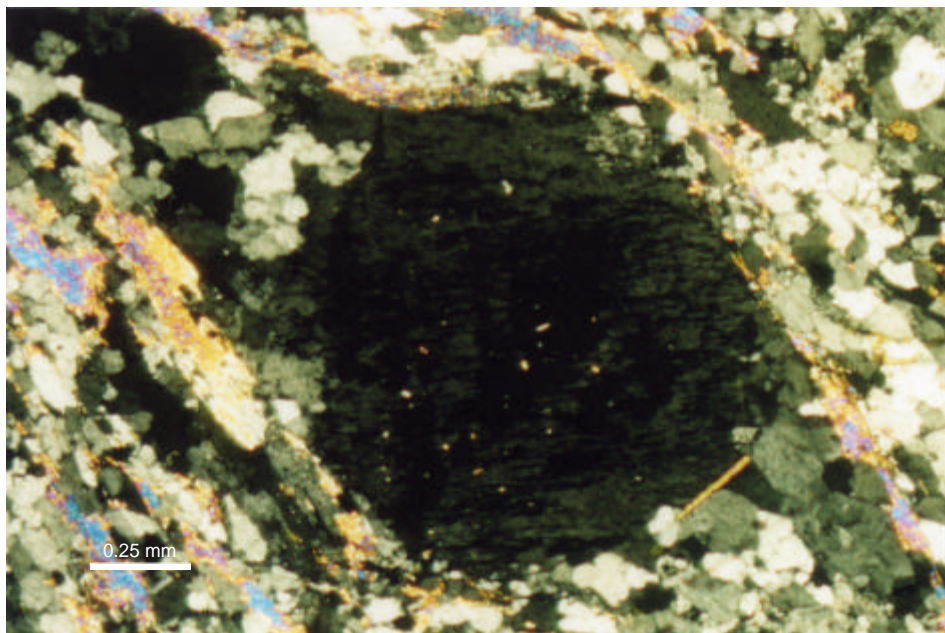


**Figure 11** (continued), (e) Sigma-type porphyroblast of perthite in mylonite indicating dextral sense of rotation. NB02-98.

(a)

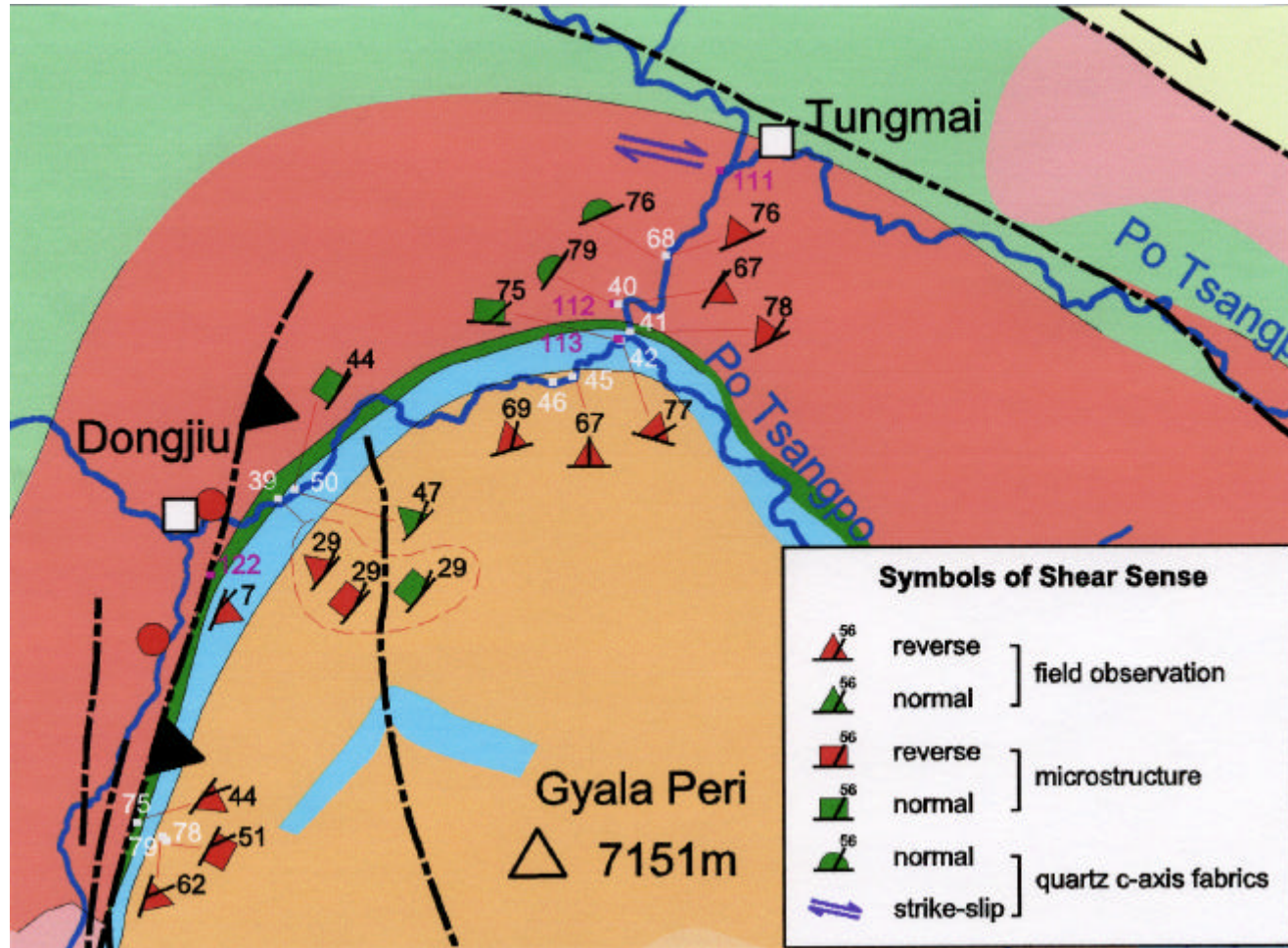


**Figure 12.** Sense of shear determined from field and microscope observations. Orientations of foliation and lineation are also shown. The number in each symbol indicate plunge of lineation. The small squares indicate outcrop locations visited during 2002 (white), 2003 (yellow), and 2005 (purple). (a) Northwestern massif boundary and vicinity of Tungmai.

(b)

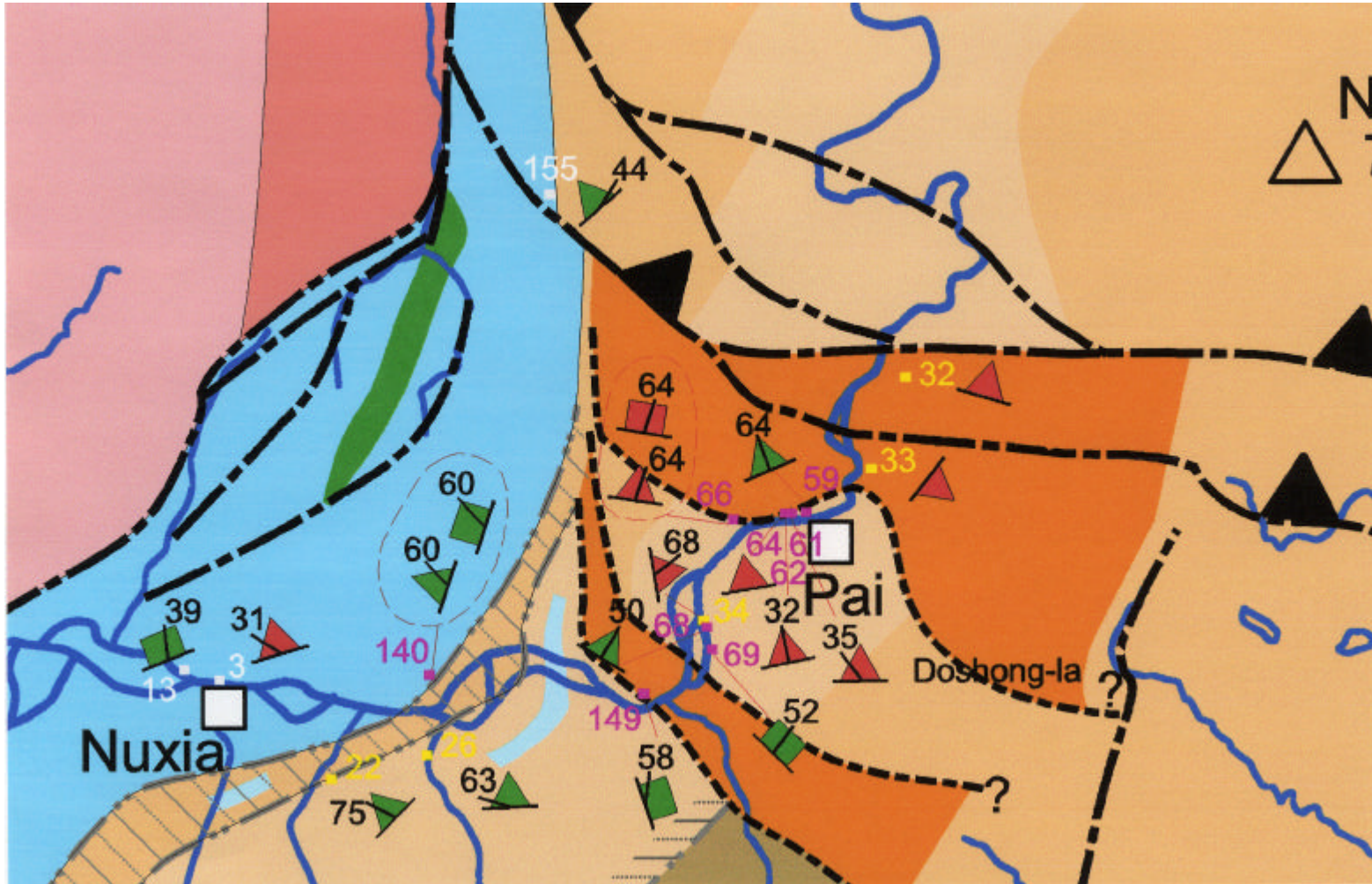


**Figure 12** (continued), Sense of shear determined from field and microscope observations. (b) Areas between and vicinity of Nuxia and Pai, and the other region to the north and northwest.

(c)

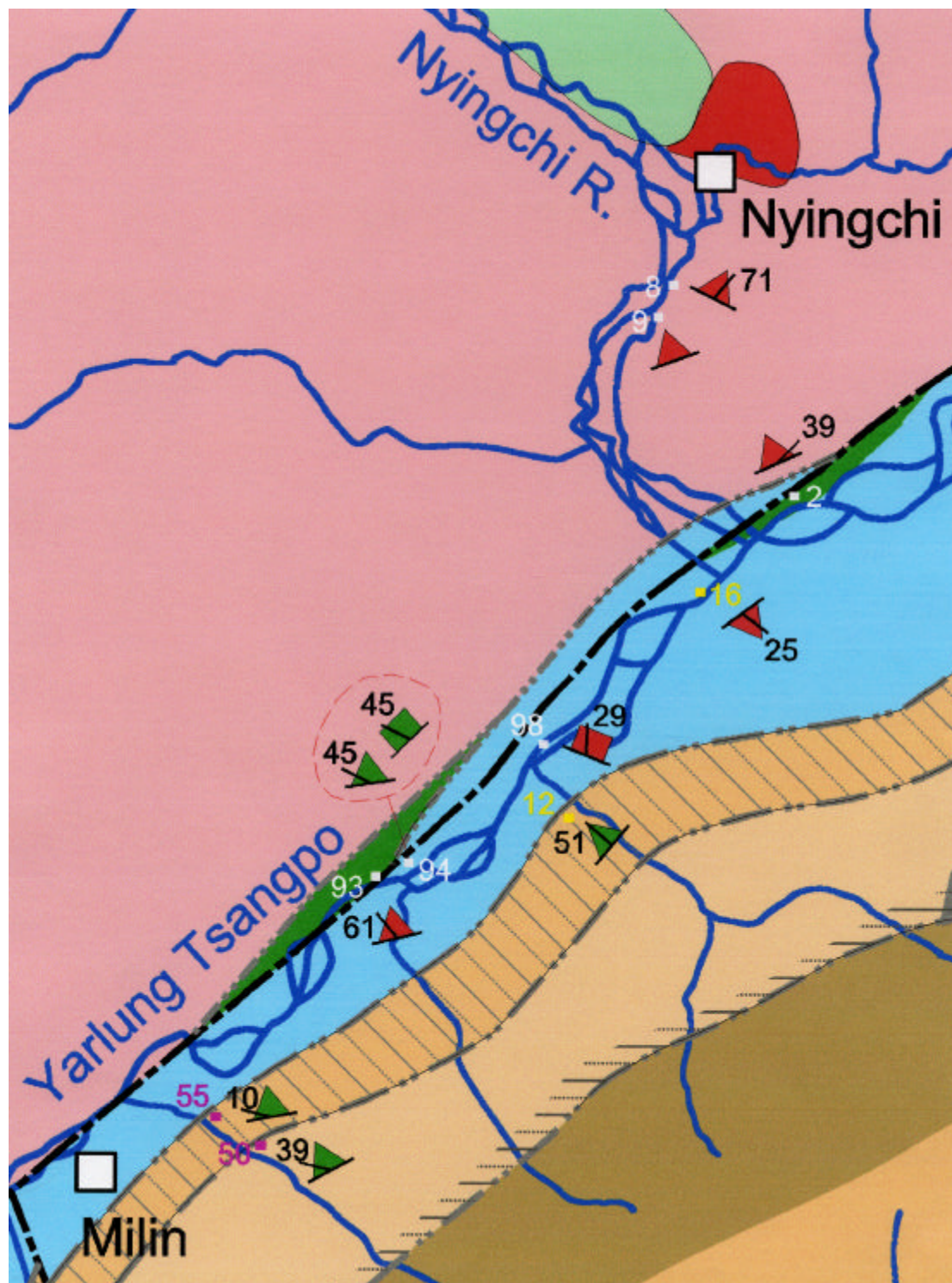


**Figure 12** (continued), Sense of shear determined from field and microscope observations. (c) The western massif boundary region.

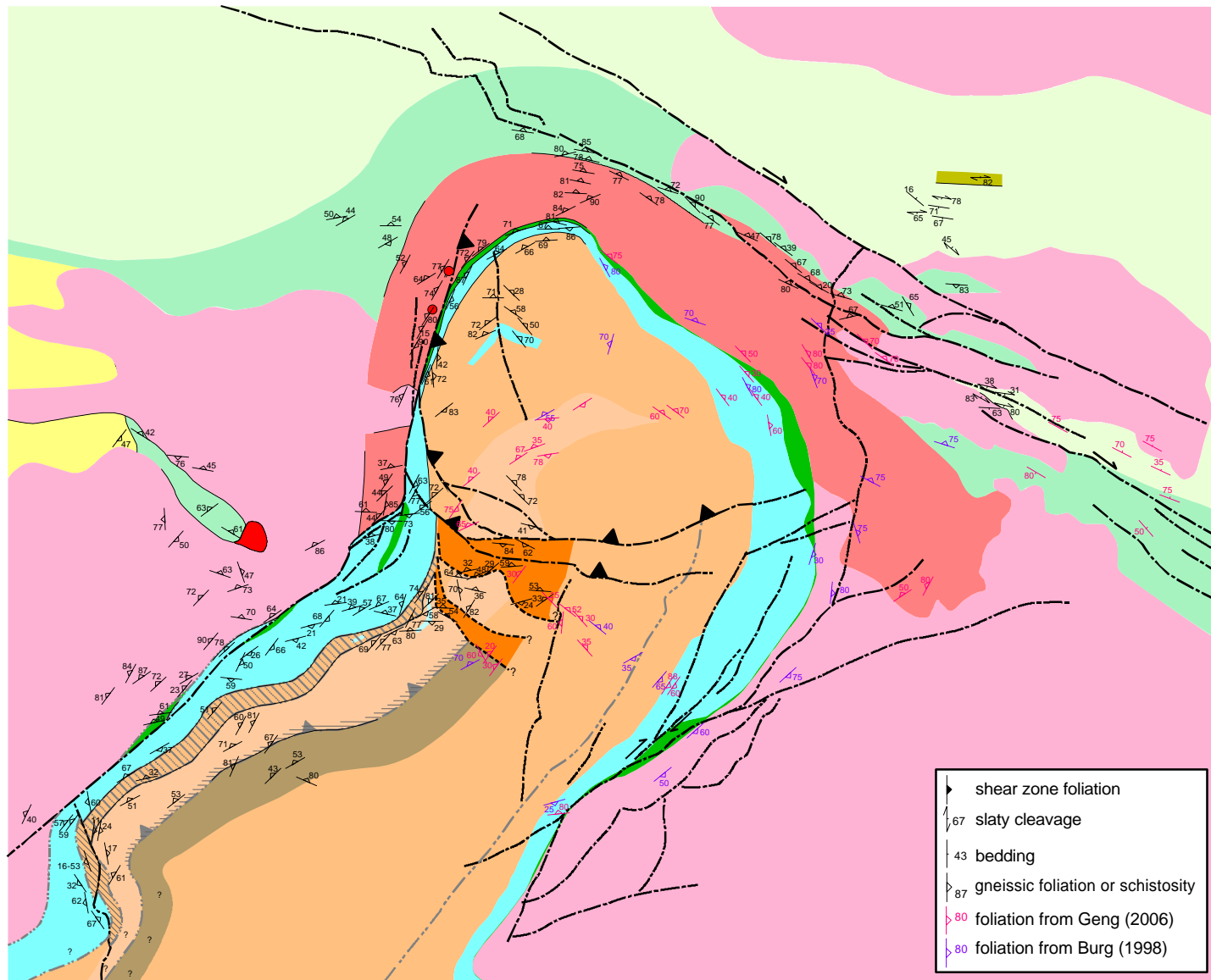


**Figure 13.** Selected orientations of gneissic foliation/schistosity within and around the Namche Barwa massif from the mapping of this project, Burg et al. (1997), and Geng et al. (2006).

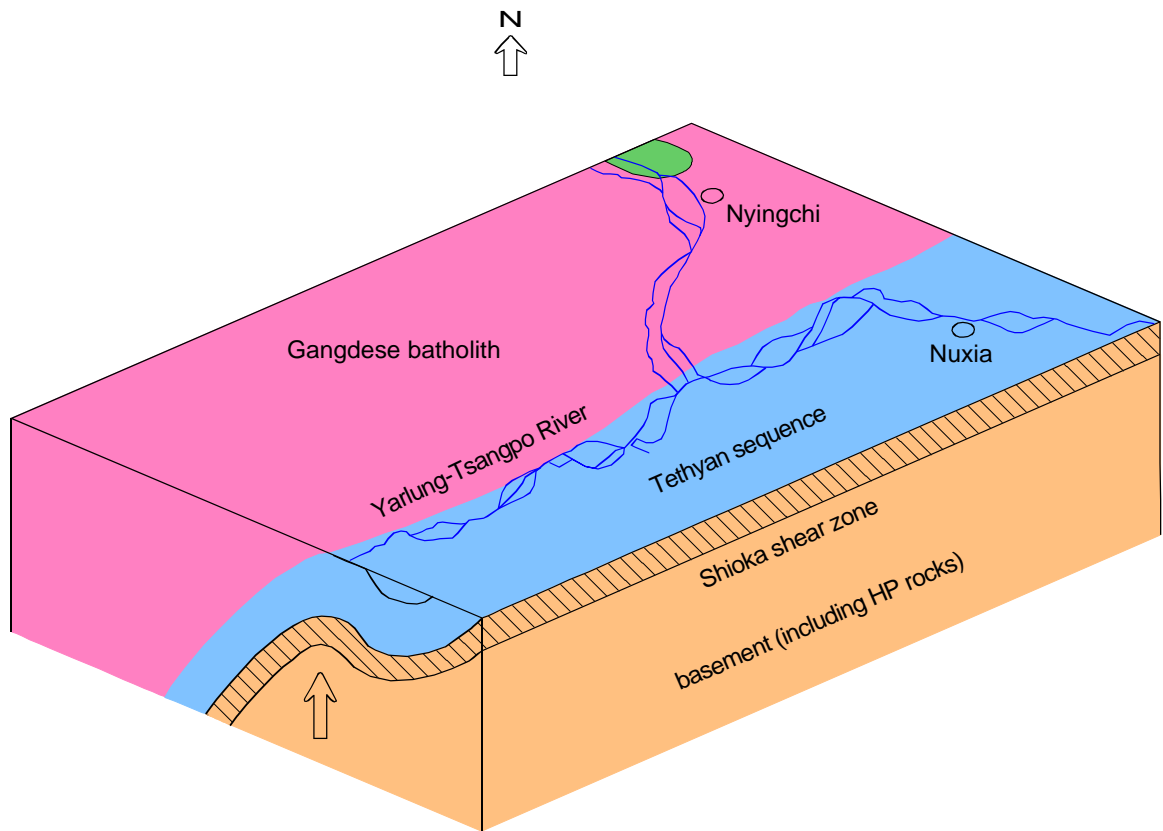


**Figure 14.** A large-scale anticline with approximate interlimb angle of  $65^\circ$  and about 36-40 km long, occurring between Nuxia and Milin.

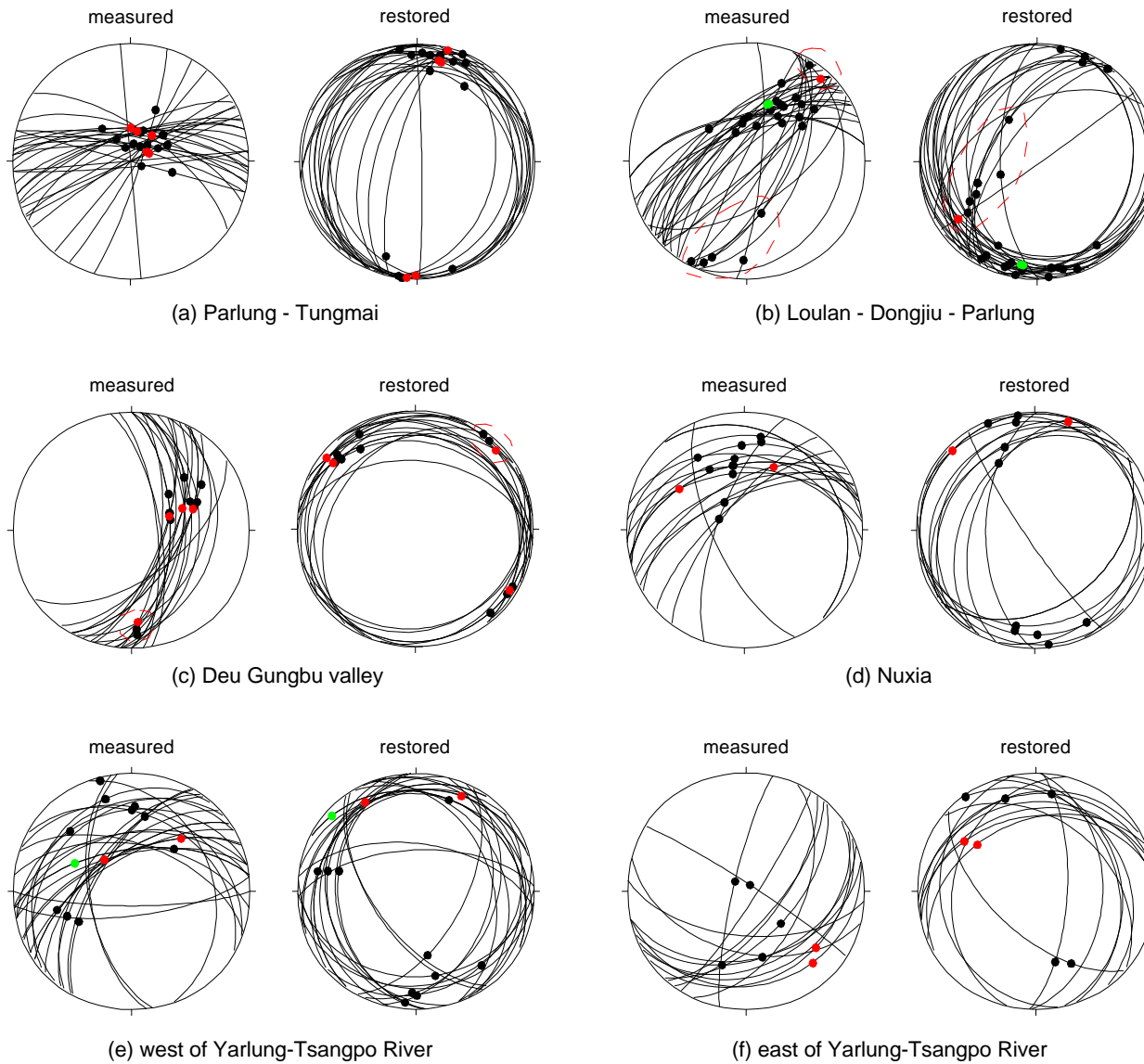


**Figure 15.** Measured and restored lineations and foliations of the Tethyan sequence in the boundary regions. An exception is the Deu Gungbu valley where the measurements are largely from the basement (Higher Himalaya). The red and green dots respectively indicate lineations with reverse and normal sense of shear in current outcrops. An exception is Parlung where the terms of reverse and normal shear do not deliver clear meaning due to the near vertical foliations, and the red dots here indicate north-up shears. The colors indicate opposite shear sense in the restored stereonets if the restoration involves overturning of foliations. For example, the two lineations (red dots) in (f) indicate normal, west-down sense of shear when they are restored. The dashed red loops enclose lineations thought to have been overprinted on foliations tilted possibly close to the current orientations during the younger N-S to NE-SW shortening.

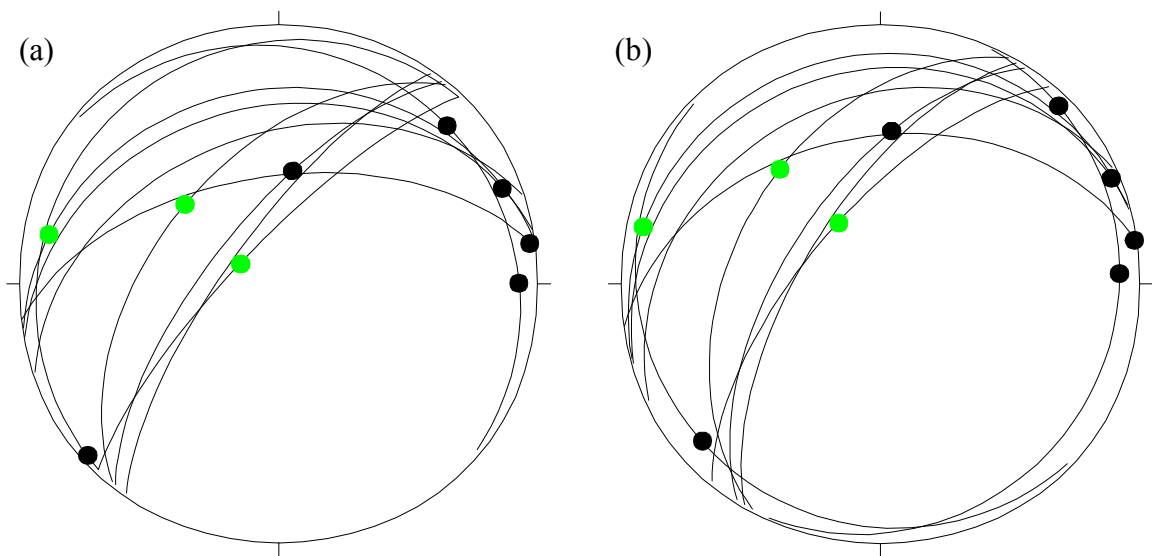


**Figure 16.** Orientations of lineations and foliations in the Shioka shear zone. (a) Measured data. (b) Rotated back by assuming a shear zone with original strike and dip of N60E and 40W, respectively. The restored orientations are similar to the current orientations. The green dots are lineations with normal sense of shear.

(a) Western margin of the Gyala Peri massif - De'u Gungbu Valley section

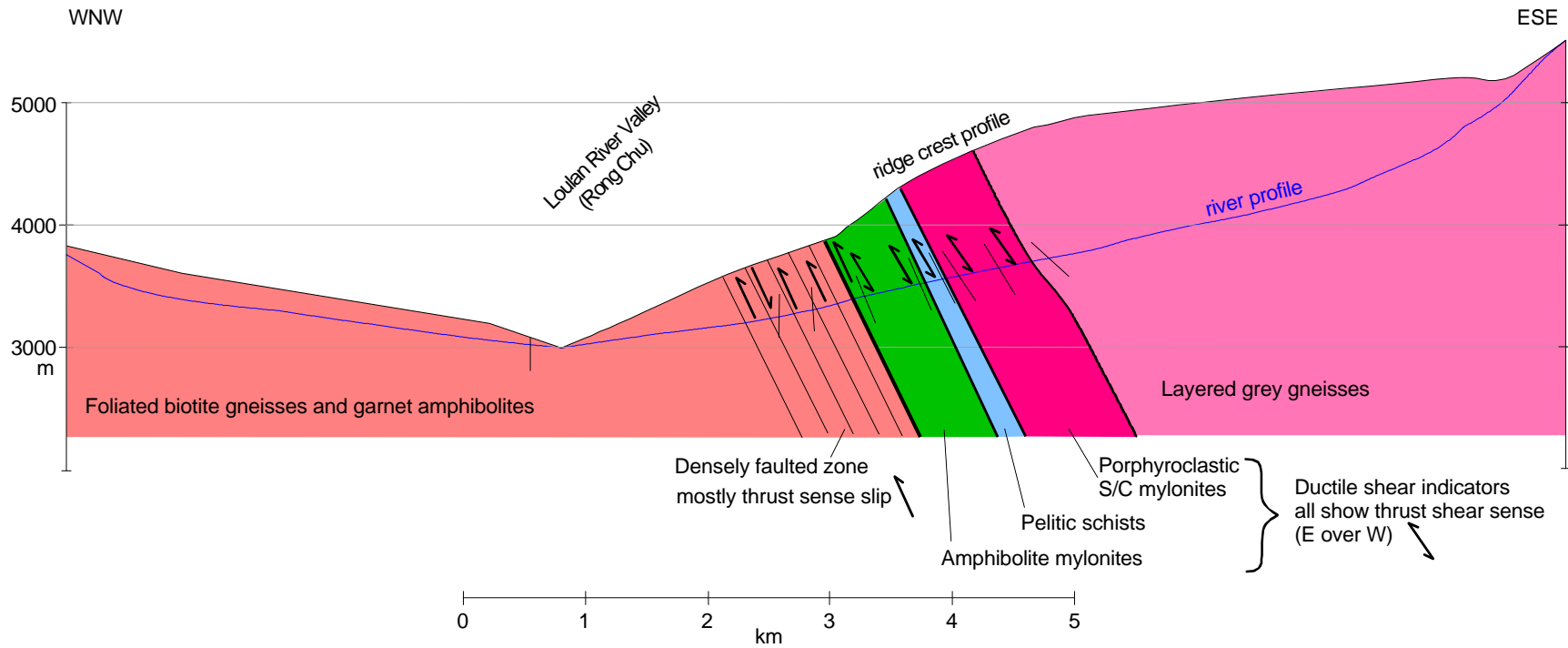


**Figure 17.** An east-west traverse along the Deu Gungbu valley. (a) A cross-section along the traverse (drawn by W. S. F. Kidd).

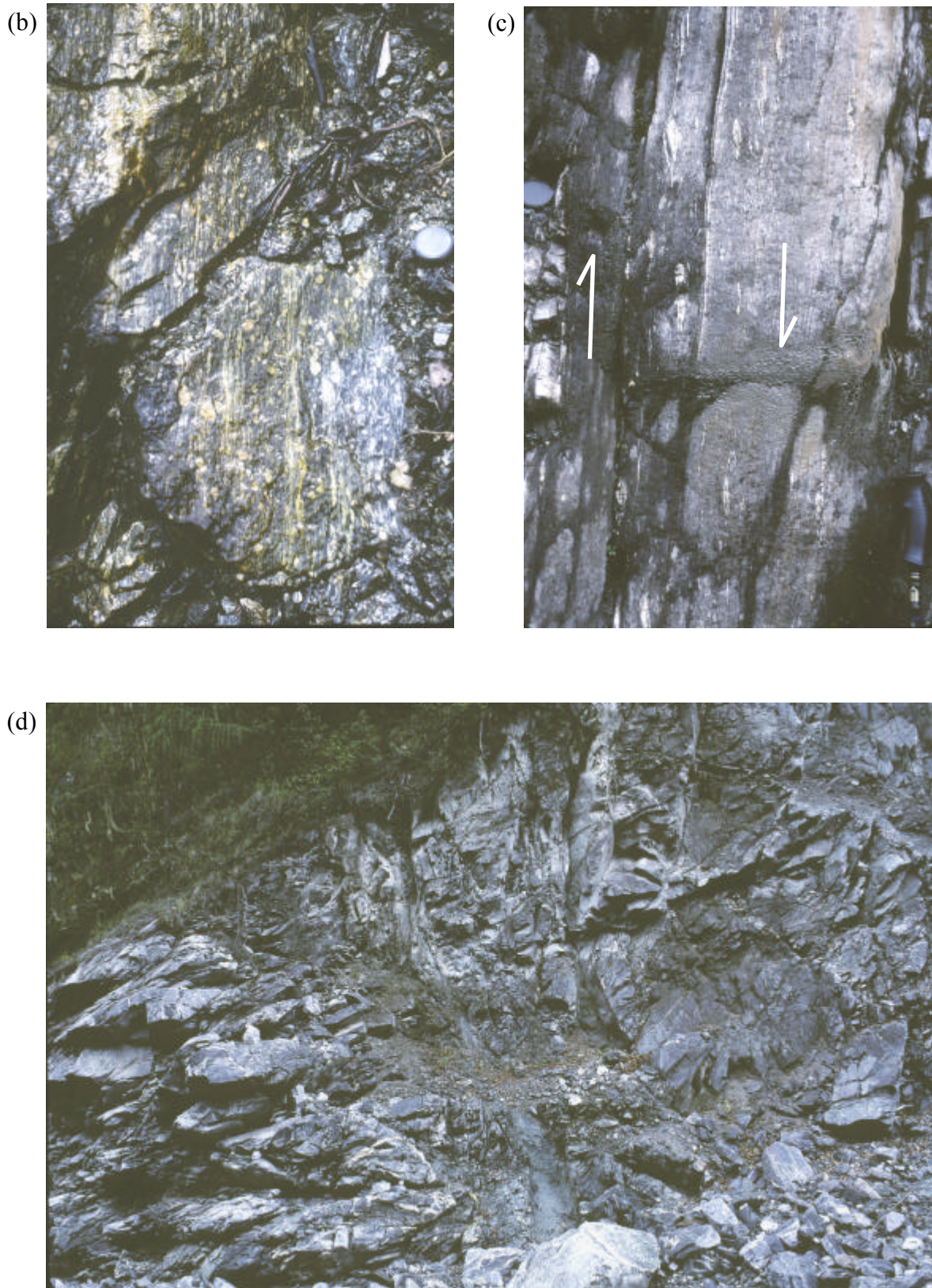


**Figure 17** (continued), All Deu Gungbu valley section. (b) A porphyroclastic quartz-feldspar mylonite. View to south. (c) A mylonitic pelitic schist with sliced-off veins indicating an east-up shear. View is toward south. (d) The densely faulted zone of quartzofeldspathic gneisses of the Lhasa Terrane.

(e)



(f)

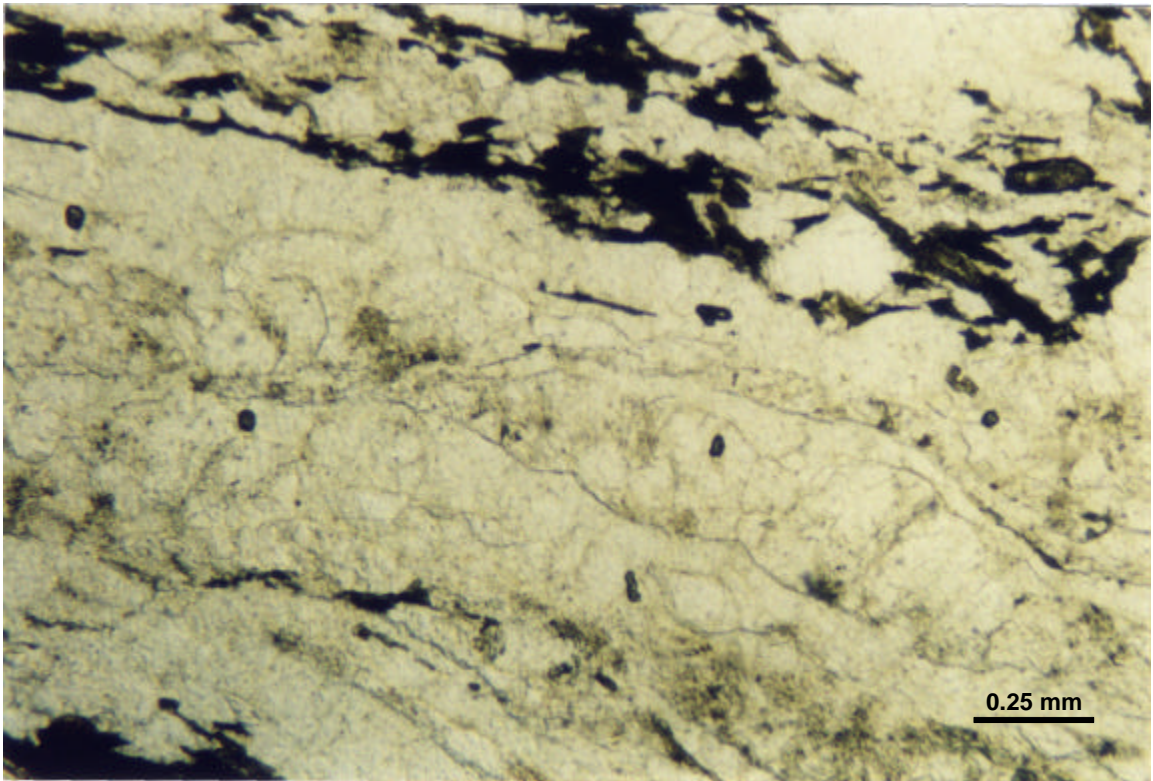


(g)



**Figure 17** (continued), Deu Gungbu valley. (e) A faulted contact between the base of mylonitic amphibolite and quartzofeldspathic schist/gneiss of the Lhasa Terrane. (f) The layered gray gneiss at the highest (easternmost) point reached during the traverse, (g) A cobble of the layered gray gneiss showing folded mylonitic foliations. All photographs by W. S. F. Kidd.

(a)



(b)

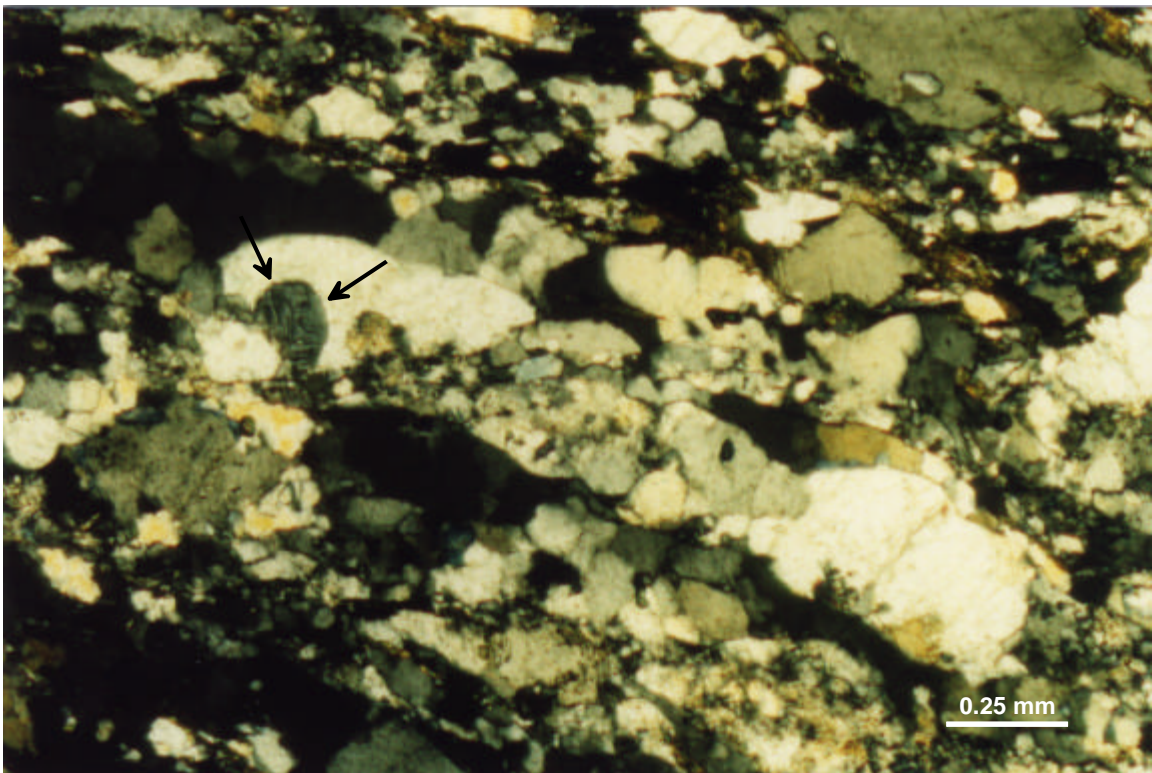
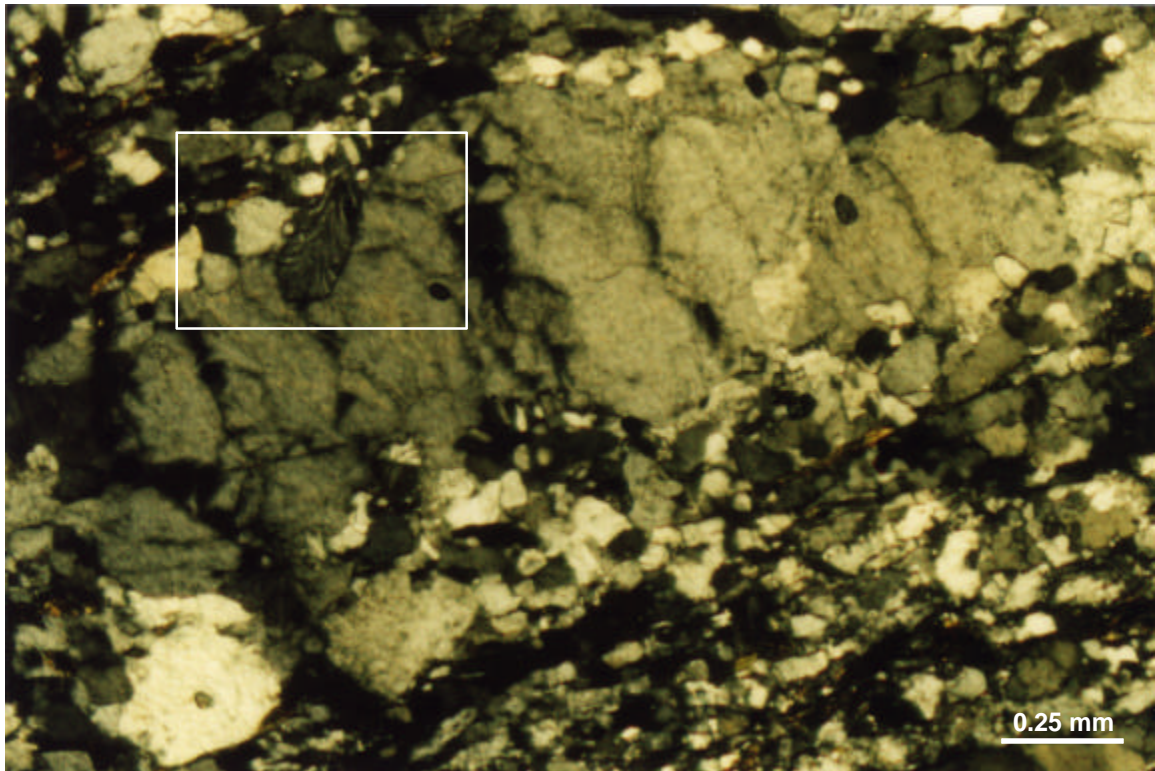


**Figure 18.** Feldspar ribbons in NB02-75. The K-feldspars were plastically deformed at high temperature conditions (above 500°C). (a) Plane light. (b) Crossed polarizer. A myrmekite is seen along the margin of the ribbon (black arrows).

(a)



(b)

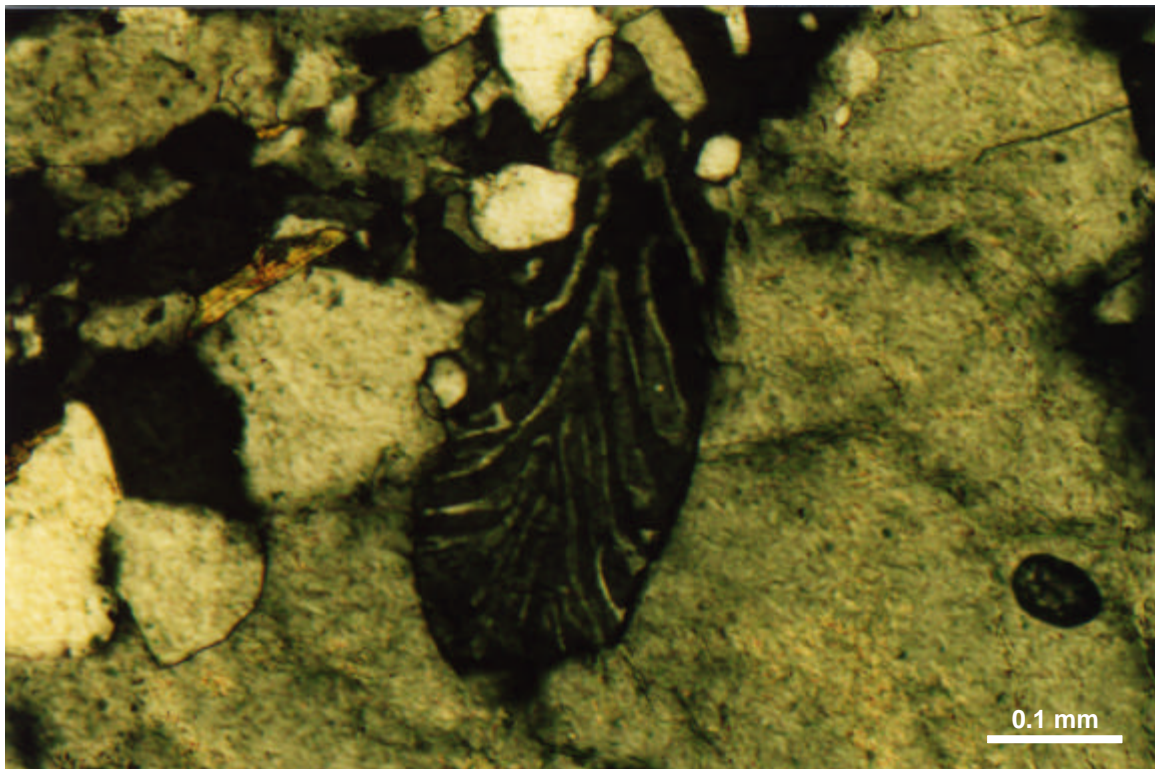
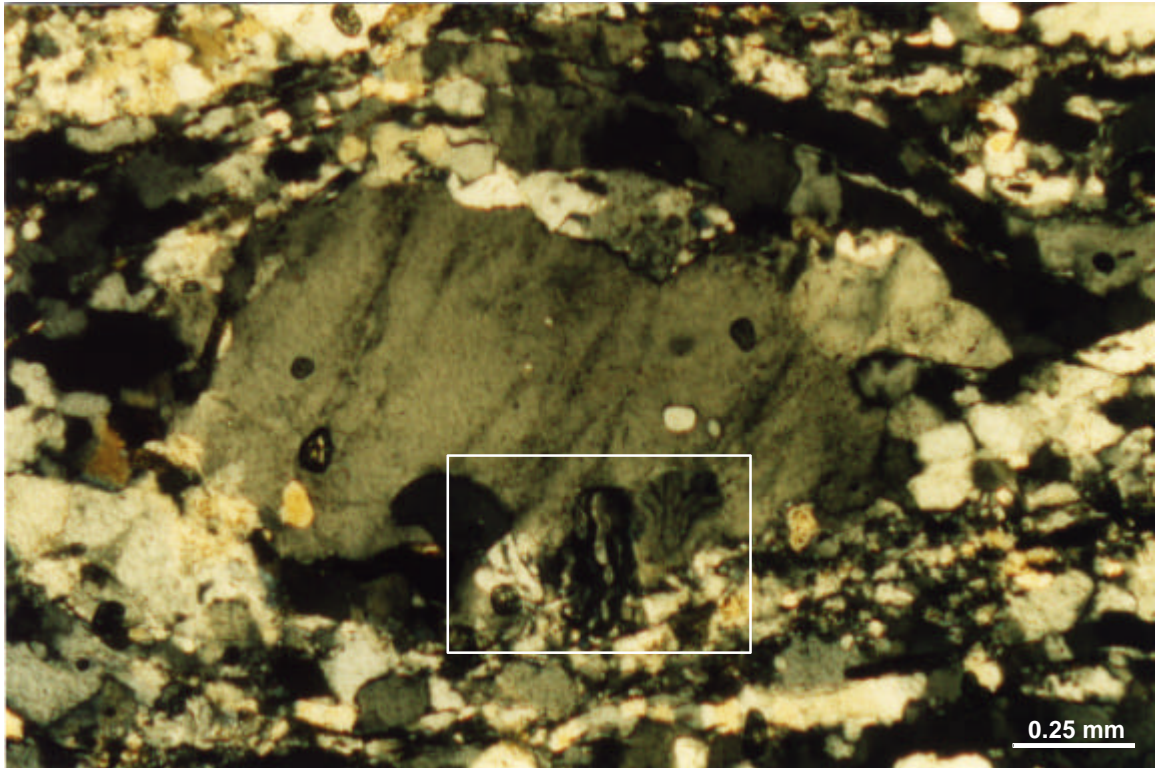


**Figure 19.** Myrmekites in NB02-74. (a) Myrmekites of various sizes are developed along edges of a K-feldspar ribbon. White box is an area enlarged in (b) where the internal texture of the myrmekite is oblique to overall foliations of this sample. Location of a large myrmekite in the shortening quadrant (a) and obliquity of its internal texture (b) indicate apparent dextral sense of shear.

(c)



(d)

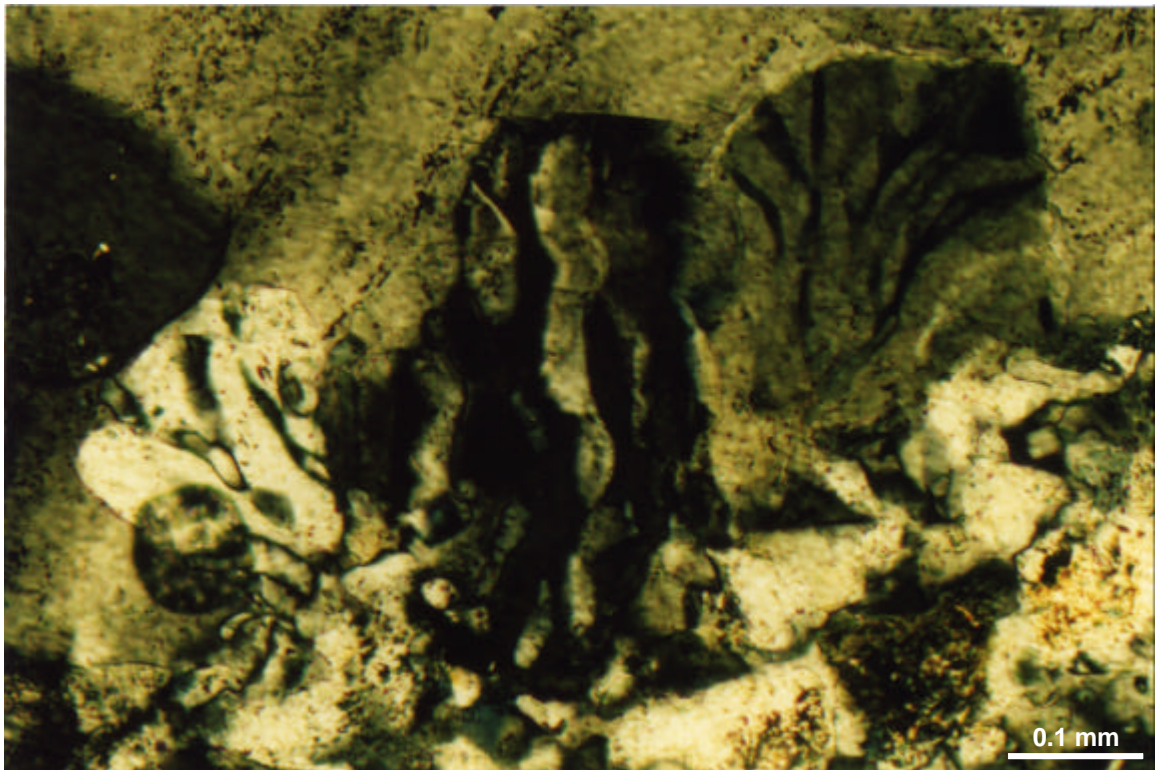


**Figure 19** (continued), Asymmetric myrmekite in NB02-75. (c) Myrmekites developed along margin of a K-feldspar porphyroblast. If the myrmekites are developed in the shortening quadrant, they indicate apparent dextral sense of shear. (d) Enlarged view of the myrmekites in the white box in (c).

(a)



(b)



**Figure 20.** The Doshong-la migmatite and shear zone.

(a) An overview to north from near Doshong-la pass. Nearly all the cliff face here consists of migmatites.

(b) A view of the same continuous cliff from the Doshong-la valley.

(c)



(d)



**Figure 20** (continued), The Doshong-la migmatite and shear zone. (c) The Doshong-la migmatite in the upper valley near the Doshong-la pass. In this outcrop, numerous felsic melt layers alternate with mafic layers which are commonly boudinaged (lower section). (d) East-west-trending folds of migmatitic foliation on the trail near Doshong-la. All photographs by W. S. F. Kidd.

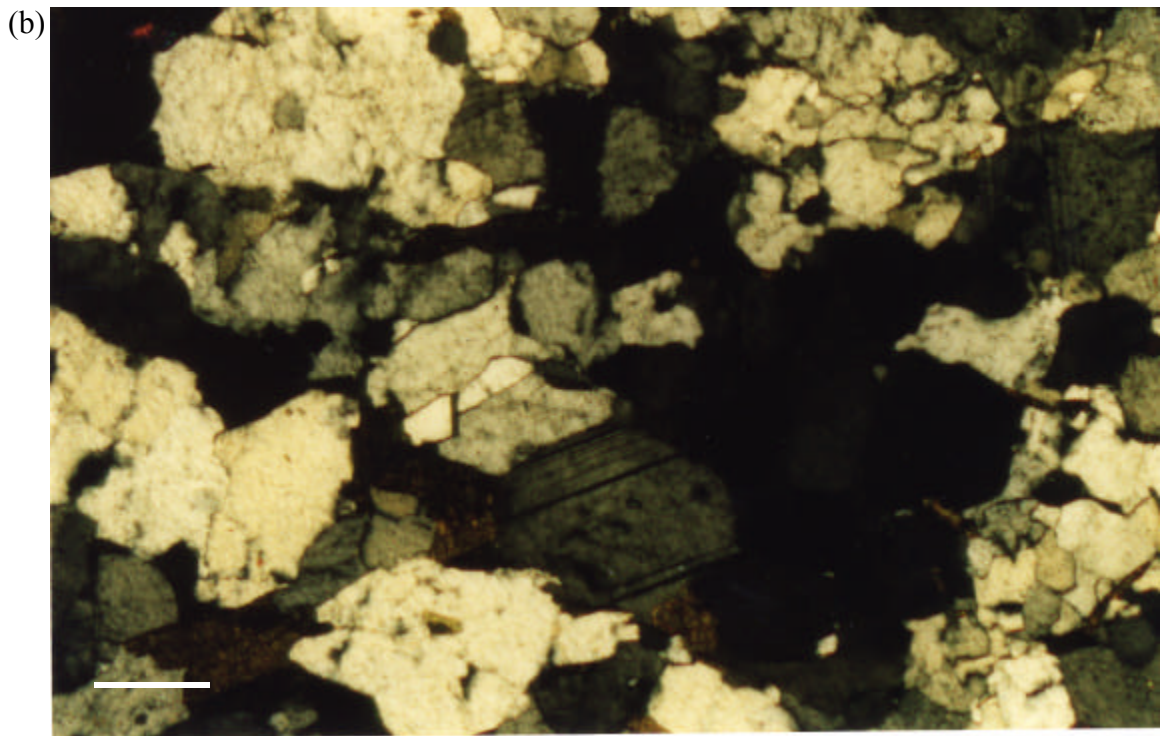
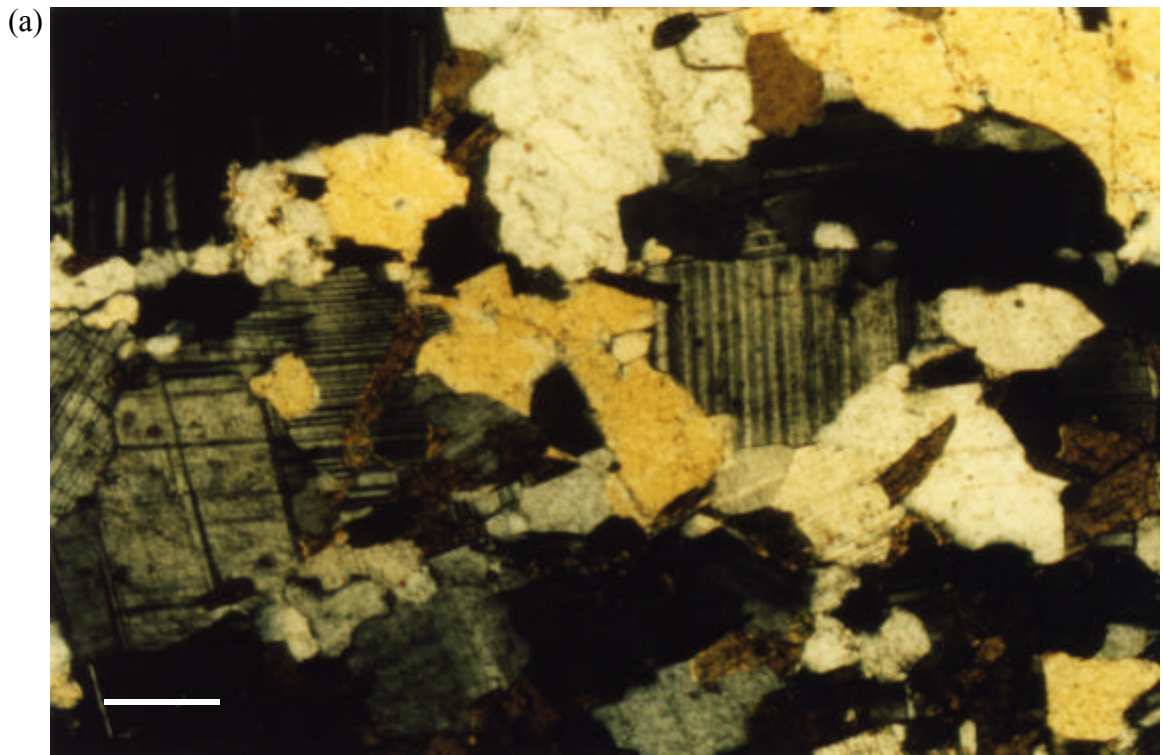


**Figure 21.** Photomicrographs of samples analyzed for quartz c-axis fabrics. The white bars on lower left are 0.25 mm long in these two photos. (a) NBK-69Y-05, and (b) NBK-71Y-05.

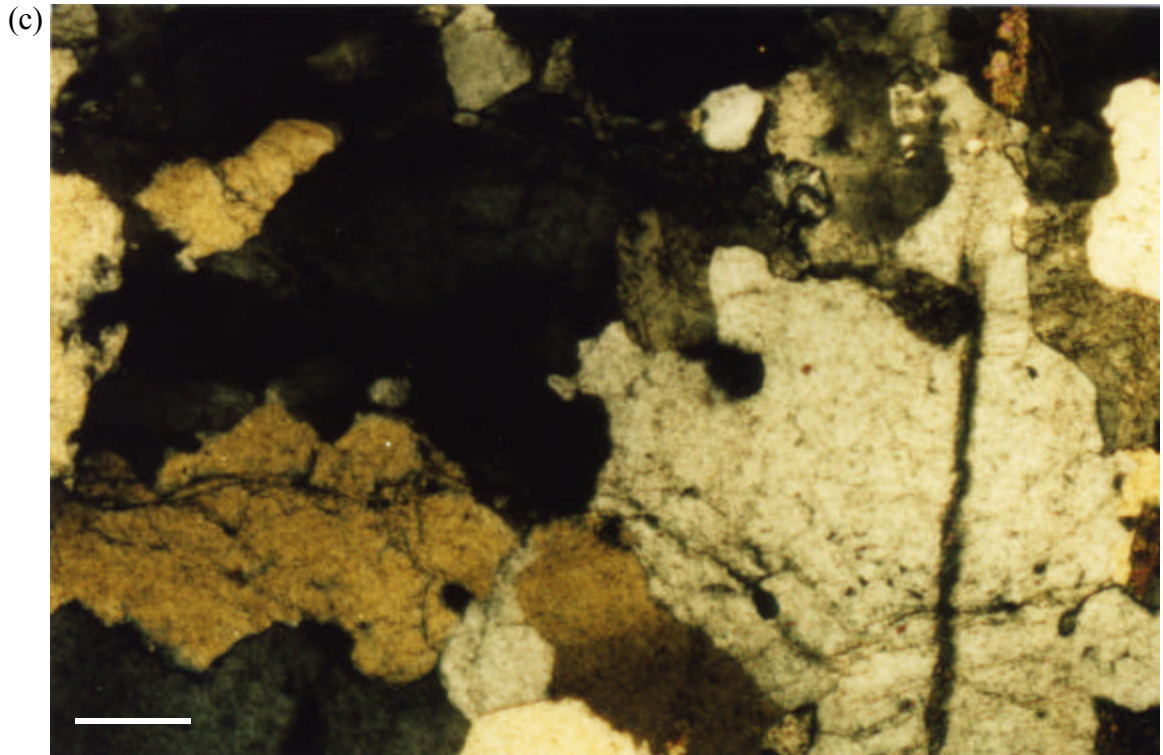


**Figure 21** (continued), (c) A photomicrograph of NBK-72Y-05 analyzed for quartz c-axis fabrics. The white bar on lower left is 0.25 mm long.

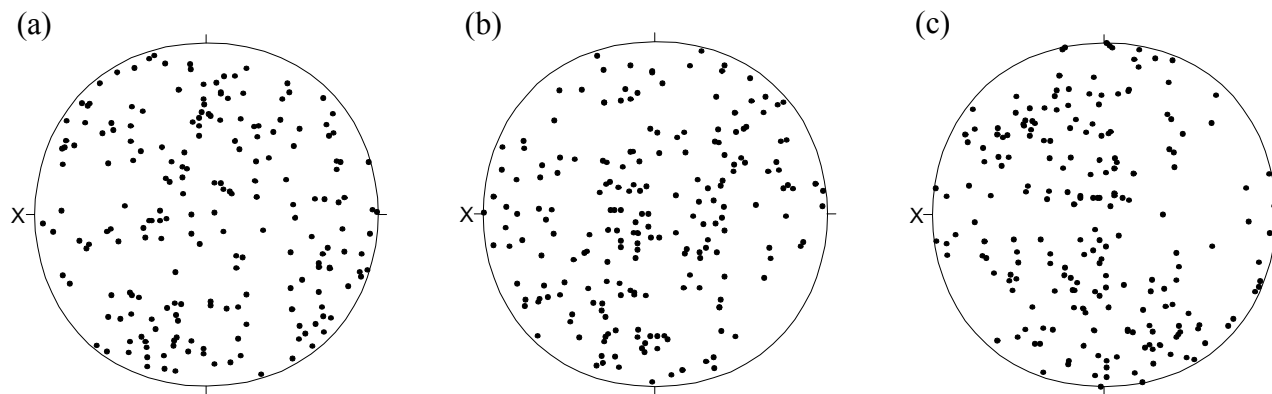


**Figure 22.** Quartz c-axis pole figures for (a) NBK-69, (b) NBK-71, and (c) NBK-72. A total of 202 measurements for each sample.

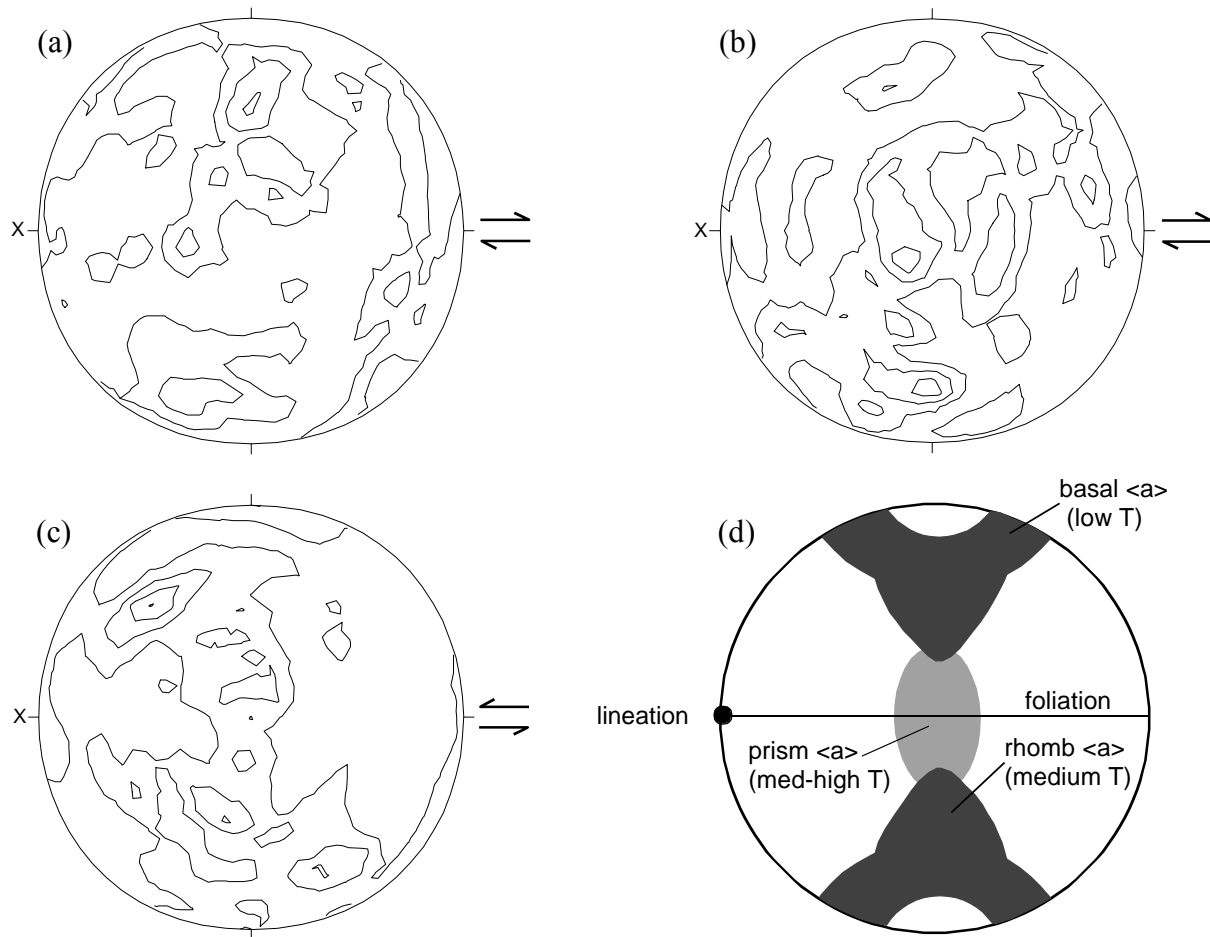


**Figure 23.** Density stereograms of the quartz c-axis pole figures. (a) NBK-69, (b) NBK-71, both contours: 3 %, 2 %, 1 %, per 1 % area. (c) NBK-72, contours: 4 %, 3 %, 2 %, 1 %, per 1 % area. (d) illustrates where quartz c-axes are plotted with respect to foliation and lineation depending on different slip systems for pure shear. In simple shear, overall c-axes are disposed oblique to foliation. Modified after Hansen and Dusel-Bacon (1998).

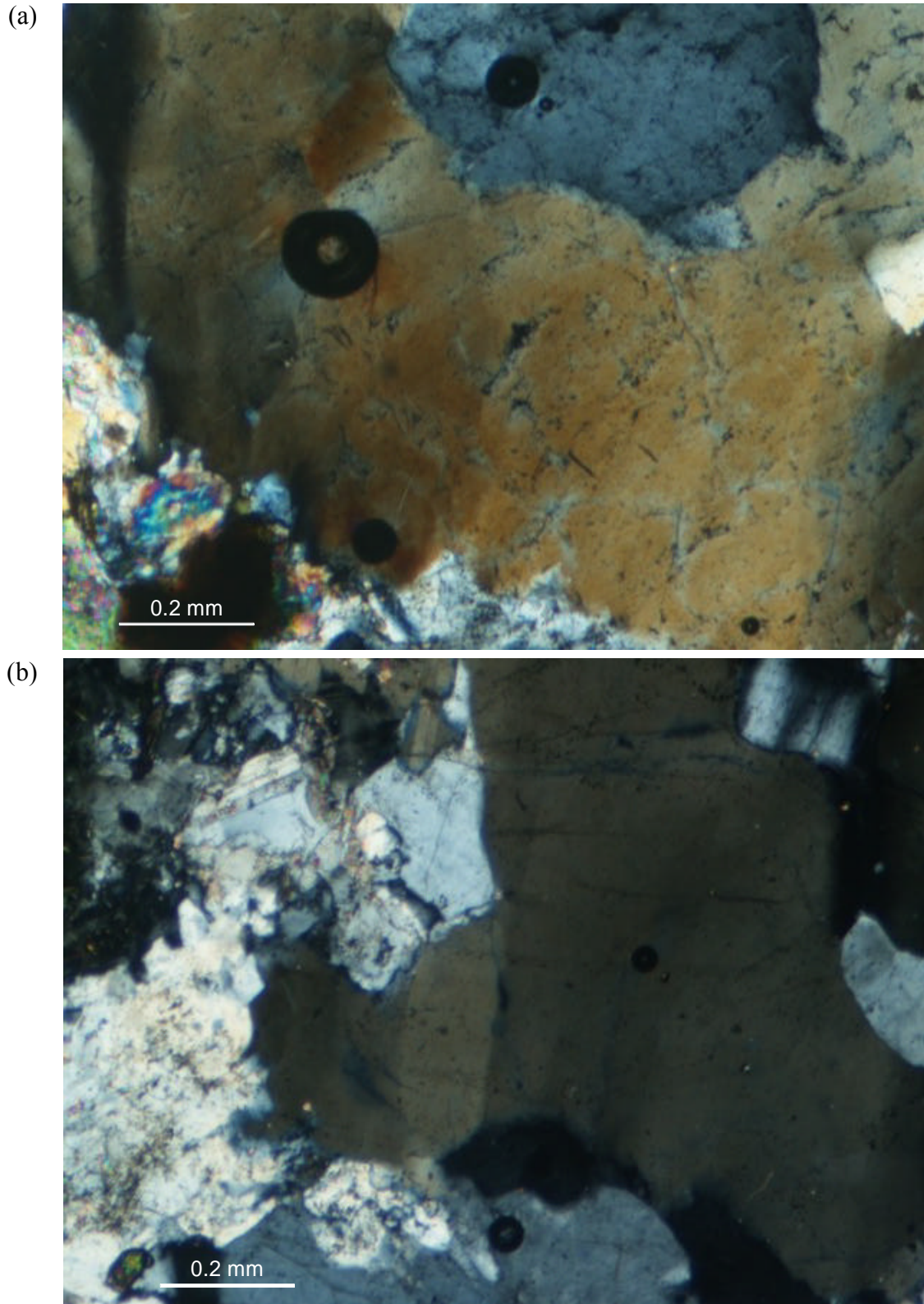


**Figure 24.** Photomicrographs of a granite dike sample (NB02-64A). (a) Quartz crystals in this sample commonly show undulatory extinction. (b) Subgrain boundaries in a large quartz. Both features indicate intracrystalline deformation after the dike intrusion.

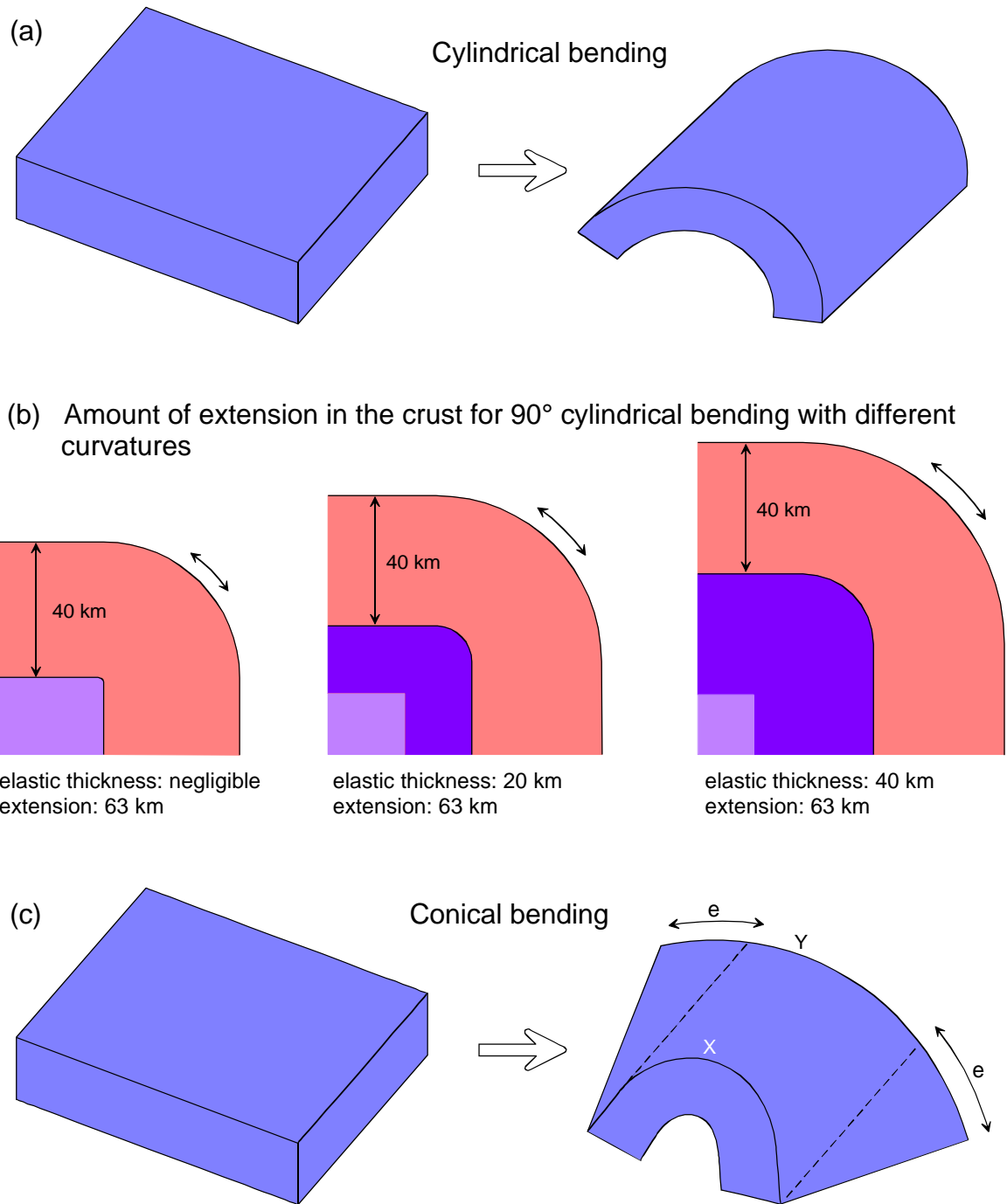


**Figure 25.** Bending of hypothetical, planar lithospheres to (a) cylindrical or (c) conical shapes. Presented in (b) is the extension amount in the crust during the cylindrical bending for different curvatures that are determined by thickness of elastic layer in the uppermost mantle. The amount of extension is 63 km in all three cases, and not affected by thickness of the elastic layer. In (c), the lithosphere is thickened at and near top of the cone (X) where the radius of curve is small, while it is thinned toward Y as the radius increases. The crust constituting the outermost layer of the lithosphere should be extended, regardless of its locations. The extension along and near the curve X occurs in the same manner and in similar amount as the cylindrical bending. By contrast, the extension along and near the curve Y mostly occurs by the fan-like expansion (e), and the component of extension caused by the cylindrical bending is small because the radius of curve is large and the lithosphere there is thin. The bending of Indian slab below the eastern Himalayan syntaxis is similar to the bending in the area around X and the kinematics of more deeply-subducted Indian slab would be similar to those in the region Y.

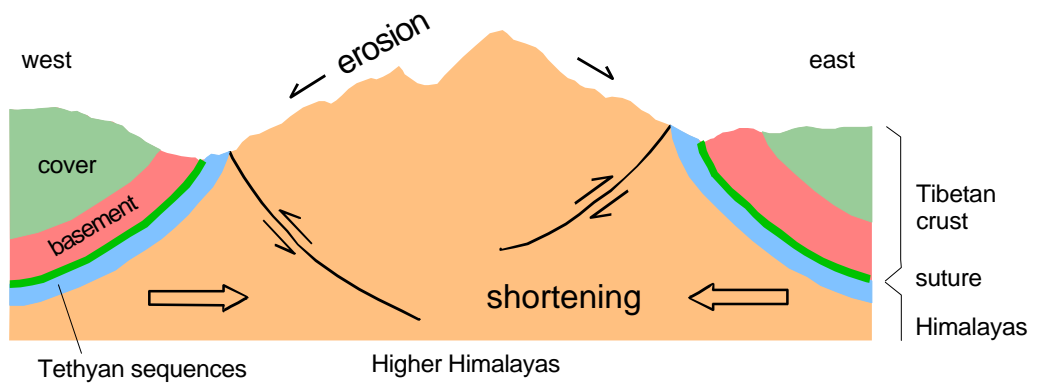


**Figure 26.** The lateral shortening model, one of possible mechanisms for the uplift and exhumation of the Namche Barwa massif. If the uplift has been driven by reverse motion along a conjugate shear zone, the exhumation could have occurred by a large amount of erosion.

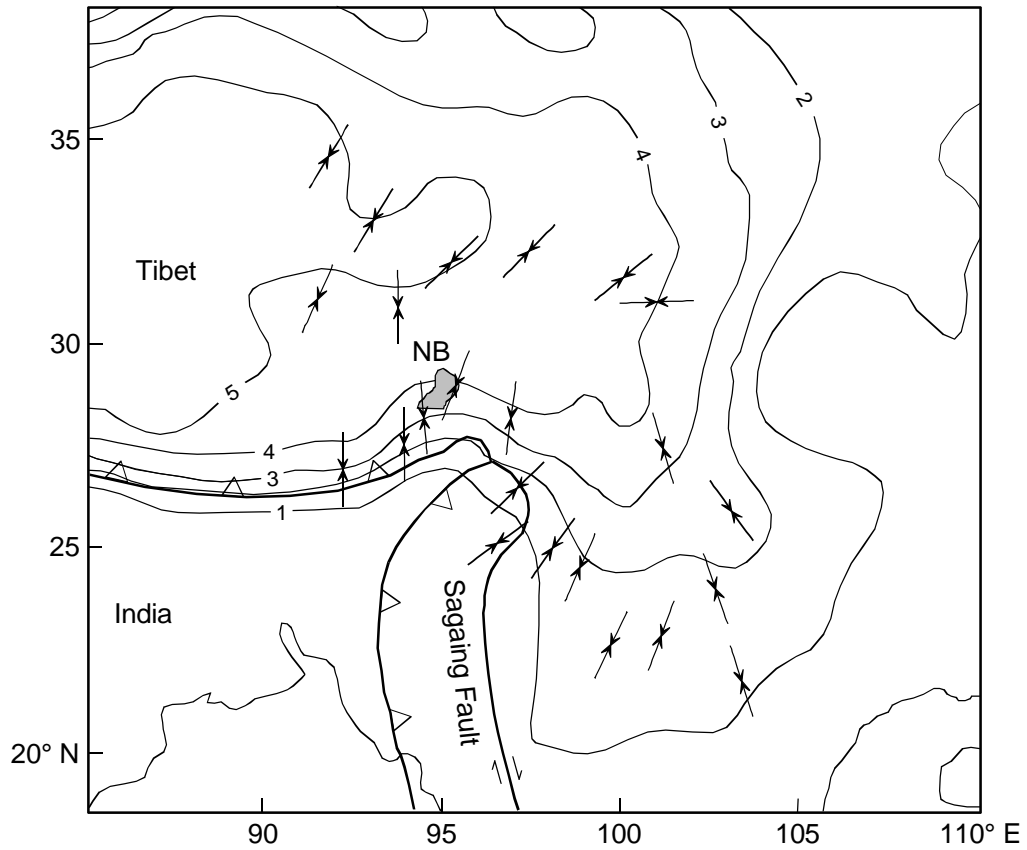


**Figure 27.** Simplified orientation map of P-axes from focal mechanisms of thrust and strike-slip events, projected onto surface. Elevation is shown by contour lines with interval of 1 km. Modified after Holt et al. (1991). NB: Namche Barwa massif.

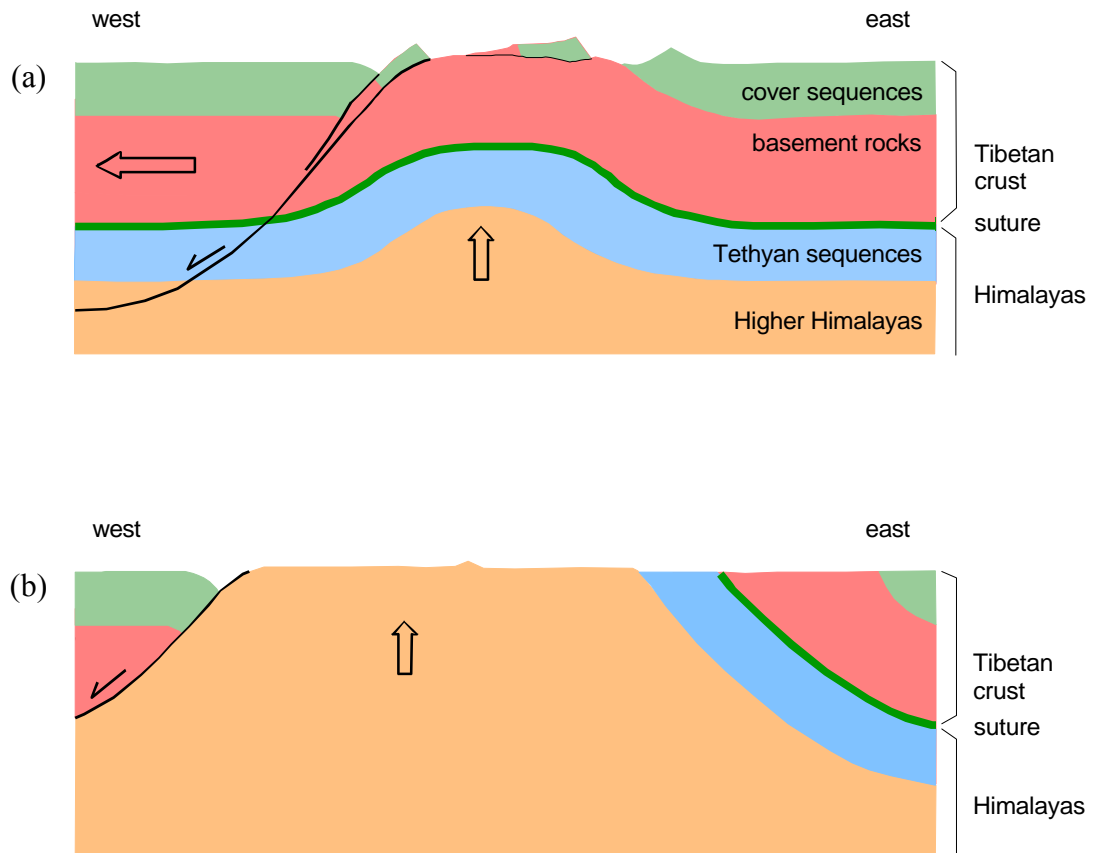


**Figure 28.** The tectonic denudation model. (a) The normal fault can exhume the structurally lower Himalayan units to the surface when it reaches the latter through the Tsangpo suture and the Tethyan sequence, and accommodates a large amount of extension. (b) This extension induces exhumation of the massif driven by isostatic rebound. In this model, the Tethyan sequence is not present along the western boundary of the massif.

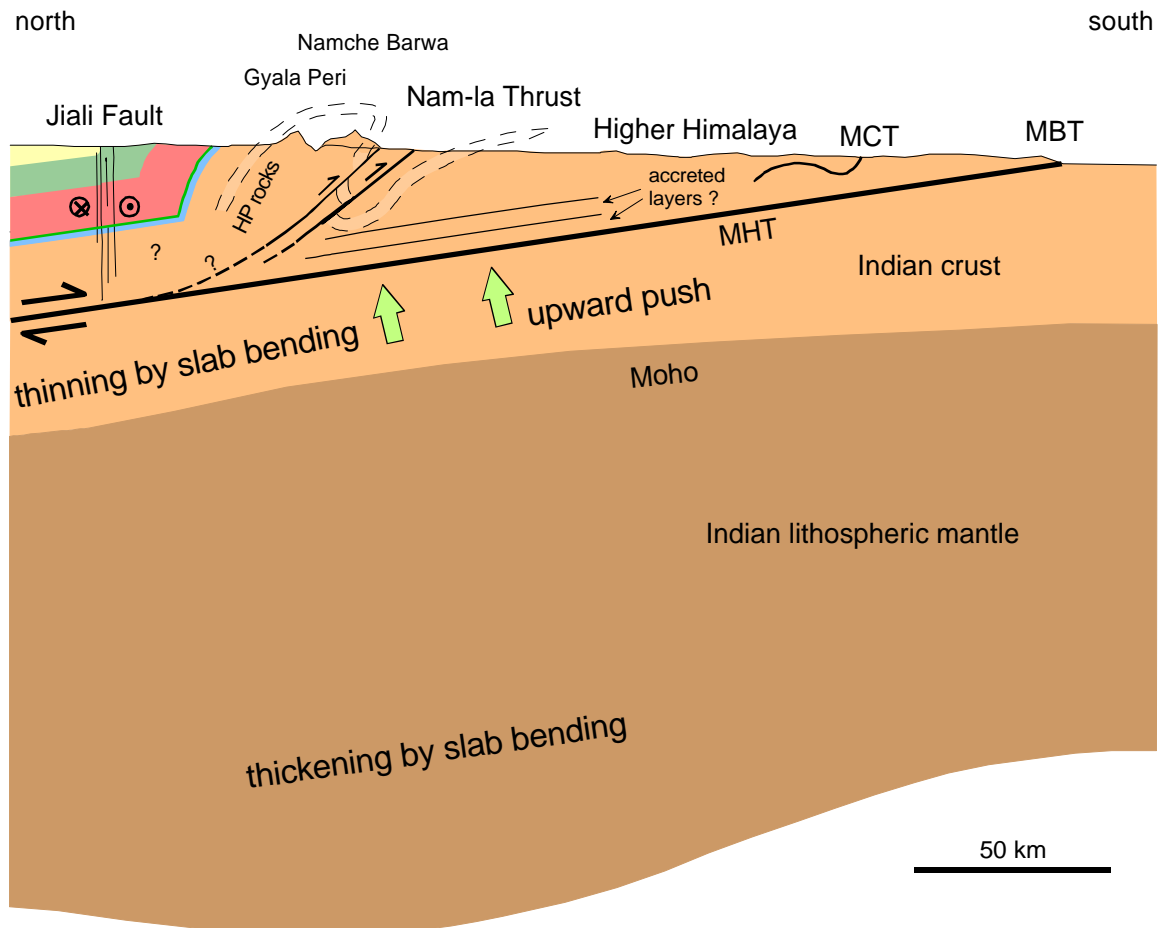
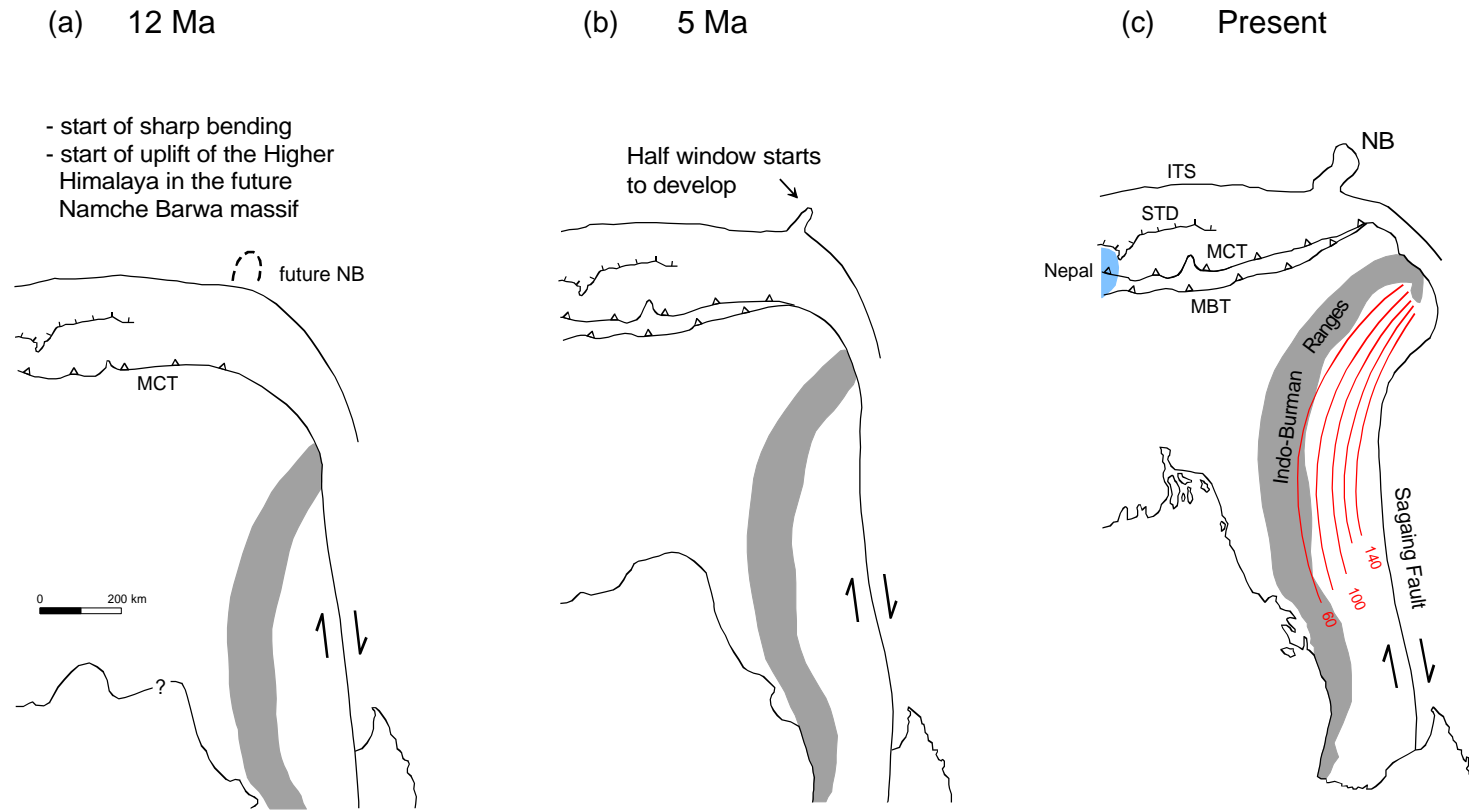


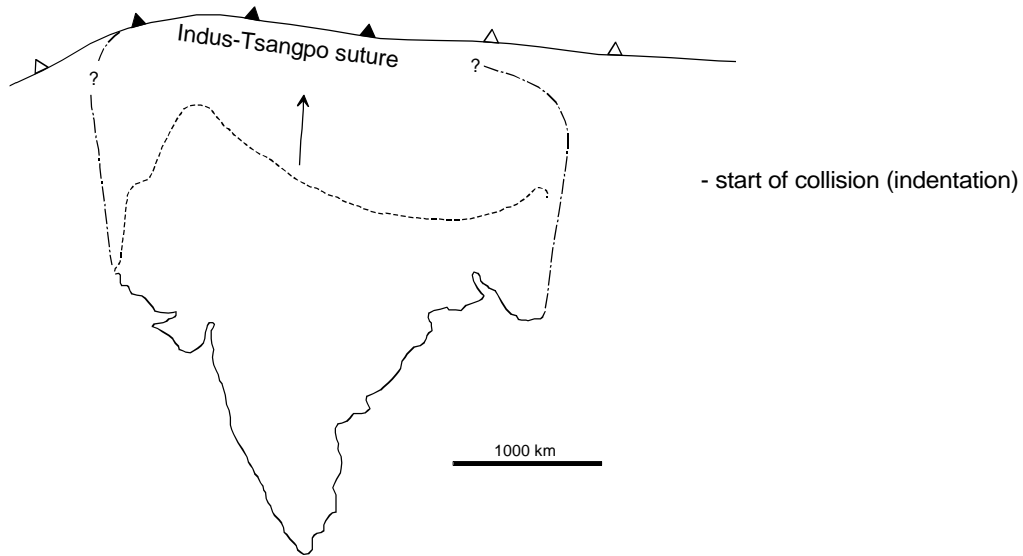
**Figure 29.** The anomalous lithospheric thickening model. The Indian slab dips about  $10^\circ$  north, west of this cross-section (toward the viewer), while it dips about  $50^\circ$  southeast below the southeastern portion of the eastern Himalayan syntaxis (away from the viewer; See Figure 30c). Such sharp bending should have thickened the Indian lithosphere in an unusual manner below the innermost syntaxis where the radius of the bending slab is minimum. As the slab passes the syntaxis with continued underthrusting, the thickened slab should undergo a large amount of extension because of increasing radius of the bent slab (See Figure 25c). Thus, the materials to thicken the Indian lithospheric mantle in the diagram have come from out of the plane of this page. MHT: Main Himalayan Thrust, MCT: Main Central Thrust, MBT: Main Boundary Thrust.



- \* India-Asia convergence rate: 40 mm/yr (based on Chen et al. (2000) and Shen et al. (2000)).
- \* Long-term right-lateral slip rate along the Sagaing Fault: 37.2 mm/yr (based on Curray et al. (1979)).
- \* Northward velocity of the Nepal Himalaya: 20 mm/yr (based on Bilham et al. (1997), Shen et al. (2000), and Paul et al. (2001)).

**Figure 30.** Reconstructed geometry of the northeastern corner of the India-Asia collision zone. Red lines show geometry of the subducted Indian plate. The numbers indicate depth to the Wadati-Benioff zone in kilometers (Ni et al., 1989). The Indo-Burman Ranges are not retrodeformed.

(a) Middle Eocene (50 Ma)



(b) Oligocene (30 Ma)

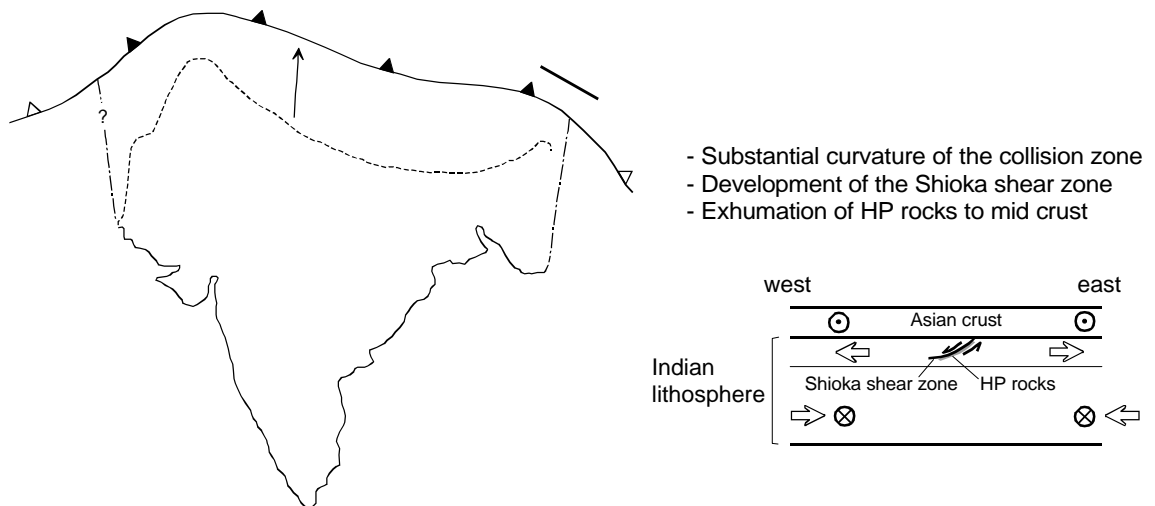
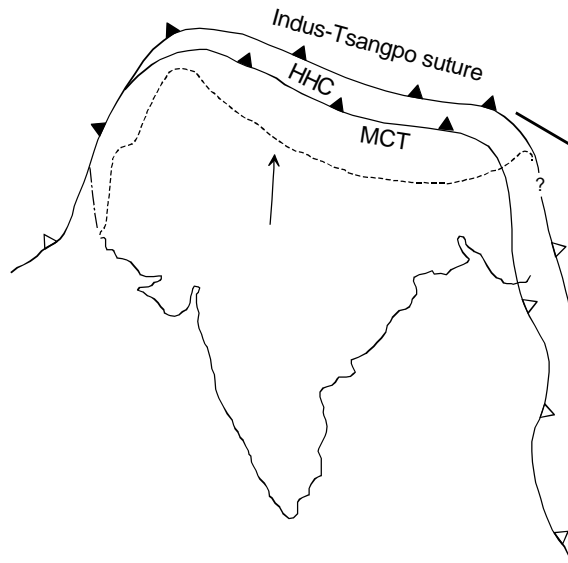
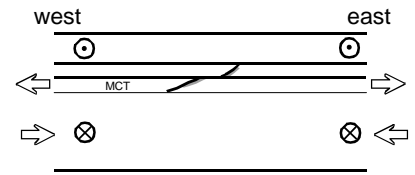


**Figure 31.** Tectonic evolution of the eastern Himalayan syntaxis region. (a) The India-Asia collision started in the Middle Eocene. (b) Since the collision started, the collision zone progressively has bent to impose extension in the upper Indian lithosphere and shortening in the lower lithosphere.

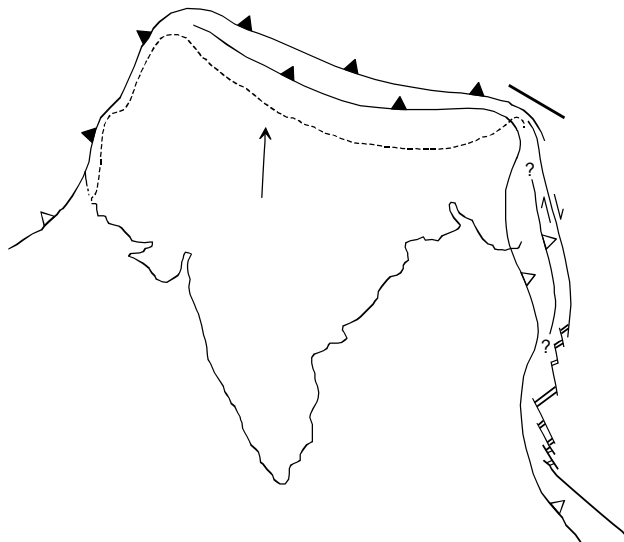
(c) Early Miocene (20 Ma)



- Development of the Main Central Thrust (MCT)
- Cessation of extension in the Shioka shear zone



(d) Middle Miocene (12 Ma)



- The eastern Himalayan syntaxis began to form.
- Sea floor spreading in the Andaman Sea

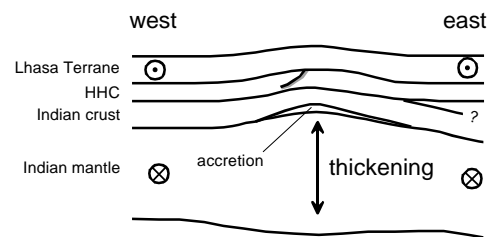
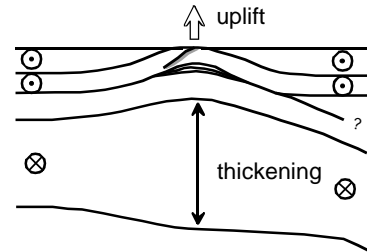
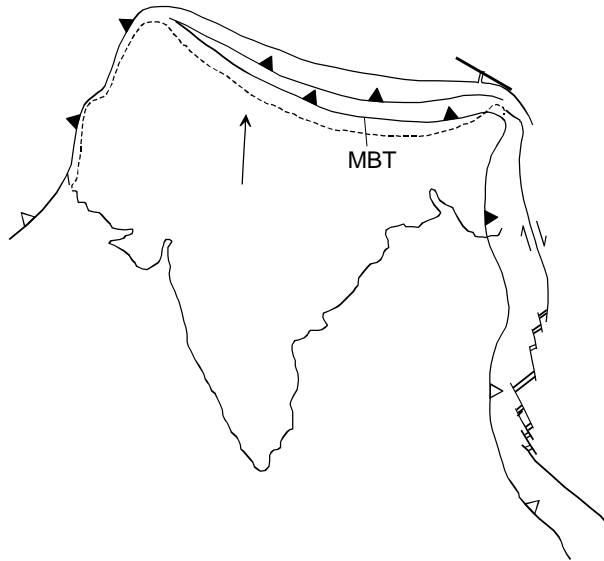


**Figure 31** (continued), (c) Thrusting of the Higher Himalayan Crystalline (HHC) along the Main Central Thrust (MCT) terminated extension along the Shioka shear zone. (d) With start of opening of the Andaman Sea, the syntaxis morphology began to appear in the eastern Himalaya.

(e) Pliocene (5 Ma)



(f) Present

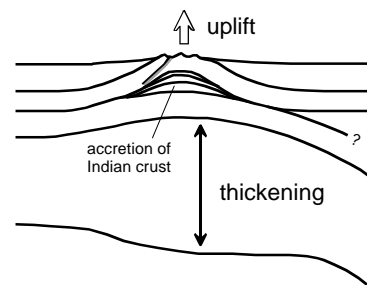
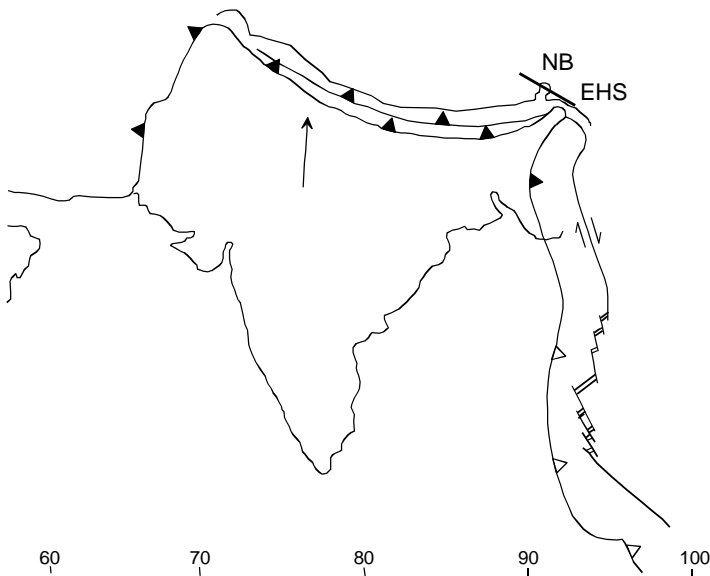


**Figure 31** (continued), (e) Northward plate motion of India, accommodated along the Sagaing Fault, resulted in thickening of the Indian lithosphere by bending. (f) Continued northward collision of the India resulted in the extreme bending of the collision zone to form the eastern Himalayan syntaxis (EHS), and the Indian lithosphere also has been bent to be thickened locally beneath the Namche Barwa massif (NB) region.